

Impact of *UGT1A* polymorphisms on inflammation and fibrogenesis in a humanized transgenic mouse model

Dissertation

zur

Erlangung des Doktorgrades (Dr. rer. nat.)

der

Mathematisch-Naturwissenschaftlichen Fakultät

der

Rheinischen Friedrich-Wilhelms-Universität Bonn

vorgelegt von

Steffen Landerer

aus

Breisach am Rhein

Bonn, 2020

Angefertigt mit Genehmigung der Mathematisch-Naturwissenschaftlichen Fakultät der
Rheinischen Friedrich-Wilhelms-Universität Bonn

1. Gutachter: Prof. Dr. Christian Strassburg

2. Gutachter: Prof. Dr. Oliver Gruß

Tag der Promotion: 18.06.2020

Erscheinungsjahr: 2020

Abstract

Fibrogenesis represents a highly dynamic scarring response of the liver resulting from different causes of hepatic injury. The stimuli leading to the excessive hepatic deposition of fibrillar collagen include obstructive biliary diseases, obesity-associated disorders of lipid metabolism or exposure to drugs and environmental xenobiotics. A key process capable of activating a broad array of profibrogenic pathways is oxidative stress. Oxidative injury, induced by reactive oxygen species, is a strong inducer of hepatic stellate cell activation which represents a critical event in fibrogenesis. UDP-glucuronosyltransferase 1A (UGT1A) enzymes detoxify a broad range of endo- and xenobiotic compounds thereby contributing to antioxidative effects, modulation of inflammation and cytoprotection. By catalyzing the covalent binding of glucuronic acid to reactive metabolites or xenobiotics, UGT1As generate hydrophilic inactive glucuronides that are more easily eliminated from the body by biliary or renal excretion.

Regarding the role of hepatic glucuronidation for the development and avoidance of liver fibrosis only limited data are available. Therefore, the overall objective of the dissertation was to show that the presence of *UGT1A* polymorphisms leading to impaired transcriptional activation and lower enzymatic UGT1A activity results in aggravated fibrogenesis as a consequence of compromised UGT1A-mediated antioxidative tissue protection. To achieve this goal, fibrosis development was assessed during different models of hepatic injury in humanized transgenic (*htg*) *UGT1A*-WT and *htgUGT1A*-SNP mice (containing a human haplotype of 10 common occurring *UGT1A* SNPs). The following studies show a considerable effect of *UGT1A* gene products on fibrosis development and progression, which is found to be dependent on the etiology of liver damage. While lower hepatic *UGT1A* expression levels correlated with a higher degree of liver fibrosis during bile duct ligation (BDL)-induced obstructive cholestasis, reduced fibrogenesis and hence a protective effect of the low-function SNP variant was observed during hepatic steatosis/steatohepatitis evoked in the experimental setting of high-fat diet-induced liver injury.

Coffee consumption is epidemiologically associated with a lower risk of fibrosis progression in humans, and has previously been shown to be a potent inducer of *UGT1A* gene expression. During BDL, coffee administration increased transcriptional *UGT1A* activation in both mouse lines accompanied by a significant reduction of liver fibrosis. Moreover, a more pronounced downregulation of fibrosis-related marker genes as well as a potent reduction of oxidative liver injury was detected in *htgUGT1A*-WT animals. Therefore, a common *UGT1A* SNP

haplotype observed in 10% of the white population, is suggested to represent a considerable risk factor for fibrosis progression in cholestasis-related disease, and could, in part, be functionally compensated by the inductive effects associated with coffee consumption. As a consequence, the beneficial effects of coffee could serve as a potential medical strategy for therapeutically activating *UGT1A* transcription in the clinical situation of cholestasis. This is the first study experimentally reporting a protective effect of this low-function Gilbert syndrome-associated haplotype leading to milder hepatic steatosis during the development of non-alcoholic steatohepatitis. Although a higher expression of *UGT1A* enzymes was observed in *htgUGT1A*-WT mice, *htgUGT1A*-SNP mice showed lower serum aminotransferase levels, reduced hepatic fat deposition and less fibrosis. The data from these experiments therefore contributes to a better understanding of one of the fastest growing hepatic disorders worldwide by identifying a novel role of *UGT1A* enzymes during the development of hepatic steatosis.

In addition to the antifibrotic effects, coffee intake has further been associated with a reduced risk of hepatocellular carcinoma (HCC) and cirrhosis, a major risk factor for the development of liver cancer in humans. The inadequate processing of carcinogenic xenobiotics, as a consequence of low-activity *UGT1A* variants, has previously been suggested to contribute or to initiate the process of liver carcinogenesis. Until now, experimental evidence for the evaluation of several case-control studies supporting this hypothesis is missing. This thesis provides experimental data for the protective influence of *UGT1A* proteins against neoplastic transformation chemically-induced by diethylnitrosamine (DEN). *HtgUGT1A*-SNP mice, which presumably show a reduced capacity of environmental carcinogen detoxification, exhibit markedly increased nodule incidence and growth, as well as higher aminotransferase activity levels. After coffee + DEN co-treatment, the number of resulting HCC-like tumor lesions decreased in both mouse lines, but was still higher in mice carrying *UGT1A* SNPs. The reduced *UGT1A* activity and carcinogen detoxification may therefore represent a relevant risk factor for individual cancer disposition, which can, at least partially, be influenced by coffee consumption. The coffee-mediated activation of human *UGT1A* genes delivers a potential explanation for the decreased risk for HCC development and other liver diseases in coffee drinkers.

Table of contents

Table of contents.....	I
List of abbreviations.....	V
List of tables.....	VIII
List of figures	IX
1 Introduction.....	1
1.1 Anatomy and function of the liver.....	1
1.1.1 Liver fibrosis	3
1.1.2 Fibrosis-related marker genes and their role in hepatic fibrogenesis.....	5
1.1.3 Incidence, pathology and pathogenesis cholestatic liver diseases	6
1.1.4 Incidence, pathology and pathogenesis of non-alcoholic fatty liver disease	8
1.2 UDP-glucuronosyltransferases	9
1.2.1 Genetic organization, substrate specificity and expression of <i>UGT1A</i> genes....	11
1.2.2 Sequence variability of the human <i>UGT1A</i> gene locus and associated diseases	13
1.2.3 Transcriptional regulation of the <i>UGT1A</i> gene locus.....	15
1.3 Hepatoprotective effects of coffee.....	20
1.4 Objectives of the dissertation	22
2 Material and Methods	25
2.1 Material.....	25
2.1.1 Humanized transgenic <i>UGT1A</i> -WT and <i>UGT1A</i> -SNP mouse lines	25
2.1.2 Oligonucleotides.....	26
2.1.3 Enzymes and dNTPs	28
2.1.4 DNA and protein makers.....	28
2.1.5 Antibodies	28
2.1.6 Secondary antibodies.....	29
2.1.7 Consumables	29
2.1.8 Technical devices	30

2.1.9	Software	31
2.1.10	Chemicals and reagents	32
2.1.11	Buffers and utility solutions	33
2.1.12	Kits	33
2.1.13	High-fat Paigen diet	34
2.2	Methods	35
2.2.1	Polymerase chain reaction (PCR) -based genotyping	35
2.2.2	Treatment, anesthesia and bile duct ligation of <i>htgUGT1A</i> mice	36
2.2.3	High-fat Paigen diet treatment of <i>htgUGT1A</i> mice.....	37
2.2.4	Diethylnitrosamine-induced liver cancer and analysis of liver tumors	37
2.2.5	Preparation of coffee	38
2.2.6	RNA-Isolation	38
2.2.7	Reverse transcription polymerase chain reaction (RT-PCR)	39
2.2.8	TaqMan PCR.....	40
2.2.9	Biochemical analysis of blood serum.....	40
2.2.10	Histological analysis	41
2.2.11	Protein isolation.....	45
2.2.12	Nuclear extraction	45
2.2.13	Western blot analysis	46
2.2.14	Peroxidase assay.....	46
2.2.15	Triglyceride assay	47
2.2.16	Computational histological analysis.....	47
2.2.17	Graphical representations and statistical analysis	48
3	Results	49
3.1	Obstructive cholestasis-induced liver fibrosis	49
3.1.1	Hepatic <i>UGT1A</i> expression during cholestatic liver injury in <i>htgUGT1A</i> mice	49
3.1.2	Serum bilirubin levels in <i>htgUGT1A</i> mice after BDL treatment	52
3.1.3	Liver histology of cholestatic <i>htgUGT1A</i> mice.....	53

3.1.4	Hepatic expression of profibrotic marker genes in cholestatic <i>htgUGT1A</i> mice...	56
3.1.5	Hepatic expression of proinflammatory marker genes in cholestatic <i>htgUGT1A</i> mice	57
3.1.6	Hepatic oxidative stress levels in cholestatic <i>htgUGT1A</i> mice.....	59
3.2	High-fat Paigen diet-induced liver injury	61
3.2.1	Hepatic <i>UGT1A</i> expression in HFPD-treated <i>htgUGT1A</i> mice	61
3.2.2	Serum aminotransferase activities in HFPD-treated <i>htgUGT1A</i> mice.....	63
3.2.3	Hepatic fat deposition in HFPD-treated <i>htgUGT1A</i> mice.....	64
3.2.4	Hepatic inflammation in HFPD-treated <i>htgUGT1A</i> mice	66
3.2.5	Quantification of liver fibrosis in HFPD-treated <i>htgUGT1A</i> mice	68
3.2.6	Hepatic expression of nuclear receptors in HFPD-treated <i>htgUGT1A</i> mice.....	71
3.3	DEN-induced carcinogenic liver injury	72
3.3.1	Incidence and size of HCC-like tumor formations in DEN-treated <i>htgUGT1A</i> mice	73
3.3.2	Serum aminotransferase activities in DEN-treated <i>htgUGT1A</i> mice.....	75
3.3.3	Hepatic <i>UGT1A</i> expression in DEN-treated <i>htgUGT1A</i> mice.....	76
4	Discussion.....	79
4.1	BDL-induced liver fibrosis	79
4.1.1	Differential hepatic <i>UGT1A</i> expression during cholestatic liver fibrosis in <i>htgUGT1A</i> -WT and SNP mice with and without coffee pre- and co-treatment	79
4.1.2	Differential effect on hepatic fibrogenesis in <i>htgUGT1A</i> -WT and SNP mice during cholestasis and coffee-dependent modulation of <i>UGT1A</i> -mediated hepatoprotection	81
4.2	HFPD-induced liver fibrosis.....	84
4.2.1	Differential outcome of hepatic fibrosis in <i>htgUGT1A</i> -WT and SNP mice.....	84
4.3	DEN-induced liver cancer	89

4.3.1	Differential incidence of HCC-like tumor formations in <i>htgUGT1A</i> -WT and SNP mice.....	89
References	93
Supplements	104
PublicationsFehler! Textmarke nicht definiert.	

List of abbreviations

4-HNE	4 hydroxynonenal
α -SMA	alpha smooth muscle actin
A	ampere
AA	amino acids
ACTA2	alpha-actin-2
AhR	aryl hydrocarbon receptor
ALT	alanine aminotransferase
AR	androgen receptor
ARNT	aryl hydrocarbon receptor nuclear translocator
AST	aspartate aminotransferase
BA	bile acid
CAR	constitutive androstane receptor
CCL2	chemokine (C-C motif) ligand 2
CDCA	chenodeoxycholic acid
CDCA-24G	chenodeoxycholic acid-24glucuronide
COL1A1	collagen type 1 alpha 1
CRE	<i>cis</i> -regulatory element
CRC	colorectal cancer
CTGF	connective tissue growth factor
CYP	cytochrome P450
CYP7A1	cholesterol 7 alpha-hydroxylase
DEN	diethylnitrosamine
dNTP	deoxyribose nucleoside triphosphate
ECM	extracellular matrix
ER	endoplasmatic reticulum
EtOH	ethanol
FFA	free fatty acids
FGF	fibroblast growth factor
FGFR	fibroblast growth factor receptor
FISH	fluorescent <i>in situ</i> hybridization
FRET	Förster resonance electron transfer
FXR	farnesoid X receptor
FXRE	FXR response elements

G	gauge
g	relative centrifugal force
GAPDH	glyceraldehyde 3-phosphate dehydrogenase
GR	glucocorticoid receptor
H&E	hematoxylin and eosin
HCC	hepatocellular carcinoma
HCl	hydrochloric acid
HCV	hepatitis C virus
HDCA	hyodeoxycholic acid
HFPD	high-fat Paigen diet
HNF	hepatocyte nuclear factor
HRP	horseradish peroxidase
HSC	hepatic stellate cell
htg	humanized transgenic
Hz	Herz
kbp	kilobase pairs
KC	Kupffer cells
LCA	lithocholic acid
LRH	liver receptor homolog
LXR	liver X receptor
mM	millimolar
mg	milligram
MMP	matrix metalloproteinase
μg	microgram
μL	microliter
μM	micromolar
NADPH	nicotinamide adenine dinucleotide phosphate
NAFLD	non-alcoholic fatty liver disease
NASH	non-alcoholic steatohepatitis
ng	nanogram
NNAL	4-(methylnitrosamino)-1-(3-pyridyl)-1-butatone
Nrf2	nuclear factor erythroid 2-related factor 2
PBS	phosphate-buffered saline
PBS-T	phosphate-buffered saline Tween 20

VII

PCR	polymerase chain reaction
PDGFB	platelet-derived growth factor subunit B
PDGFRB	beta-type platelet-derived growth factor receptor
PFA	paraformaldehyde
PhIP	2-amino-1-methyl-6-phenylimidazo[4,5-b]pyridine
PNPLA3	patatin-like phospholipase domain-containing protein 3
PPAR α	peroxisome proliferator-activated receptor alpha
PXR	pregnane X receptor
qPCR	quantitative real-time PCR
RIPA	radioimmunoprecipitation assay
RLL	right lateral lobe
ROS	reactive oxygen species
rpm	revolutions per minute
RT	reverse transcription
RXR	retinoid X receptor
SD	standard deviation
SDS-PAGE	sodium dodecyl sulfate polyacrylamide gel electrophoresis
SHP	small heterodimer partner
SNP	single nucleotide polymorphism
SREBP	sterol regulatory element-binding protein
TBS-T	tris buffered saline with Tween
tBHQ	<i>tert</i> -butylhydroquinone
TGF- β	transforming growth factor beta
TIMP	tissue inhibitor metalloprotease
TNF- α	tumor necrosis factor alpha
U	units
UDCA	ursodeoxycholic acid
UDP	uridine-5'-diphosphate
UGT	UDP-glucuronosyltransferase
V	volt
VDR	vitamin D receptor
WT	wild type
x	fold
XAP2	X-associated protein 2

List of tables

Table 1: Listing of primers used for amplification.....	26
Table 2: Listing of primers and probes used for gene expression analysis by TaqMan PCR	26
Table 3: Listing of assays used for gene expression analysis by TaqMan PCR.....	27
Table 4: Listing of enzymes and dNTPs	28
Table 5: Listing of primary antibodies used for western blot analysis.....	28
Table 6: Listing of consumables and their suppliers.	29
Table 7: List containing all used technical devices and corresponding manufacturers.....	30
Table 8: Listing of software and corresponding manufacturers	31
Table 9: Listing of chemicals, reagents and their suppliers	32
Table 10: Setting for the <i>UGT1A3</i> PCR-program	35
Table 11: Settings for dehydrogenation protocol of the Microm STP 120	41
Table 12: Hematoxylin and Eosin staining protocol	42
Table 13: Sirius red staining protocol	43
Table 14: Immunofluorescence staining protocol	44

List of figures

Figure 1: Graphical illustration of the microscopic liver architecture in humans	2
Figure 2: Graphical illustration of the morphological changes in a fibrotic liver	4
Figure 3: Localization and principle function of UDP-glucuronosyltransferases	10
Figure 4: Functional groups used for conjugation reactions performed by UDP-glucuronosyltransferases.....	11
Figure 5: Graphic representation of the human <i>UGT1A</i> gene locus.....	12
Figure 6: Schematic diagram of the negative feedback and feed-forward regulation of bile acid synthesis.....	17
Figure 7: Schematic representation of the human <i>UGT1A3</i> gene	18
Figure 8: AhR- and Nrf2-mediated transcriptional <i>UGT1A</i> regulation.....	20
Figure 9: Hypothesis overview of a potential UGT1A-mediated protective function in fibrosis initiation and progression.....	23
Figure 10: Hypothesis overview of a putative UGT1A-mediated protection against development and progression of liver cancer.....	24
Figure 11: Graphic illustration of the human <i>UGT1A</i> gene locus and the corresponding genes in <i>htgUGT1A</i> -WT and SNP mice.....	25
Figure 12: Bile duct ligation of <i>htgUGT1A</i> mice	37
Figure 13: Hepatic UGT1A mRNA expression in <i>htgUGT1A</i> -WT mice after sham operation (sham) or 14 days bile duct ligation (BDL) with and without coffee pre- and co-treatment	50
Figure 14: Hepatic UGT1A mRNA expression in <i>htgUGT1A</i> -SNP mice after sham operation (sham) or 14 days bile duct ligation (BDL) with and without coffee pre- and co-treatment.....	51
Figure 15: Determination of serum bilirubin levels after 14 days sham or bile duct ligation (BDL) operation in <i>htgUGT1A</i> -WT and SNP mice with and without coffee pre- and co-treatment	53
Figure 16: Representative hepatic sections of histological Sirius red staining in <i>htgUGT1A</i> -WT mice	54
Figure 17: Representative hepatic sections of histological Sirius red staining in <i>htgUGT1A</i> -SNP mice	54
Figure 18: ImageJ-based quantification of Sirius red histological staining in <i>htgUGT1A</i> -WT and SNP mice after sham operation (sham) or 14 days bile duct ligation (BDL) with and without coffee pre- and co-treatment	55
Figure 19: Expression levels of hepatic collagen in <i>htgUGT1A</i> -WT and SNP mice after sham operation (sham) or 14 days bile duct ligation (BDL) with and without coffee pre- and co-treatment	56

Figure 20: Hepatic expression of marker genes for fibrogenic activity in <i>htgUGT1A</i> -WT and SNP mice after sham operation (sham) or 14 days bile duct ligation (BDL) with and without coffee pre- and co-treatment	57
Figure 21: Hepatic expression of proinflammatory marker genes in <i>htgUGT1A</i> -WT and SNP mice after sham operation (sham) or 14 days bile duct ligation (BDL) with and without coffee pre- and co-treatment	58
Figure 22: Total hepatic peroxidase concentration of <i>htgUGT1A</i> -WT and SNP mice after sham or 14 days bile duct ligation (BDL) operation with and without coffee pre- and co-treatment	59
Figure 23: Representative pictures of 4-HNE immunofluorescent stained liver sections of <i>htgUGT1A</i> -WT and SNP mice after 14 days bile duct ligation (BDL) with and without coffee pre- and co-treatment	60
Figure 24: Hepatic UGT1A mRNA expression in <i>htgUGT1A</i> -WT and SNP mice after 24 weeks of control or high-fat Paigen diet (HFPD).....	62
Figure 25: Hepatic UGT1A3 protein expression in <i>htgUGT1A</i> -WT and SNP mice after 24 weeks of control or high-fat Paigen diet (HFPD).....	63
Figure 26: Serum aminotransferase activity levels of high-fat Paigen diet (HFPD)-treated <i>htgUGT1A</i> -WT and SNP mice	64
Figure 27: Macroscopic pictures of <i>htgUGT1A</i> -WT and SNP mice livers 24 weeks after control or high-fat Paigen diet (HFPD)	65
Figure 28: Representative H&E stained liver sections of <i>htgUGT1A</i> -WT and SNP mice 24 weeks after control or high-fat Paigen diet (HFPD).....	65
Figure 29: Hepatic triglyceride content of <i>htgUGT1A</i> -WT and SNP mice after 24 weeks of control or high-fat Paigen diet (HFPD)	66
Figure 30: Hematoxylin & Eosin stained liver sections of <i>htgUGT1A</i> -WT and SNP mice after 24 weeks of high-fat Paigen diet (HFPD).....	67
Figure 31: Hepatic expression of proinflammatory marker genes in <i>htgUGT1A</i> -WT and SNP mice after 24 weeks of control or high-fat Paigen diet (HFPD).....	68
Figure 32: Representative liver sections of Sirius red histological staining of <i>htgUGT1A</i> -WT and SNP mice after 24 weeks of control or high-fat Paigen diet (HFPD)	69
Figure 33: Computational evaluation of Sirius red stained areas and hepatic collagen expression in <i>htgUGT1A</i> -WT and SNP mice after 24 weeks of control or high-fat Paigen diet (HFPD)	70
Figure 34: Hepatic expression of fibrosis marker genes in <i>htgUGT1A</i> -WT and SNP mice after 24 weeks of control or high-fat Paigen diet (HFPD)	71
Figure 35: Hepatic mRNA expression and nuclear protein of nuclear receptors in <i>htgUGT1A</i> -WT and SNP mice after 24 weeks of control or high-fat Paigen diet (HFPD).....	72

Figure 36: Representative liver images of *htgUGT1A*-WT and SNP mice 40 weeks after diethylnitrosamine (DEN) injection with and without coffee co-treatment..... **73**

Figure 37: Characterization of all visible liver nodules in *htgUGT1A*-WT and SNP mice 40 weeks after diethylnitrosamine (DEN) injection with and without coffee co-treatment **74**

Figure 38: Detailed overview of tumor susceptibility in *htgUGT1A*-WT and SNP mice 40 weeks after diethylnitrosamine (DEN)-induced hepatocarcinogenesis..... **75**

Figure 39: Serum aminotransferase activities of *htgUGT1A*-WT and SNP mice 40 weeks after diethylnitrosamine (DEN)-induced hepatocarcinogenesis..... **76**

Figure 40: Hepatic expression of UGT1A1, UGT1A3 and UGT1A4 in *htgUGT1A*-WT and SNP mice after 40 weeks of diethylnitrosamine (DEN)-induced hepatocarcinogenesis **77**

Figure 41: Hepatic expression of UGT1A6, UGT1A7 and UGT1A9 isoforms in *htgUGT1A*-WT and SNP mice after 40 weeks of diethylnitrosamine (DEN)-induced hepatocarcinogenesis **78**

Figure 42: Schematic illustration of a putative mechanism of action involving the reduced expression of UGT1A3 due to the presence of SNPs **85**

Figure 43: Graphical overview of potential factors possibly contributing to the protective effects of *htgUGT1A*-SNP mice in non-alcoholic fatty liver disease..... **86**

Figure 44: Manually written protocol used for computational quantification of liver fibrosis from Sirius red stained liver sections..... **104**

Figure 45: Western blot analysis of nuclear retinoid X receptor protein in *htgUGT1A*-WT and SNP mice after 24 weeks of control or high-fat Paigen diet (HFPD) **104**

1 Introduction

1.1 Anatomy and function of the liver

With a weight of about 1200 - 1500 grams, the liver is the body's heaviest internal organ and the largest exocrine gland. As central metabolic organ it performs multiple substantial functions closely involved in glucose, lipid and protein metabolism [1]. In doing so, the liver is not only accountable for the production of essential proteins such as blood clotting factors or albumin, but also fulfills a plethora of other crucial functions related to gluconeogenesis, cholesterol synthesis, lipogenesis and the formation of transporter lipoproteins. Representing the primary organ for detoxification, the liver is responsible for the biotransformation of various xenobiotics including therapeutic drugs, dietary components and environmental carcinogens. Moreover, it is also active in the clearance of endobiotic by-products (e.g. bilirubin, the lipid-soluble end product of heme degradation), thus protecting the organism against harmful compounds from internal and external sources. The synthesis of biomolecules (e.g. bile) necessary for digestion, the breakdown of hormones and insulin as well as the storage of vitamins, glucose and minerals are further important functions performed by the liver [2].

The unique and highly complex architecture allows the reddish-brown organ to complete its innumerable different functions. Macroscopically, the human liver is divided into four lobes (*Lobus hepatis sinister*, *Lobus hepatis dexter*, *Lobus caudatus* and *Lobus quadratus*) which are covered by a fine elastic layer of connective tissue referred to as Glisson's capsule. Based on their vascular supply, these lobes can be subdivided into eight functional segments. The hepatic vasculature is composed of two distinct blood vessels, the hepatic artery (*Arteria interlobularis*) and the portal vein (*Vena interlobularis*). The former supplies the liver with oxygenated blood, whereas the latter distributes venous blood from the spleen and the digestive system [3]. Accordingly, the portal vein transports all substances to the liver that enter the bloodstream with the diet, regardless of whether they are nutrients or toxins. In the liver, both blood vessels branch into a fine capillary network thereby enabling the transport of substances for further procession to individual liver cells called hepatocytes. At the microscopic level, roughly 1-1.5 million hepatic lobules form the morphological-functional units of the liver lobes. They possess a hexagonal columnar structure and predominantly consist of radially arranged hepatocyte cords (or hepatic cords) that surround a central vein localized in the middle of each hepatic lobule (Fig. 1) [4]. At each corner of two adjacent hepatic lobules are the portal triads, through each of which passes one branch of the hepatic

artery, one branch of the hepatic portal vein and one branch of the intrahepatic bile duct (*Ductus biliferus interlobularis*) [5]. Lymphatic vessels and a branch of the *nervus vagus* are two additional structures localized in the portal triad (not depicted in figure 1). In between the hepatic cords are the hepatic sinusoids where the arterial and portal blood mixes before draining to the central vein.

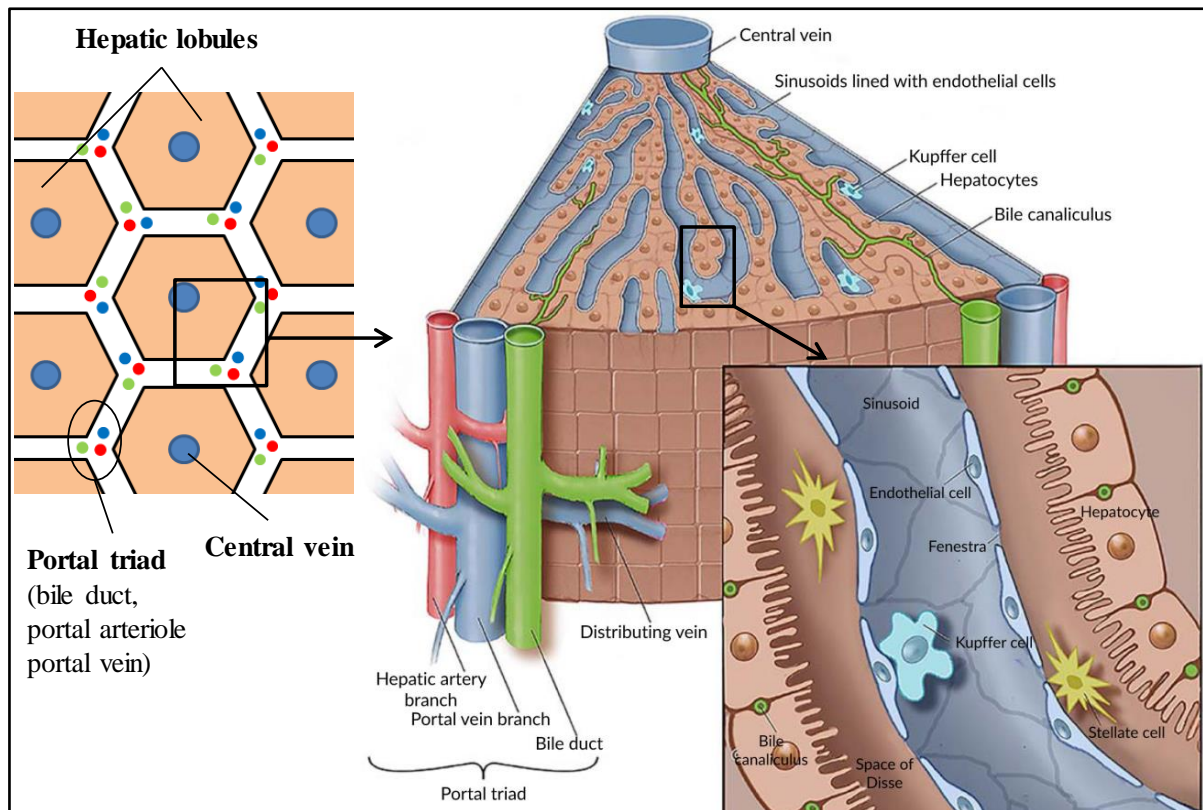


Figure 1: Graphical illustration of the microscopic liver architecture in humans. The hexagonal arrangement of the hepatic lobules that surround the central vein and the portal triads (each harboring one branch of the hepatic artery, portal vein and bile duct) at the periphery is depicted on the left side. The microvascular units of the hepatic lobules, the hepatic sinusoids, are shown in more detail on the right side of the illustration [2, modified].

The inner surface of the hepatic sinusoids is an endothelial lining with a porous/fenestrated structure. These pores or "*fenestrae*" enable the metabolic exchange of solutes between hepatocytes and blood. Specific liver macrophages named Kupffer cells (KCs) colonize the hepatic sinusoids. KCs are involved in the degradation of senescent erythrocytes and in the removal of bacteria or unwanted external particles. Endothelial cells and hepatocytes are separated by the subendothelial space of Disse which inhabits vitamin A storing hepatic stellate cells (HSCs) and a thin layer of basement membrane matrix proteins [6].

The biliary tree or biliary tract represents another important hepatic element and enables the bile flow throughout the entire organ. Bile, synthesized and secreted by hepatocytes, is collected through a fine network of bile canaliculi which are situated between two

neighboring hepatocytes. The bile canaliculi merge into intrahepatic bile ducts, which again fuse into the bigger left and right hepatic ducts and finally merge to form the common hepatic duct. Together with the cystic duct from the gallbladder they unite to form the common bile duct which leaves the liver to enter the duodenum [7].

1.1.1 Liver fibrosis

Hepatic fibrogenesis is the consequence of either acute or sustained liver injury leading to the pathological proliferation of fibrous scar tissue due to hepatic deposition of fibrillar collagen. It is a reversible wound-healing response characterized by the massive accumulation of extracellular matrix (ECM, 6 times more compared to healthy livers) proteins and concomitant structural changes of the liver architecture [8]. In case of acute liver damage, pathological alterations are transient and the liver restores its natural structure. During chronic liver injury, regeneration cannot keep pace with hepatocyte death and scarring occurs. The progressive replacement of hepatocytes by collagen and other ECM proteins as well as self-perpetuation of inflammatory processes result in serious morphological alternations of the liver architecture and uncontrolled metabolic abnormalities with potentially devastating consequences [9]. Chronic hepatitis C virus (HCV) infection, non-alcoholic steatohepatitis (NASH), inappropriate alcohol consumption, cholestasis-related diseases and drug intoxication are among the primary reasons for hepatic fibrogenesis in developed countries [10]. Fibrosis occurs in most types of chronic liver diseases and usually leads to no or sometimes minor clinical symptoms. If the underlying cause of liver injury is not identified and eliminated, fibrosis will proceed to cirrhosis and liver failure representing the end-stage of advanced fibrosis that is associated with an increased mortality rate [11].

The pathomechanisms responsible for the formation of fibrous scar tissue are based on interactions between ECM producing HSCs, liver resident and liver infiltrating cells. In healthy livers, HSCs reside in a quiescent state. Upon liver injury, HSCs become activated and highly proliferative. Once activated, they lose their vitamin A storage capacity, acquire a contractile myofibroblast-like phenotype and become the primary source for fibrillar collagen and other ECM proteins [12]. Although the pathogenesis of liver fibrosis depends on the origin of liver injury, the activation of HSCs represents a common pathological feature and is therefore considered as key event in hepatic fibrogenesis. Damaged hepatocytes and the associated uncontrolled release of cytokines, chemokines and the subsequent activation of KCs together with increased oxidative stress are the primary effectors of HSC activation [13].

A schematic overview of the morphological consequences for the liver as a result of the excessive HSC-mediated production of ECM proteins is shown in figure 2.

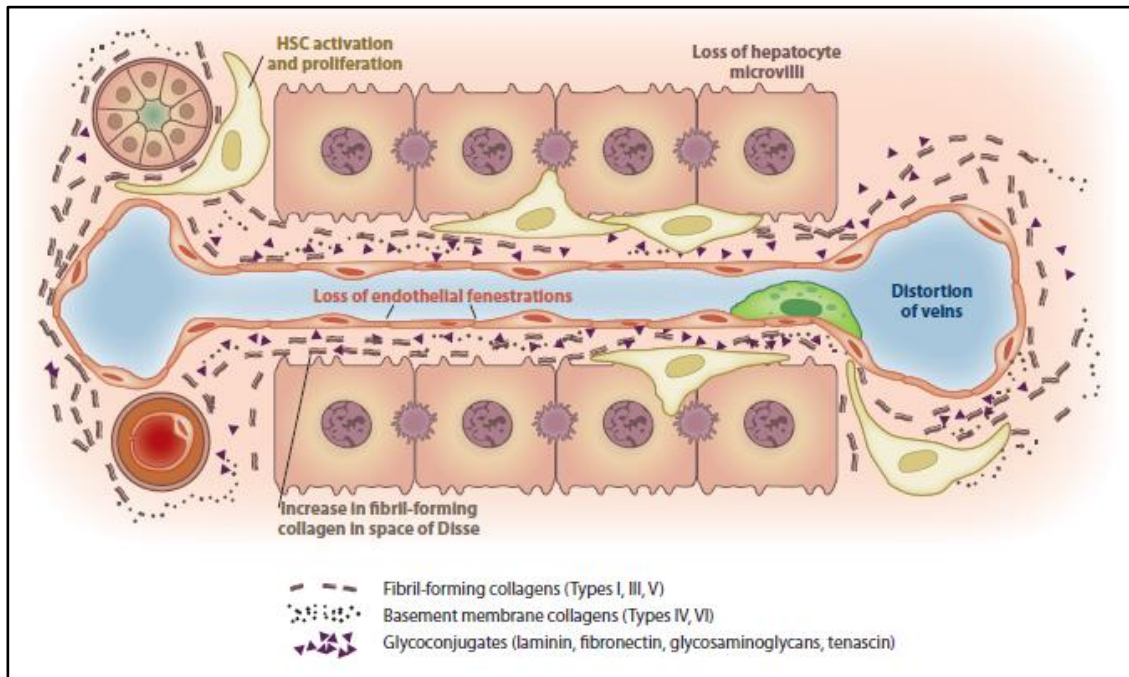


Figure 2: Graphical illustration of the morphological changes in a fibrotic liver. Accumulation of extra cellular matrix (ECM) proteins and the associated loss of endothelial fenestrations as a consequence of hepatic stellate cell (HSC) activation are important characteristics of liver fibrosis. Remodeling of ECM composition leads to a substitution of basement membrane collagens of type IV and VI to fibril-forming collagens of type I and III which are particularly abundant in fibrotic livers [6].

ECM is defined as tightly organized network that provides functional and structural integrity of surrounding parenchymal cells [14]. The persistent synthesis of ECM in the space of Disse, in combination with the reduced degradation leads to the capillarization of sinusoids [15]. The resulting loss of the endothelial fenestrations causes a physical obstruction of the bidirectional plasma flow and impairs the exchange of solutes between portal vein and hepatocytes. Consequently, perturbations of hepatocyte function ensue leading to apoptosis. This, in turn, activates KCs and the subsequent release of fibrogenic mediators causes the infiltration of additional inflammation cells and enhances the already established inflammatory state contributing to the initiation, progression and maintenance of liver fibrosis [6, 16]. The roles of those profibrotic mediators that are of higher importance for the present work are briefly described in the section below.

1.1.2 Fibrosis-related marker genes and their role in hepatic fibrogenesis

Following liver injury, a multitude of factors promote hepatic fibrogenesis and contribute to the activation, proliferation and survival of HSCs. Among the many different profibrotic factors released during the pathological course of liver fibrosis, transforming growth factor beta (TGF- β) is certainly the most powerful cytokine. Predominantly generated by monocytes, macrophages and damaged hepatocytes, TGF- β binds to transforming growth factor beta receptor type II, causes the dimerization of receptor type I and initiates a signaling cascade that involves phosphorylation and activation of the intracellular proteins SMAD 2/3, which then interact with SMAD 4 to form an active complex that enters the nucleus to enhance the transcription of fibrogenic TGF- β target genes [17, 18]. Moreover, it stimulates HSCs to synthesize the fibrillar ECM components *procollagen type I* (encoded by the *COL1A1* gene) and *procollagen type III* [19]. TGF- β is also involved in the transcriptional regulation of its downstream mediator connective tissue growth factor (CTGF) which amplifies its profibrotic action. Primarily produced by activated HSCs, CTGF is highly overexpressed in fibrotic livers and crucial for tissue remodeling, collagen production, maintenance of activation and proliferation of HSCs [20]. Moreover, tissue inhibitor of metalloproteinase (TIMP) is generated under the action of TGF- β in activated HSCs. These endogenous protease inhibitors mediate the inhibition of two key features involved in fibrosis resolution. On the one hand, they promote HSC survival by exerting anti-apoptotic effects and on the other hand they antagonize the anti-fibrotic effects of matrix metalloproteinases (MMPs) which are key enzymes responsible for fibrillar ECM degradation [21]. Especially the significant overproduction of the TIMP1 isoform causes perturbations in the thoroughly regulated MMP-TIMP balance and leads to defective ECM remodeling. Together with TGF- β , platelet-derived growth factor (PDGF) is one of the key growth factors involved in fibrogenesis. Primarily released by KCs, it is the major mitogen for activated HSCs boosting them to excessive proliferation. PDGF-stimulated proliferation is transmitted *via* the specific platelet-derived growth factor receptors (PDGFR) localized at the surface of activated HSCs. Both, PDGF and PDGFR are upregulated in activated HSCs and correlate with the severity of fibrosis and inflammation [22].

As sustained hepatic inflammation nearly always precedes liver fibrosis, inflammatory mediators play a key role in hepatic fibrogenesis. Tumor necrosis factor alpha (TNF- α) is a proinflammatory cytokine produced by activated macrophages and injured hepatocytes [23]. Upon binding to tumor necrosis factor receptor 1 or 2, TNF- α exerts a variety of profibrotic effects. It is a potent chemoattractant for neutrophils, a powerful mediator of the inflammatory

response and an essential effector for the activation of HSCs. In this connection, it promotes the production of reactive oxygen species (ROS) by interfering with the mitochondrial respiratory chain. Furthermore, the TNF- α -mediated induction of the NF κ B signaling pathway contributes to transcriptional initiation of genes involved in HSC activation. In particular during NASH it is an important mediator of hepatocyte cell death and a crucial inducer of insulin resistance in adipocytes [24, 25]. C-C chemokine ligand 2 (CCL2) is another proinflammatory cytokine with chemotactic activity. It is secreted by damaged hepatocytes, KCs, dysfunctional adipocytes and activated HSCs. When released, it causes additional macrophage recruitment and consequently enhances the production of cytokines [26].

Alpha-smooth muscle actin (α -SMA) is an actin isoform encoded by the *alpha-actin-2* gene (*ACTA2*) present in the contractile apparatus of vascular smooth muscle cells. If liver injury ensues, the expression of α -SMA correlates with the activation of HSCs and is therefore commonly used as a surrogate marker of myofibroblast transformation [27].

1.1.3 Incidence, pathology and pathogenesis cholestatic liver diseases

Apart from HCV infection, alcohol consumption and NASH, cholestatic liver injury is one of the major causes for liver fibrosis in industrialized countries [28]. Encompassing a wide field of clinical conditions that range from rather benign cholestatic disorders with good chances of recovery to malignant cancers with poor prospects for survival, cholestasis-related diseases are diagnosed in all age groups, ethnicities and both sexes [29]. High prevalence rates have been reported for gallstone diseases, drug-induced cholestasis as well as gallbladder cancer, whereas primary biliary cholangitis, primary sclerosing cholangitis and cholangiocarcinoma are rather rarely observed [30]. Especially gallstone diseases (also known as cholelithiasis) belong to the most frequent types of cholestasis reaching a prevalence range of roughly 6 - 22% in Europe and the United States [31, 32]. Depending on the causative pathological condition, cholestatic disorders can further be subdivided into obstructive or metabolic (non-obstructive) types of cholestasis. While the first-mentioned develop usually as a result of gallstone-caused mechanical blockage of the common bile duct, genetic defects leading to disturbances in bile formation belong to the latter type. The histopathological findings are disease specific. In cholestasis these generally involve the presence of bile within hepatocytes, portal expansion and bile duct proliferation whereas at the biochemical level, elevated serum BA levels and direct hyperbilirubinemia (more than 50% of total bilirubin content is conjugated) can be observed [33, 34]. Irrespective of their etiology, if left untreated

cholestasis will proceed to liver fibrosis, biliary cirrhosis and ultimately to end-stage liver disease [35].

The defining feature of cholestatic liver diseases is impaired bile flow from the liver to the duodenum and the subsequent hepatic accumulation of bile acids (BAs) [36]. BAs are directly synthesized from cholesterol and exert several biological functions that are predominantly mediated *via* the farnesoid X receptor (FXR, see chapter 1.2.3) [37]. Upon food intake, the amphipathic molecules are secreted into the small intestine where their detergent properties are required for absorption of dietary lipids and lipid-soluble vitamins [38]. Moreover, BAs can act as signaling molecules not only capable of influencing bile formation and synthesis, but also lipid and glucose homeostasis, liver regeneration and carcinogenesis [39, 40]. The hepatic retention of toxic bile components can initiate deleterious consequences and is considered to be the major effector of liver damage during cholestasis [41, 42]. Therefore, the molecular mechanisms underlying the BA-triggered hepatocyte damage have been extensively studied. The combination of prolonged exposure to cytotoxic BAs, increased concentrations as well as their detergent action on lipid components leads to the disruption of cell membranes and induction of hepatocyte apoptosis [43]. This, in turn, promotes the generation of ROS which are playing a critical role in the pathogenesis of BA-induced tissue injury. Elevated ROS levels result in lipid peroxidation, oxidative modification of proteins, nucleic acids and the activation of KCs through increased exposure to biomolecules that stimulate damage-associated molecular patterns [44, 45]. Activated KCs amplify the inflammatory response through generation of various cytokines and further increase intracellular ROS levels eliciting additional oxidative hepatocyte injury [46]. In early stages of cholestatic liver injury, oxidative stress mainly occurs through BA-mediated impairment of the respiratory chain and electron transport in hepatic mitochondria as well as by depletion of antioxidative defense mechanisms such as peroxidase concentrations or mitochondrial glutathione contents [44]. Ursodeoxycholic acid (UDCA), a secondary bile acid and sole approved medical drug used in the treatment of cholestasis-related diseases, in part contributes to anticholestatic action through reduction of oxidative injury [47]. Identification of compounds either possessing inherent antioxidative properties or capable to activate BA detoxifying enzymes, or both, are therefore suitable candidates to limit the susceptibility to fibrosis progression during cholestasis.

1.1.4 Incidence, pathology and pathogenesis of non-alcoholic fatty liver disease

The growing number of patients with non-alcoholic fatty liver disease (NAFLD) renders this condition one of the most common liver disorders worldwide and consequently to a central medical challenge of the 21st century. It has been estimated that one third of the adult American population is affected by NAFLD. With more than 85% of them being morbidly obese, the prevalence of NAFLD is closely related to obesity and associated comorbidities that lead to an increased mortality rate [48, 49]. Since the number of overweight individuals has nearly doubled during the past decades, it is predictable that the global incidence of patients with NAFLD will continue to increase [50]. Apart from dietary habits, other influences such as genetic disorders (e.g. polymorphisms in *PNPLA3*), gender, age and ethnicity have been identified as additional risk factors for NAFLD development [51]. As NAFLD is considered to be the hepatic manifestation of the metabolic syndrome it usually comes along with other clinical conditions that almost always occur in the pathological setting of obesity. These include dyslipidemia, cardiovascular diseases and/or insulin resistance [25]. The hallmark of NAFLD is hepatic steatosis. A condition defined as the hepatic accumulation of triglycerides in more than 5% of hepatocytes without or with insignificant (less than 10-20 g per day) alcohol consumption [52]. Often beginning as simple steatosis, NAFLD has the potential to progress to NASH or cirrhosis and eventually results in liver failure or hepatocellular carcinoma (HCC) [53]. NASH as the next stage is a more severe condition of fatty liver damage, which is characterized by several molecular events comprising lobular inflammation, hepatocyte apoptosis and fibrosis [54]. NASH is often regarded as the most worrisome intermediate state of NAFLD, as with the progressive deposition of hepatic collagen, cirrhosis is likely to ensue. NAFLD-related cirrhosis has been estimated to emerge in about 20-25% of individuals with NASH making it the second most common cause for liver transplantation in the United States [55, 56].

The pathogenesis of NAFLD is a complex process and the molecular mechanisms are still poorly understood. It has been suggested that obesity-induced adipose tissue dysfunction and subsequent immune-mediated injury by inflammatory cells triggers the initiation of hepatic steatosis [57]. As a result of continuously enlarging adipocytes, oxygen demand increases and exceeds the blood supply leading to hypoxic adipocytes and successive production of the proinflammatory cytokines TNF- α and CCL2 [58]. While TNF- α induces insulin resistance in dysfunctional adipocytes and the release of free fatty acids (FFAs) into the blood circulation, CCL2 reinforces cytokine production and perpetuates the already existing insulin resistance through recruitment of macrophages. Consequently, the liver is exposed to elevated levels of

circulating FFAs which are absorbed from hepatocytes by fatty acid up-take transporters [59]. In the liver, excess FFA are esterified to triglycerides for storage forcing the liver to become an ectopic fat reservoir. Insulin-mediated stimulation of *de novo* lipogenesis, impaired fatty acid oxidation and the reduced export of hepatic lipids by very-low density lipoproteins of hepatocytes are additional factors leading to hepatic steatosis in obese individuals [60]. According to the “two-hit hypothesis”, in which the progression to liver fibrosis after liver injury requires at least two hits, hepatic lipid accumulation represents the first hit, while the second hit can take different forms. FFA-mediated lipotoxicity, hepatocyte cell death, oxidative stress and the resultant inflammatory processes have been proposed as possible second hits for liver damage capable to promote steatosis to NASH or worse [61]. Clinical data indicates that whenever fibrosis occurs in NAFLD and NASH the prognosis in the affected individual is reduced [62, 63].

Since hepatic lipid homeostasis includes a precisely regulated network of nuclear receptors, transcription factors and their ligands, perturbations of involved pathways have the potential to cause serious hepatic consequences [64]. Growing evidence suggests an important role of fatty acids as modulators of cell-signaling pathways. As such, fatty acids might be capable to induce the activation of various nuclear receptors such as retinoid X receptor (RXR) or peroxisome proliferator-activated receptor alpha (PPAR α) [65]. Steatosis-associated pathological features such as oxidative stress and inflammatory mediators are further factors possibly influencing the activity of nuclear receptors [66]. Thus, NAFLD-caused dysregulation of nuclear receptor signaling pathways due to aberrant FFA concentrations would not only affect lipid homeostasis and liver histopathology, but could also have considerable effects on nuclear receptor-regulated drug metabolizing enzymes and hence on xenobiotic metabolism.

1.2 UDP-glucuronosyltransferases

The process of glucuronidation represents an important, specialized and highly conserved metabolic detoxification pathway performed by a subgroup of drug metabolizing enzymes entitled uridine-5'-diphospho-glucuronosyltransferases (UDP-glucuronosyltransferases, UGTs) [67]. UGTs are enzymes of the so-called phase II metabolism that utilize the co-substrate UDP-glucuronic acid as a sugar donor to covalently attach glucuronic acid to a broad array of different substrates. This biotransformation process generates β -glucuronidase-sensitive sugar conjugates referred to as glucuronides [68]. Localized in the inner membrane

of the endoplasmatic reticulum (Fig. 3) they catalyze the conversion of lipophilic substrates to water soluble, usually inactive glucuronides that can be easily eliminated from the body *via* bile, urine or feces [69, 70]. Since endo- and exogenous compounds are excreted through coordinated metabolism between phase I and II enzymes, most of the UGT target substrates encompass reactive molecules that have been previously generated by oxidation of cytochrome P450 (CYP) enzymes in phase I metabolism. Substances that undergo glucuronidation include a huge variety of endo- and xenobiotics such as bile acids, hormones, bilirubin, dietary constituents and approximately 40-70% of all commercially available drugs, making UGTs the most important group of phase II enzymes [71-74].

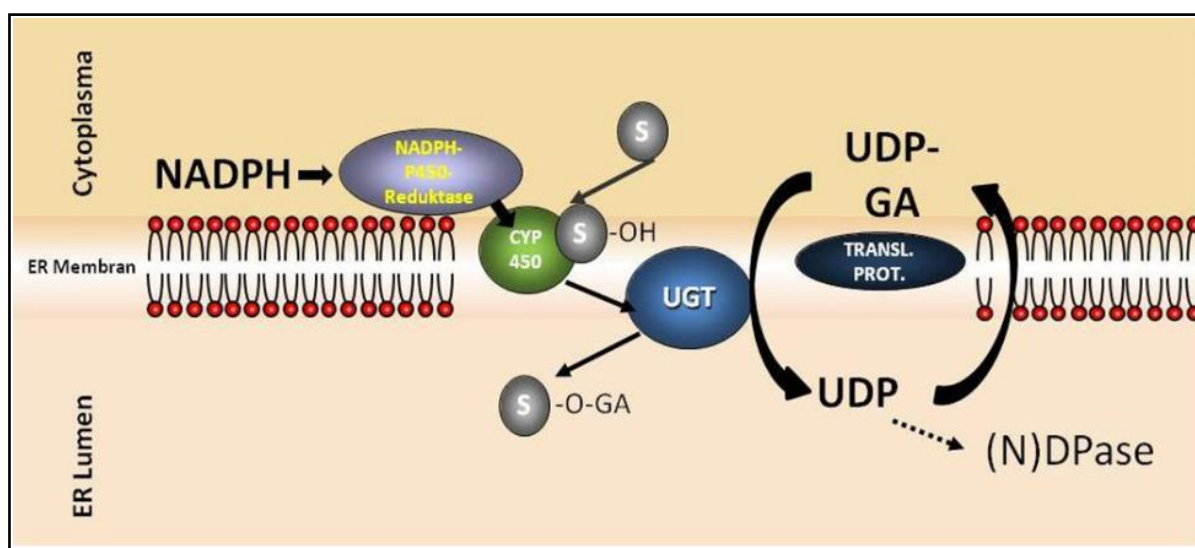


Figure 3: Localization and principle function of UDP-glucuronosyltransferases. (NADPH) Nicotinamide adenine dinucleotide phosphate, (CYP450) cytochrome P450, (S) substrate, (OH) hydroxyl group, (UGT) uridine-diphosphate-glucuronosyltransferase, (UDP-GA) uridine 5'-diphospho-glucuronic acid, (ER) endoplasmatic reticulum [75].

Together with other phase II biotransformation reactions, UGTs also play an essential role for cellular defense against a broad array of chemically diverse compounds including environmental toxins and carcinogens [76, 77]. The broad spectrum of substrates is based on the ability of UGTs to use hydroxyl, sulfuryl, carboxyl, carbonyl and amine groups (Fig. 4) for the formation of glucuronides in various tissues [78, 79].



Figure 4: Functional groups used for conjugation reactions performed by UDP-glucuronosyltransferases. UGT-mediated covalent addition of UDP-sugar to hydroxyl (OH), carboxyl (COOH), amine (NH₂) or sulfur (SH) groups [79].

UGT expression was detected in liver, stomach, esophagus, bile ducts, small and large intestines, colon, lungs, kidney, brain, breast and other tissues with tissue-specific expression profiles. Since the highest UGT mRNA levels have been detected in hepatic specimens, the liver is considered as major glucuronidation site for systematic excretion of toxic lipophilic compounds [80].

1.2.1 Genetic organization, substrate specificity and expression of *UGT1A* genes

The human UGT superfamily comprises four families divided into UGT1, UGT2, UGT3 and UGT8 with a total of 22 identified members [81]. While the UGT1 and UGT2 subfamilies preferentially use UDP-glucuronic acid as glycosyl donor for substrate glucuronidation, UGT3 and UGT8 show other UDP-sugar preferences (e.g. UDP-glucose or UDP-xylose) and to date, are supposed to play a minor part in drug metabolism and biotransformation of environmental xenobiotics [82, 83]. UGT1A enzymes are primarily involved in the detoxification of pharmacological and xenobiotic compounds but also show important exceptions in endobiotic substrate choice [84]. The *UGT1A* gene locus is localized on chromosome 2q37, spans nearly 220 kbp and encompasses 13 genes encoding for nine functional UGT1A proteins (UGT1A1, UGT1A3, UGT1A4, UGT1A5, UGT1A6, UGT1A7, UGT1A8, UGT1A9 and UGT1A10) and four pseudogenes (*UGT1A2P*, *UGT1A11P*, *UGT1A12P* and *UGT1A13P*) [85]. The pseudogenes exhibit one to several mutations in their

respective first exon resulting in an improper transcription or translation and consequently fail to generate functional UGT1A proteins [86]. All individual *UGT1A* gene products are generated through the transcription process of exon sharing (Fig. 5). This strategy enables the transcription of all functional *UGT1A* genes by combining the isoform-specific first exon with a downstream set of the four common exons 2-5, resulting in 13 individual *UGT1A* transcripts with unique 5' ends and identical 3' ends. The divergent amino terminal region encoded by exon 1 spans 287 ± 2 amino acids (AA) and contains the substrate binding domain. The identical, highly conserved 245 AA comprising carboxyl terminal portion encoded by the shared set of exons, is composed of a ER residing UDP-glucuronic acid binding domain, a hydrophobic transmembrane domain (17 AA) and a small cytoplasmic domain (20 AA). The N-terminal signal peptide is cleaved after integration of the proteins into the endoplasmatic reticulum [87-89].

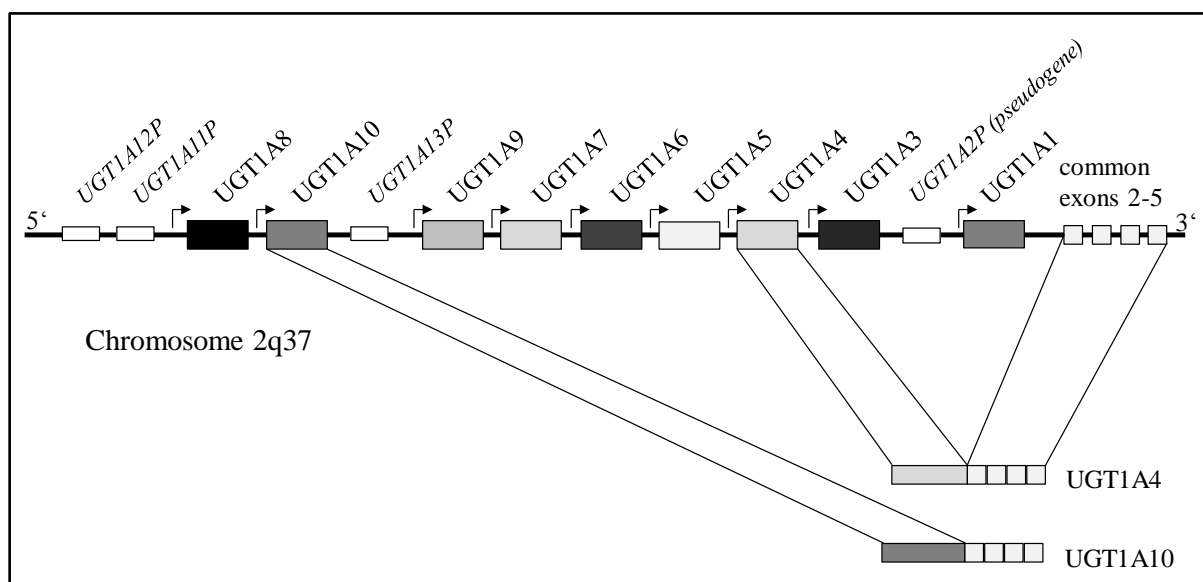


Figure 5: Graphic representation of the human *UGT1A* gene locus. 13 individual first exons each containing a unique 5'- promoter region are spliced to the shared exons 2-5 to generate nine functional *UGT1A* genes and four pseudogenes with identical 3' ends. (P) pseudogene [68, modified].

The use of many different first exons, which all contain individual promoters, presumably contributes to the wide substrate range of structurally dissimilar lipophilic molecules and also defines substrate specificity of each individual UGT1A protein as well as isoform-specific gene regulation. Nevertheless, a broad overlap of substrate specificities is observed within the UGT1A enzyme family reflecting the high sequence similarity of up to 95% between the individual isoforms [90]. As a consequence, there are compounds which become glucuronidated from a number of distinct UGT1As (e.g. methylumbelliferone) and others, such as the heme catalytic byproduct bilirubin, that are exclusively detoxified by the specific

UGT1A1 isoform [91, 92]. Furthermore, UGT1As show a tissue-specific expression profile resulting in a unique combination of UGT1A enzymes in each tissue. The liver, for instance, was shown to express UGT1A1, UGT1A3, UGT1A4, UGT1A6 and UGT1A9, whereas UGT1A7, UGT1A8 and UGT1A10 are exclusively expressed in extrahepatic tissues [93, 94]. This is likely the result of specific glucuronidation requirements in the respective tissue [95]. Accordingly, as a first contact point for many xenobiotics, the metabolically highly active gastrointestinal mucosa is faced with different challenges for glucuronidation and consequently has a different requirement for detoxification leading to the tissue-specific UGT1A enzyme composition [72]. The complex organization of the human glucuronidation system is further underlined by varying UGT1A expression and protein levels in different tissues resulting in a unique complement of UGT1A mRNA levels in almost every organ [96]. The identification of additional factors (such as genetic variations) capable to affect *UGT1A* gene expression and function is therefore of significant interest for a better understanding of individual's capacity to eliminate lipophilic compounds and potential therapeutic interventions involving UGT1As.

1.2.2 Sequence variability of the human *UGT1A* gene locus and associated diseases

With over 100 identified single nucleotide polymorphisms (SNPs) within the promoters and coding regions a huge variety of genetic variants affecting UGT1A function and/or transcription has been described so far. Since many of these SNPs were found to exist in linkage-disequilibrium with each other, inter-individual *UGT1A* sequence variation is further increased [97]. Individual variability within in the *UGT1A* gene locus is widely spread and exhibits allelic frequencies of up to 40-50% among the white population. In most carriers of these variants, clinical studies linked *UGT1A* polymorphisms to changes in clearance or detoxification of endo- and xenobiotics. In addition, genetic *UGT1A* variants were associated with altered drug metabolism and increased susceptibility towards unwanted drug side effects or drug-mediated toxicity [98, 99].

Bilirubin is a hydrophobic degradation product of heme catabolism and cannot be excreted from the body without being converted into water-soluble metabolites. While being a powerful antioxidant at low blood concentrations, bilirubin is a potent toxicant at high concentrations, which is why bilirubin levels need to be precisely controlled [100]. In the liver, bilirubin is mainly inactivated through glucuronidation by UGT1A1, the sole biologically relevant enzyme for effective bilirubin elimination in humans [101]. As most *UGT* genes, *UGT1A1* is highly polymorphic and until today a total of 113 different *UGT1A1*

variants (*UGT1A1*1* to *UGT1A1*113*) have been reported throughout the gene [102]. Having regard to the special importance of this isoform, genetic *UGT1A1* variations leading to inactive or variable degrees of transcriptional regulation and/or protein activity are among the best studied polymorphisms of the entire UGT superfamily. One example is the Gilbert syndrome-associated *UGT1A1*28* variant that occurs in individuals with an additional thymine-adenine (TA) insertion in the TATA box element within the promoter of the *UGT1A1* gene. The resulting A(TA)₇TAA promoter sequence is accompanied by a 70% lower transcriptional activity compared to the more common A(TA)₆TAA wild type variant and is found in approximately 11-16% of the European population [103]. As a result of reduced promoter activity, homozygous *UGT1A1*28* (+/+) carriers can develop a mild unconjugated hyperbilirubinemia (plasma levels between 2.1 and 7.1 mg/dl) provoking a yellowish discoloration of skin and eyes under particular conditions (e.g. when fasting). The genetic *UGT1A1*37* variant, which has been associated with Crigler-Najjar syndrome type II, is defined by the presence of eight consecutive TA repeats in the promoter sequence. This genotype leads to an even lower transcriptional activity of roughly 10% of the normal level, whereas individuals homozygous for the *UGT1A1*36* (TA₅) allele exhibit higher activity than carriers of the wild type genotype [104, 105]. Accordingly, the transcriptional activity inversely correlates with the number of TA repeats of the *UGT1A1* promoter. The inheritable Crigler-Najjar syndrome type I represents another, more serious genetic *UGT1A* variant. Several inactivating mutations lead to the complete loss of *UGT1A1* function and consequently to severe unconjugated hyperbilirubinemia [106]. This condition may cause the accumulation of bilirubin in the central nervous system (kernicterus) leading to irreversible brain damage or infantile death shortly after birth [78, 107].

The low-activity *UGT1A7*3* allele is characterized by the combination of a promoter polymorphism (-57T>G) and three amino acid substitutions (Asn129Lys, Arg131Lys and Trp208Arg) in the first exon of the *UGT1A7* gene [68]. This genetic variation has also been found to exist simultaneously in 97% of homozygous *UGT1A1*28* carriers [108]. For HCC, a significant correlation between the low-activity *UGT1A7*3* variant and the incidence of liver cancer has been reported in several case-control studies among patients with hepatitis B or C [109-112]. In this context, it has been supposed that the overall increased risk of HCC development is likely the result of the lower glucuronidation activity of these variant *UGT1A7*3* alleles towards particular dietary carcinogens. Especially 2-amino-1-methyl-6-phenylimidazo(4,5-b)pyridine (PhIP), its major metabolite *N*-hydroxy-PhIP as well as hydroxylated benzo[a]pyrene are among the best known examples for food-borne carcinogens

detoxified by UGT1A7 [113-116]. Moreover, genetic modifications of the human *UGT1A7* gene, including *UGT1A7*3*, have been associated with a more severe fibrosis and cirrhosis progression in patients with hepatitis B and C [117]. Although the *UGT1A7* gene is not expressed in the liver, these studies emphasize the central meaning of this isoform in the intestinal first-pass metabolism of dietary and environmental carcinogens and hence for the risk of HCC initiation. Similar to HCC, *UGT1A7* polymorphisms are also a well-recognized risk factor contributing to the increased susceptibility of colorectal cancer (CRC). The lower carcinogen-metabolizing activity and the associated increased exposure to harmful dietary components is an identified risk factor for an elevated CRC outcome. In 2002, *Strassburg et al.* were the first who could substantiate an association between *UGT1A7*3* alleles and the incidence of CRC in a case-control study with CRC patients and healthy Caucasians [114]. This correlation was confirmed and expanded by *Tang* and colleagues who reported an increased CRC outcome in carriers of the *UGT1A1*6* and *UGT1A7*3* variants [118]. Breast, ovarian, head and neck cancer are further cancer types which have been associated with polymorphisms of *UGT1A* genes [119-122]. However, it is important to keep in mind that additional factors such as age, environment or eating habits (e.g. coffee intake, see chapter 1.3) further influence the risk of developing a certain type of cancer.

1.2.3 Transcriptional regulation of the *UGT1A* gene locus

The transcriptional regulation of *UGT1A* genes is a crucial determinant for the distribution and glucuronidation capacity of UGTs in various organs of the human body. Furthermore, it is a decisive factor for the variable rates of glucuronidation between the same organs in different individuals [99]. The underlying molecular mechanisms responsible for *UGT1A* expression and activity have been the subject of countless studies over the past decades. To date, major advances in deciphering the complex regulation of *UGT1A* genes were made. Collectively, these studies have shown that the constitutive and inducible regulation of UGT1As are modulated at multiple levels [122]. These include pre-transcriptional (e.g. *via* DNA methylation and histone modification), transcriptional (e.g. *via* transcription factors), post-transcriptional (e.g. by alternative splicing and microRNAs) and post-translational regulation (e.g. modification of UGTs by phosphorylation) [123-126]. In addition, the constitutive as well as the inducible *UGT1A* expression are further regulated in dependence of tissue-specific and ligand-activated transcription factors through interaction with *cis*-regulatory elements (CREs) in the promoters and enhancers of the different *UGT1A* isoforms. The liver-enriched transcription factors hepatocyte nuclear factor (HNF) 1 α / β and HNF4 α were identified to

work in concert with the ubiquitously expressed transcription factors to regulate constitutive *UGT1A* transcription [127-130]. As mentioned above, inducible *UGT1A* expression is regulated by ligand-activated transcription factors (often nuclear receptors), sensing the contemporary need for substrate glucuronidation of endo- or exogenous molecules in the respective tissue. The farnesoid X receptor (FXR), constitutive androstane receptor (CAR), pregnane X receptor (PXR), vitamin D receptor (VDR), liver X receptor (LXR), androgen receptor (AR), estrogen receptor alpha (ER α), glucocorticoid receptor (GR) and the peroxisome proliferator-activated receptors (PPARs) are nuclear receptors involved in the inducible *UGT* gene regulation [131-135]. The aryl hydrocarbon receptor (AhR) and nuclear factor erythroid 2-related factor 2 (Nrf2) are additional ligand-inducible transcription factors involved in *UGT1A*-mediated responses to stress but do not belong to the nuclear receptor superfamily [136, 137]. Those transcription factors, which are of central importance within the scope of this work, are described in more detail below.

Farnesoid X receptor

The FXR, also referred to as bile acid receptor or NR1H4 (nuclear receptor subfamily 1, group H, member 4), belongs to the nuclear hormone receptor superfamily and is highly expressed in enterohepatic tissues [138, 139]. The receptor plays a pivotal role in synthesis, secretion and transport of BAs, which were identified as natural endogenous FXR ligands more than 20 years ago [140, 141]. Similar to other nuclear receptors, FXR translocates into the nucleus after ligand activation, dimerizes with RXR and binds as a heterodimer to specific FXR response elements (FXREs) in target gene promoters to regulate transcriptional activity of various physiological pathways and metabolic processes [142, 143]. An essential function of FXR is the hepatic suppression of BA synthesis from cholesterol. A tightly controlled network of negative feedback and positive feed-forward mechanisms regulates the activity of BA transporters and the expression of cholesterol 7 α -hydroxylase (CYP7A1), the rate-limiting enzyme for BA synthesis, thereby preventing excessive hepatic accumulation of the amphipathic molecules [144-146]. In doing so, BA-activated FXR does not directly inhibit the transcriptional regulation of CYP7A1, but induces the expression of small heterodimer partner (SHP), which in turn interacts with the liver receptor homolog-1 (LRH-1) and subsequently functions as inhibitor of CYP7A1 transcription (Fig. 6) [147]. In contrast, FXR activation in the intestine leads to the expression and release of fibroblast growth factor 19 (FGF19, FGF15 in mice) into the portal vein and reaches the liver through enterohepatic circulation. Once there, FGF19 binds to the fibroblast growth factor receptor 4 (FGFR4)

whose subsequent activation represses CYP7A1 transcription through involvement of the Jun N-terminal kinase pathway [148-150]. The enterohepatic circulation, also known as gut-liver axis, is essential for the regulation of BA metabolism in which FXR constitutes a key player for BA-modulated signaling pathways. The receptor supports the effective ileal absorption, hepatic re-uptake and re-secretion of BAs into the biliary system so that only 5% of entire bile salt pool need to be replaced by hepatic *de novo* synthesis due to fecal excretion [151, 152].

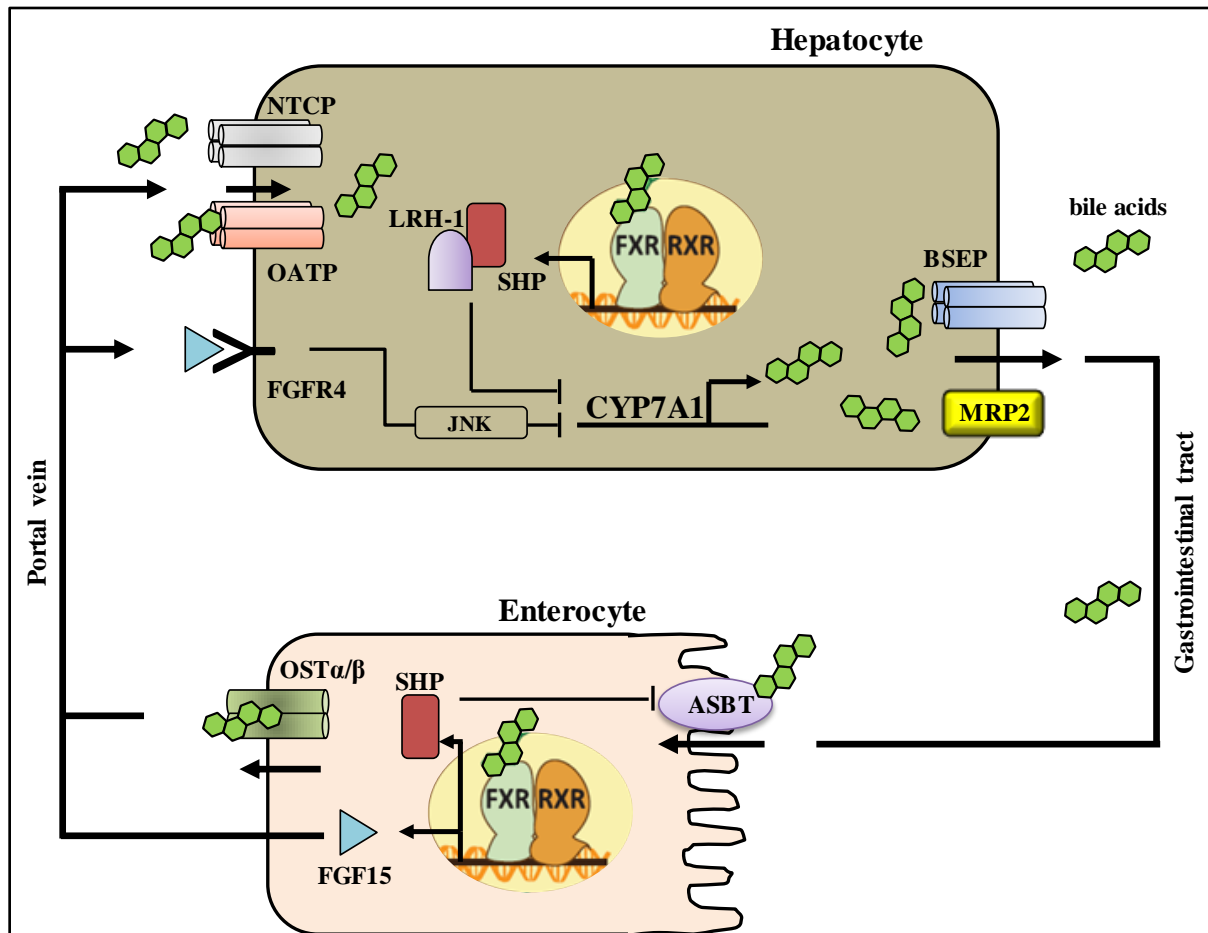


Figure 6: Schematic diagram of the negative feedback and feed-forward regulation of bile acid synthesis. In hepatocytes, BA-activated FXR stimulates the activation of SHP which reduces transcriptional activity of CYP7A1 causing the inhibition of BA synthesis. In enterocytes, FXR-mediated SHP activation stops the ileal BA uptake through inhibition of ASBT. FXR activation also leads to the release of FGF15 (FGF19 in humans), which in turn is transported to the liver and initiates the inhibition of CYP7A1. (ASBT) apical sodium-dependent bile acid transporter, (BSEP) bile salt export pump, (FGFR4) fibroblast growth factor receptor 4, (FXR) farnesoid X receptor, (JNK) Jun N-terminal kinase, (LRH-1) liver receptor homolog-1, (MRP2) multidrug resistance protein 2, (NTCP) Na⁺ dependent taurocholate cotransport peptide, (OATP) organic anion transporting polypeptides, (OST α/β) organic solute transporter α/β , (RXR) retinoid X receptor [153, modified].

The role of FXR in homeostasis and signaling of BAs has been extensively investigated in numerous studies. Defects in FXR-mediated processes can cause serious hepatobiliary diseases leading to the hepatic retention of cytotoxic BAs and subsequent hepatocellular damage [154-156]. During cholestasis, FXR activation increases the expression of BA export

pumps and mediates the stimulation of enzymes involved in BA detoxification and excretion [141]. These include CYP3A4, sulfotransferases and UGTs [157, 158]. Serum concentrations of BA glucuronides have shown to be significantly increased in patients with cholestatic liver injury [159, 160]. Together with UGT2B4 and UGT2B7, UGT1A3 is one of the major isoforms involved in the hepatic conversion of BAs into more hydrophilic and therefore less toxic BA glucuronides [161, 162]. *In vitro* studies identified a FXR binding motif in the *UGT1A3* promoter (Fig. 7), whose functionality is highly affected by the presence of common promoter polymorphisms (-66A→T and A→G at the -204 position) [163]. This indicates a potential impact of genetic *UGT1A* variations on BA detoxification especially under cholestatic conditions.

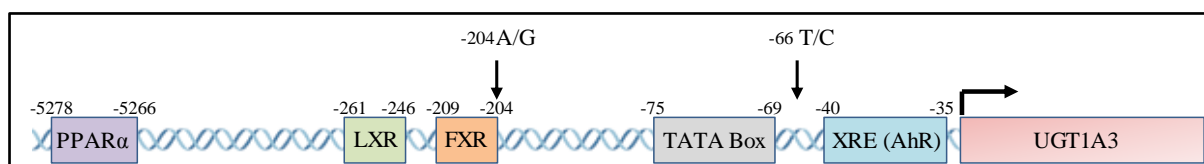


Figure 7: Schematic representation of the human *UGT1A3* gene. Overview of the regulatory promoter elements involved in inducible *UGT1A3* transcription. Two common occurring SNPs and the respective mutations are indicated by black arrows. (AhR) aryl hydrocarbon receptor, (FXR) farnesoid X receptor, (LXR) liver X receptor, (PPAR α) peroxisome proliferator-activated receptor alpha, (XRE) xenobiotic response element [67, modified].

UGT1A3 catalyzes the C24-glucuronidation of the primary BA chenodeoxycholic acid (CDCA) as well as the by intestinal bacteria produced secondary BAs lithocholic acid (LCA) and hyodeoxycholic acid (HDCA) through formation of acyl glucuronides [157]. Since acyl-glucuronidation of BAs is considered to have minor importance under normal physiological conditions, it has been suggested to become more relevant during cholestasis. The detoxification of retained BAs together with the modulation of interactions between BAs and their transporters represent important functions of BA glucuronidation [164] and thus provides a biochemical link between UGTs, BA metabolism and cholestasis progression. Moreover, BA glucuronides have been suggested to influence the regulation of BA-modulated gene expression mediated through FXR activation [165]. Accordingly, the modulation of BA-dependent signaling is likely to be another function of BA glucuronidation, indicating deep-reaching effects of BA glucuronides, and consequently UGTs, on FXR-dependent biological effects [83, 166].

Besides the well-defined functions of BAs as biological detergents required for dietary lipid absorption and regulators of their own homeostasis, they are also capable to act as endogenous signaling molecules which exert, *via* FXR activation, hormonal-like effects on signaling pathways involved in lipid and glucose metabolism [167]. In line with this, animal

studies have shown that hepatic triglyceride and cholesterol levels were increased in FXR knock-out mice [168, 169]. Thus, the dysregulation or impairment of BA-mediated receptor signaling has been proposed to not only affect development of cholestatic liver diseases, but maybe also the pathogenesis of NAFLD [170]. In addition, the presence of a xenobiotic response element (XRE) identified in the promoter of the *UGT1A3* gene (Fig. 7), further creates a natural connection between endogenous BA-dependent regulatory processes and xenobiotic metabolism [171]. Accordingly, AhR-mediated activation of UGT1A3 enzymes, triggered by environmental xenobiotics, could therefore influence BA glucuronidation and consequently BA-mediated biological effects in certain diseases.

Oxidative stress sensor nuclear factor erythroid 2-related factor 2 and xenobiotic-activated aryl hydrocarbon receptor

Oxidative stress results from an imbalance between oxidant and antioxidant agents and represents a crucial factor for the initiation of liver fibrosis [172]. The Nrf2 transcription factor has key functions in the (up)-regulation of genes involved in intracellular responses against ROS-induced oxidative stress caused by injury and/or inflammation [173]. Furthermore, it is a central regulator of antioxidative activity and maintenance of the metabolic oxidative balance that recognizes antioxidant response elements (AREs) in the promoter sequences of its target genes. These include NAD(P)H quinone oxidoreductase 1, glutamate-cysteine ligase, glutathione-S-transferases and cytoprotective UGT1As [174]. Involvement of Nrf2 in hepatic fibrogenesis has been provided by animal experiments using Nrf2-null mice. In a chronic model of toxin-induced (carbon tetrachloride; CCL₄) liver injury, Nrf2 knockout mice exhibited more severe fibrosis and increased expression of inflammatory cytokines compared to their WT counterparts with normal Nrf2 activity [175]. Similarly, a higher degree of hepatocyte damage has been reported in Nrf2 (-/-) mice treated with a high-fat diet. Although these harmful effects were primary attributed to the decreased antioxidative defense in Nrf2-null mice, it has also been suggested that Nrf2 is responsible for the suppression of genes involved in lipogenic signaling pathways [176]. As a consequence, the capacity of Nrf2 to induce antioxidative *UGT1A* genes is supposed to contribute to the Nrf2-mediated beneficial effects on hepatic fibrosis.

Interestingly, cross-talk between Nrf2 and AhR pathways has been reported for certain *UGT1A* genes (Fig. 8) [177, 178]. The central meaning of AhR to act as sensor for xenobiotic chemicals and key regulator of enzymes involved in the metabolic conversion of these substances has been elucidated in countless studies. Activated AhR binds as a heterodimer

with aryl hydrogen receptor nuclear translocator (ARNT) to specific XRE DNA-binding motifs and subsequently initiates target gene transcription. XREs were identified in the promoters of many drug-metabolizing enzymes including members of the CYP450 family and UGT1A isoforms [179-181]. Xenobiotic inducibility not only highlights the significance of *UGT1A* gene products in the protection against environmental toxins or mutagens, but also points to the ability of naturally occurring compounds (for instance particular coffee constituents) or pharmaceuticals to transcriptionally activate *UGT1A* genes.

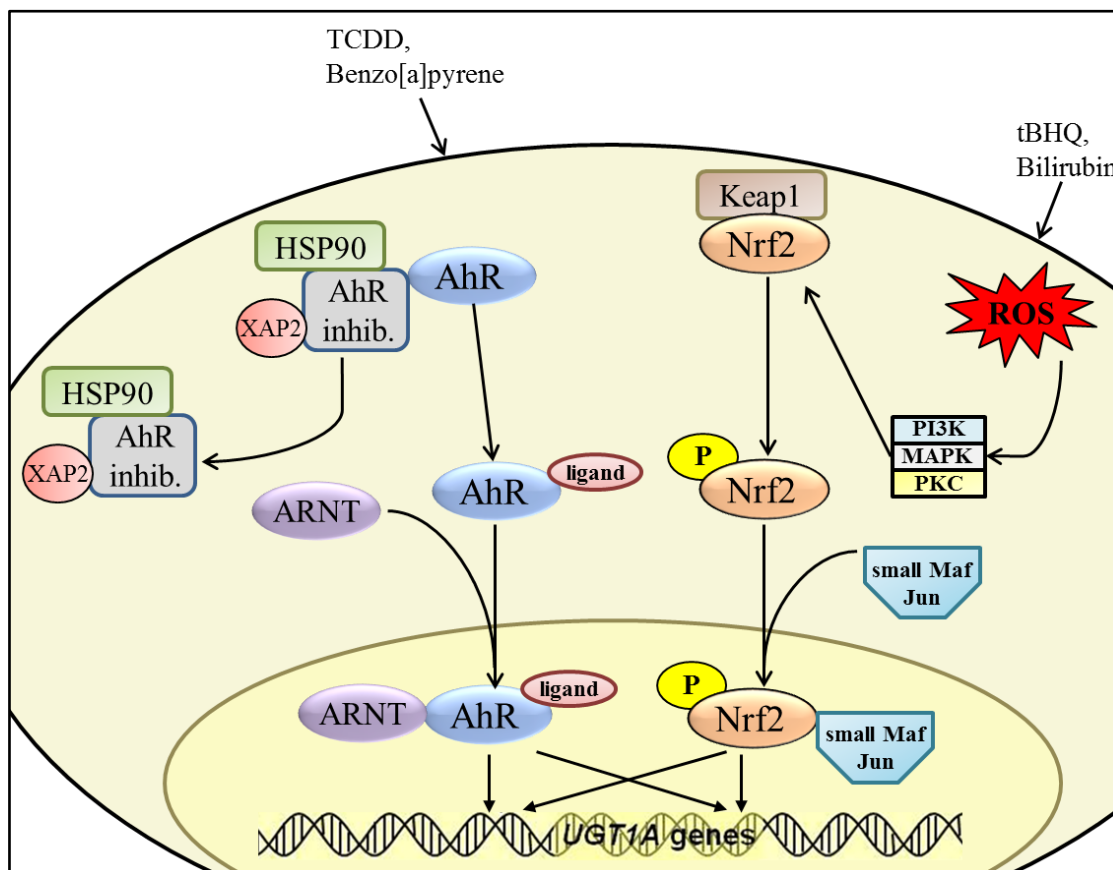


Figure 8: AhR- and Nrf2-mediated transcriptional *UGT1A* regulation. Cross-talk between AhR and Nrf2 signaling pathways has been reported for certain *UGT1A* genes. (AhR) aryl hydrocarbon receptor, (ARNT) AhR nuclear translocator, (HSP90) heat shock protein 90, (MAPK) mitogen-activated protein kinase, (Nrf2) nuclear factor erythroid 2-related factor 2, (PI3K) phosphoinositid-3-kinase, (PKC) protein kinase C, (ROS) reactive oxygen species, (tBHQ) *tert*-butylhydroquinone, (TCDD) 2,3,7,8-tetrachlorodibenzo-*p*-dioxin, (XAP2) X-associated protein 2 [182, modified].

1.3 Hepatoprotective effects of coffee

Believed to have been first discovered in a region of southwest Ethiopia called Kaffa, coffee has seen an unprecedented rise to become one of the most widely consumed beverages worldwide [183, 184]. Besides its sought-after taste and stimulating effect, coffee has been associated with a variety of hepatoprotective properties. A growing number of

epidemiological studies reported an inverse association of coffee consumption with hepatic fibrosis progression, liver cirrhosis and HCC [185, 186]. In a population-based study, *Ruhl* and colleagues assessed the effects of coffee intake in individuals with a high risk for liver injury (alcoholics, overweight people or patients with viral hepatitis infection). The research group reported an association between coffee consumption and reduced hepatic inflammation indicated by lower ALT levels [187]. These findings were expanded in a prospective cohort study involving patients with hepatitis C-related liver damage. The presented analysis revealed an inverse correlation in coffee-consuming patients with the progression of liver fibrosis and cirrhosis [188]. Moreover, a large meta-analysis of epidemiological and case-control studies discovered a 40% lower risk for HCC development for coffee-drinkers versus non-coffee-drinkers [189].

The molecular mechanisms underlying the protective effects of coffee are not fully understood. To this point, a body of literature has been published regarding the specific ingredients of coffee potentially accountable for the observed beneficial effects. Currently, polyphenols (such as chlorogenic acid), diterpenes (cafestol, kahweol) and caffeine are among the best-studied coffee constituents in association with chronic liver diseases [190]. Thus, for instance, the coffee-related hepatoprotective effects were *inter alia* attributed to the ability of caffeine and other methylxanthines to decrease TGF- β -induced CTGF activation by stimulating the proteasomal degradation of the TGF- β signaling mediator SMAD 2 [191, 192]. The hepatic antioxidative properties of coffee were in turn ascribed to other bioactive coffee components such as caffeic acid or chlorogenic acid capable to activate the Nrf2 signaling pathway [193]. Additional studies characterized the hepatoprotective impact of coffee-stimulated antioxidative defense system and measured a lower content of malondialdehydes, reduced ROS formation and increased hepatic glutathione levels [194, 195]. A preventive anti-tumorigenic mechanism has been proposed for cafestol and kahweol. Both biomolecules are potentially associated with the reduced incidence of HCC in coffee-drinkers by either inhibiting phase I enzymes responsible for bioactivation of carcinogens or by induction of phase II detoxifying enzymes [196]. Interestingly, *in vitro* and *in vivo* studies performed by *Kalthoff* et al. demonstrated the coffee-induced expression and activity of human UGT1A enzymes independent of caffeine, methylxanthines or diterpenes [181]. In this study, the induction of *UGT1A* genes by coffee was shown to be coordinately mediated by the Nrf2/ARE and AhR/XRE signaling pathways (Fig. 8). Although the responsible compounds have not yet been identified, the study suggests that glucuronidation may represent a coffee-dependent protective mechanism which is in part based on the cytoprotective, genoprotective

and indirect antioxidative activities of UGT1A enzymes. Accordingly, the AhR- and Nrf2-mediated activation of downstream phase II antioxidative enzymes might be crucial for the prevention of oxidative liver injury and consequently for restriction of fibrosis progression. However, more experiments are needed to elucidate the molecular determinants and mechanisms of coffee to achieve the ultimate goal of developing coffee-based pharmaceuticals applicable for therapeutic treatment against initiation or progression of chronic liver diseases.

1.4 Objectives of the dissertation

UGT1A enzymes are part of phase II metabolism capable of detoxifying a broad range of endo- and xenobiotic substances. By catalyzing the conjugation of glucuronic acid to small lipophilic molecules they facilitate their renal and biliary excretion. Moreover, UGT1As act as indirect antioxidants for their ability to eliminate reactive molecules such as quinines, aldehydes, epoxides or peroxides and consequently contribute to cytoprotection by improving the hepatic antioxidative capacity. The impact of altered *UGT1A* expression on initiation and development of chronic liver injury is not well understood. Common polymorphisms in the promoters and coding regions of individual UGT1A isoforms are associated with various liver diseases including a more severe fibrosis progression and an increased risk for HCC. *UGT1A* transcription is known to be regulated by ligand-activated transcription factors including BA-activated FXR, oxidative stress sensor Nrf2 and xenobiotic inducible AhR. Since liver fibrosis proceeds as a result of elevated oxidative stress levels following to liver injury, the generation of ROS represents a common effector for HSC activation resulting in inflammation, the production of profibrotic cytokines and increased formation of fibrillar collagens. The identification of AREs in specific *UGT1A* genes provides a functional link between Nrf2-mediated antioxidative cytoprotection and the indirect antioxidative capacities of *UGT1A* gene products. The FXR-, AhR-, and Nrf2-dependent regulation of *UGT1A* genes further links glucuronidation to BA detoxification, xenobiotic-induced cellular protection as well as defense against oxidative stress and consequently to a putative protective role during hepatic fibrogenesis. Accordingly, the transcriptional regulation and function of *UGT1A* genes is supposed to be central process for the maintenance of the cellular antioxidative defense in the pathological setting of cholestasis or steatosis-induced liver injury which may be influenced by the presence of particular low-activity *UGT1A* SNPs. The overarching hypothesis of the dissertation is therefore based on the assumption that these SNPs exacerbate hepatic

fibrogenesis due to reduced *UGT1A* gene expression and impaired responsiveness towards typical *UGT1A* inducers (Fig. 9).

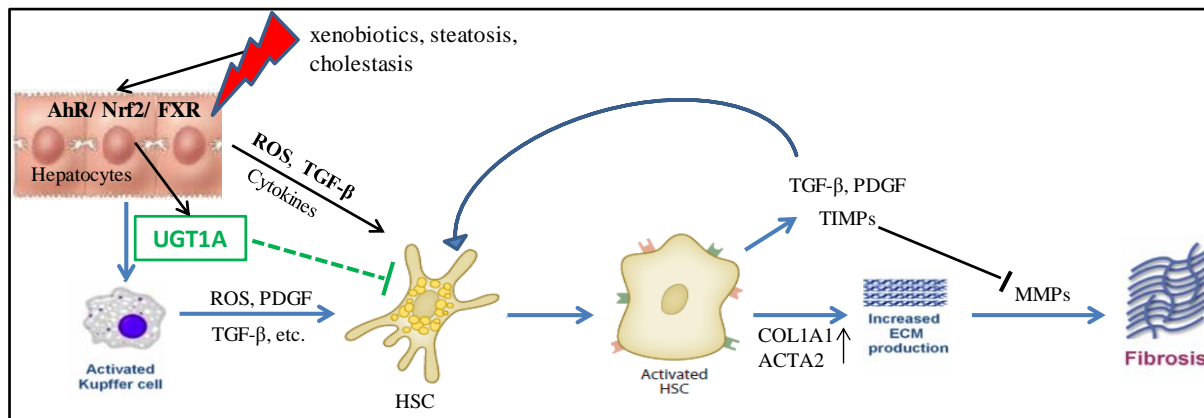


Figure 9: Hypothesis overview of a potential *UGT1A*-mediated protective function in fibrosis initiation and progression. (ACTA2) alpha-actin-2, (AhR) aryl hydrocarbon receptor, (COL1A1) collagen type 1 alpha 1, (FXR) farnesoid X receptor, (ECM) extracellular matrix, (HSC) hepatic stellate cell, (MMP) matrix metalloproteinase, (Nrf2) nuclear factor erythroid 2-related factor 2, (PDGF) platelet-derived growth factor, (ROS) reactive oxygen species, (TGF- β) transforming growth factor beta, (TIMP) tissue inhibitor of metalloproteinase [46, modified].

This resulted in the following aims for this work:

- 1) To date, no systematic data on the hepatic regulation of human *UGT1A* genes after 14 days of cholestatic liver injury (surgically-induced by BDL) has been published. Therefore, the expression of human *UGT1A* genes should be determined in *htgUGT1A*-WT and SNP mice.
- 2) Assessment of the functional contribution of *UGT1A* polymorphisms on fibrosis initiation, progression and severity during obstructive cholestasis, by determining oxidative stress levels and the severity of fibrosis in *htgUGT1A*-WT and SNP mice. The use of *htgUGT1A*-SNP mice aims to clarify the influence of a common Gilbert syndrome-associated SNP haplotype, present in roughly 10% of the white population, on hepatic fibrogenesis and may contribute to a better understanding of fibrosis risk factors and development of potential anti-fibrotic therapies.
- 3) Coffee consumption is epidemiologically associated with a reduced risk of liver fibrosis and has previously been shown to induce antioxidative *UGT1A* genes. For that reason, a further objective was to analyze the role of *UGT1A* genes as effectors of the protective antioxidative effects of coffee in BDL-induced liver fibrosis and to investigate whether the induction of *UGT1A*s ameliorates the effects of chronic cholestatic liver injury. The co-treatment with coffee should further clarify whether the coffee-mediated hepatoprotective effects are based on the ability to induce cytoprotective *UGT1A* genes.

- 4) A metabolic model of liver injury was selected to elucidate the role of *UGT1A* polymorphisms during hepatic steatosis, NASH development and, as a consequence, the progression to liver fibrosis. Similar to the objectives listed in point number two, profibrotic markers indicating the severity of liver fibrosis as well as the histopathological consequences for the liver should be assessed in both mouse lines.

Liver cirrhosis, which often results as a consequence of hepatic fibrosis due to persistent liver injury, is a major risk factor for HCC development in humans. Impaired responsiveness towards carcinogens and the associated reduced clearance of cancer-promoting molecules are the basis for the hypothesis of numerous case-control studies reporting an increased cancer incidence in carriers of low carcinogen-metabolizing *UGT1A* SNP variants (Fig. 10).

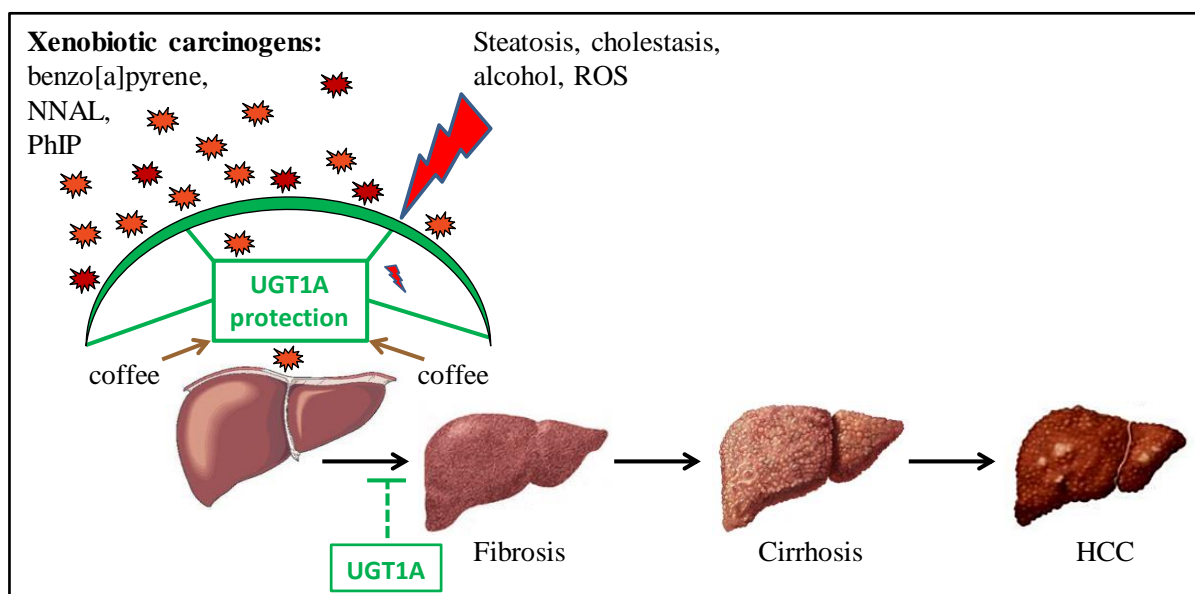


Figure 10: Hypothesis overview of a putative UGT1A-mediated protection against development and progression of liver cancer. (HCC) hepatocellular carcinoma, (NNAL) 4-(methylnitrosamino)-1-(3-pyridyl)-1-butatone, (PhIP) 2-amino-1-methyl-6-phenylimidazo[4,5-b]pyridine, (ROS) reactive oxygen species.

- 5) Experimental evidence for the association between an increased risk of cancer development and a human haplotype of 10 common occurring *UGT1A* SNPs could not yet be provided. Therefore, the aim of this subproject was to examine the effect of multiple *UGT1A* polymorphisms on HCC susceptibility and outcome in *htgUGT1A* mice after chemical induction (diethylnitrosamine, DEN) of hepatocarcinogenesis.

2 Material and Methods

2.1 Material

2.1.1 Humanized transgenic *UGT1A*-WT and *UGT1A*-SNP mouse lines

To investigate the transcriptional regulation of *UGT1A* genes under the condition of hepatic steatohepatitis or obstructive cholestasis leading to hepatic fibrosis, a humanized transgenic (*htg*) *UGT1A*-WT [197] and a *htgUGT1A*-SNP mouse line was used. Apart from *UGT1A8* and *UGT1A10*, both mouse lines contained the entire human *UGT1A* gene locus. The *htgUGT1A*-SNP mouse model was created to simulate a frequent human variant haplotype containing 10 common occurring *UGT1A* SNPs (*UGT1A1**28, *UGT1A3* -66T>C, *UGT1A3* V47A, *UGT1A3* W11R, *UGT1A6**2a (S7A/ T181A/ R184S), *UGT1A7**3 (N129K/ R131K/ W208R/ -57T>G)). This haplotype is present in about 10% of the white population leading to decreased *UGT1A* basal expression and reduced *UGT1A* inducibility (Fig. 11). The genetic variants *UGT1A1**28, *UGT1A3* -66T>C and *UGT1A7* -57T>G are promoter polymorphisms that alter the transcriptional regulation and activation of these genes [198].

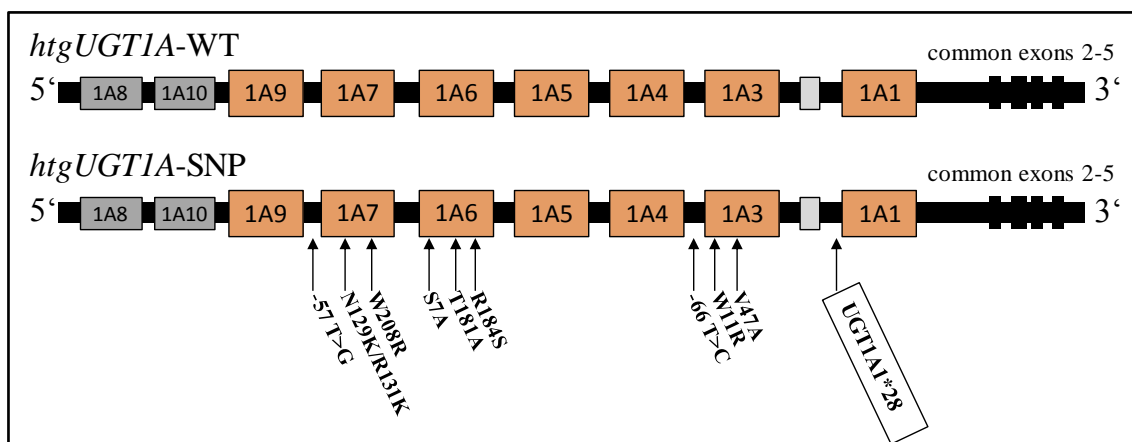


Figure 11: Graphic illustration of the human *UGT1A* gene locus and the corresponding genes in *htgUGT1A*-WT and SNP mice. *TgUGT1A* mice are containing *UGT1A1*, *UGT1A3*, *UGT1A4*, *UGT1A5*, *UGT1A6*, *UGT1A7* and *UGT1A9* genes, which, in case of the SNP haplotype, comprised several polymorphisms present at high frequencies in the Caucasian population [197].

Analysis of gene copy numbers by quantitative real-time PCR (qPCR) revealed six gene copy numbers in *htgUGT1A*-WT mice and five gene copy numbers in the low-function *htgUGT1A*-SNP mouse line. Fluorescence *in situ* hybridization (FISH) demonstrated that all gene copies were localized on the same chromosome. Both *htgUGT1A* mouse lines were bred with non-transgenic C57BL/6J-mice and descendants have been tested for the human *UGT1A3* gene. Positively tested mice were taken for experiments in the age of 8-12 weeks. Transgenic *UGT1A* mice were housed in a temperature controlled environment with a 12 hour light-dark

cycle in the Central Animal Facility of the University Hospital Bonn. All experiments were performed in accordance to the “German Animal-Protection Law” and approved by the relevant North Rhine-Westphalia state-agency for Nature, Environment and Consumer Protection (LANUV, Germany).

2.1.2 Oligonucleotides

Oligonucleotides used for amplification

Table 1 comprises a list of primers used for analysis of ear samples for genotyping of potentially transgenic *UGT1A* mice. A listing of the oligonucleotides applied in TaqMan PCR is shown in table 2 and 3.

Table 1: Listing of primers used for amplification (all primers were purchased form MWG).

Indication	Nucleotide sequence (5' - 3')
Allgen	CCAATGAAGACCATGTTGGGC
GT1A3	TGTTGAACAATATGTCTTTGGTCTA

Oligonucleotides used for gene expression analysis by TaqMan PCR

Table 2: Listing of primers and probes used for gene expression analysis by TaqMan PCR (all primers and TAMRA probes were purchased from MWG, all MGB probes were purchased from Applied Biosystems).

Gene	Primer and probe (5' - 3')
UGT1A1	Forward: GAATCAACTGCCTTCACCAAAT Revers: AGAGAAAACCACAATTCCATGTTCT Probe: FAM – CTATCCCAGGAATTTGAA – MGB
UGT1A3	Forward: CAGAAGTATGGCAATGTTGAACAATA Revers: GCCTCATTATGTAGTAGCTCCACACA Probe: FAM – TCTTTGGTCTATCATAGGTC – MGB
UGT1A4	Forward: TTTTCTGCCCCTTATGCAAGT Revers: ACAGCCACACGGATGCATAG Probe: FAM – TCAGAGAGAGGTGTCAGTGGTGGATCTTGT – TAMRA

UGT1A6	Forward: CTCATTGGAGGTATCAACTGTAAGAA Revers: AAGAGAAAACCACAATTCCATGTTC Probe: FAM – AGGAAAGACTTGTCTCAGGAATTTGAAGCC – TAMRA
UGT1A7	Forward: GAGGATCAGGACCGGGAGTT Revers: GAAAATGCACTTCGCAATGGT Probe: VIC – TGGTTTTTGCCGATGCT – MGB
UGT1A9	Forward: AAACCCGTGATGCCCAAC Revers: GGCTTCAAATTCCATAGGCAAC Probe: FAM – TGATCTTCATTGGTGGTATCAACTGCCATC – TAMRA
Mouse beta-actin	Forward: ACGGCCAGGTCATCACTATTG Revers: CAAGAAGGAAGGCTGGAAAAG Probe: FAM – CAACGAGCGGTTCCGATGCCC – MGB

Table 3: Listing of assays used for gene expression analysis by TaqMan PCR (all assays were purchased from ThermoFischer Scientific).

Gene	Assay ID
Acta2	Mm00725412_s1
FXR (Nr1h4)	Mm01240553_m1
Ccl2	Mm00441442_m1
Colla1	Mm00801666_g1
Pdgfb	Mm00440677_m1
Pdgfrb	Mm00435546_m1
Tgf- β	Mm01178820_m1
Timp1	Mm01341361_m1
Tnf- α	Mm00443260_g1

2.1.3 Enzymes and dNTPs

Table 4 summarizes the enzymes, dNTPs and the respective manufacturer used in this thesis.

Table 4: Listing of enzymes and dNTPs.

Enzyme	Units (U)/ μ L	Manufacturer
DNase I	100	Invitrogen
Proteinase K	20	VWR
DNA-Polymerases		
BioTherm™ Taq DNA Polymerase	5	Genecraft
SuperScript™ III RT	200	Invitrogen
dNTPs (dATP, dCTP, dTTP, dGTP)		Genecraft

2.1.4 DNA and protein makers

100 bp DNA Ladder (Genecraft)

1 kb DNA Ladder (Genecraft)

SDS-PAGE Standards, Low Range (Bio-Rad)

Precision Plus Protein™ Dual Color Standards (Bio-Rad)

Page Ruler Prestained Standard (Thermo-Fischer)

2.1.5 Antibodies

The following table 5 provides a list of the antibodies used in this thesis.

Table 5: Listing of primary antibodies used for western blot analysis.

Antibody	Exact designation	Species	Manufacturer
4 Hydroxynonenal	ab46545	rabbit	Abcam
GAPDH	SC-32233	mouse	Santa Cruz
Histone H3	ab12079	goat	Abcam
PPAR α	SC-398394	mouse	Santa Cruz
UGT1A3	H-00054659-M02	mouse	Abnova

2.1.6 Secondary antibodies

Mouse IgG _K , BP-HRP conjugated	(Santa Cruz)
Goat anti rabbit IgG, HRP conjugated	(Santa Cruz)
Goat anti rabbit, Alexa Fluor® 488	(Abcam)
Rabbit anti goat IgG, HRP conjugated	(Santa Cruz)

2.1.7 Consumables

Consumables and corresponding manufacturers are listed in table 6.

Table 6: Listing of consumables and their suppliers.

Consumable	Manufacturer
0.2 mL 8-Strip PCR Tubes	Starlab GmbH
8-Strip PCR Caps, domed	Starlab
96-Well Hard-Shell® PCR plates	Bio-Rad
Bepanthen® Eye and Nose cream	Bayer Vital GmbH
Coffee filter classic	Melitta
Cover glasses	VWR
CryoPure tube 1.8 mL	Sarstedt
Disposable needle, Sterican, 19 G x 1 ¼” and 23 G	BBraun
Falcon tubes 15 mL, 50 mL	Sarstedt
Filter tips 10 µL	Starlab GmbH
Filter tips 200 µL and 1000 µL	Sarstedt
Frosted microscope slides	Thermo Scientific
Gelloader pipette tips 200 µL	Sarstedt
Microplates, 96-Well, F-bottom	Greiner bio-one
Micro tubes 0.5 mL and 1.5 mL	Sarstedt
Midi-size nitrocellulose membrane	Bio-Rad
Midi-size transfer stacks	Bio-Rad
MX35 PREMIER+ microtome blades	Thermo Scientific
Pipette tips 10 µL, 200 µL and 1000 µL	Sarstedt
Polystyrene cuvettes	Sarstedt
Rotilabo® embedding cassettes	Roth
Safe-lock tubes 2.0 mL	Eppendorf
Serological pipettes 5 mL, 10 mL and 25 mL	Corning B.V. Life Science

Single-use syringes, 3 piece, 1 mL	BBraun
Staining jars	Marienfeld
Stainless steel beads, 5 mm	Qiagen
Surgical sutures (polyester, 5-0) non absorbable (Ethicon Mersilene)	Johnson&Johnson
Surgical sutures (Silk, 6-0, C1 needle) non absorbable (Ethicon)	Johnson&Johnson
Underpads MoliNea® Plus L	IVF Hartmann AG

2.1.8 Technical devices

Table 7 contains a list of all used devices and its corresponding manufacturers.

Table 7: List containing all used technical devices and corresponding manufacturers.

Device	Manufacturer
Anesthesia Induction Chamber	Xenogen Corporation
Blotting chamber system	Bio-Rad
C1000 Touch™ Thermal Cycler	Bio-Rad
Camera for fluorescence microscope, Nikon-Digital Sight DS-Vi1	Nikon
Centrifuge 5424 R	Eppendorf
CFX96™ Real-Time system	Bio-Rad
Chemoluminescence detection, ChemiDoc™ MP Imaging System	Bio-Rad
Colibri retractor	Fine Science Tools
Cooling plate, Microm EC 350-2	Thermo Scientific
Fluorescence microscope, Eclipse 50i	Nikon
Gel electrophoresis chamber	Bio-Rad, SCIE-PLAS
Heating block, ThermoMixer C 1.5 mL	Eppendorf
Incubator shaker, Stuart®	Bibby Scientific
Inverted light microscope	Leica
Isoflurane Vaporizer, Funnel - Fill	VetEquip
Magnetic stirrer and hotplate	Heidolph
Micro scales	Sartorius
Micro-serrations forceps, Moria	Fine Science Tools
Microplate reader, MultiSkan GO	Thermo Scientific
Microscope, Axio Scope.A1	Zeiss

Microtome, Microm HM 355 S	Thermo Scientific
Mini G centrifuge	IKA®
Multichannel pipette 300 µL	VWR
PCR machine, peqSTAR thermocycler	VWR
Photometer, BioPhotometer PLUS	Eppendorf
Pipette 0.1-2.5 µL	Eppendorf
Pipette 100-1000 µL	Eppendorf
Pipette 1-10 µL	Eppendorf
Pipette 20-200 µL	Eppendorf
Pipetting aid, Pipetus®	Hirschmann®
Serum analyzer, DRI-CHEM NX500i	Fujifilm
Sonicator, Sonopuls HD 2200	Bandelin
Spin tissue processor, Microm STP 120	Thermo Scientific
Sterile bench, SCANLAF	Thermo Fischer Scientific
Tissue embedding center, Microm EC 350-1	Thermo Scientific
TissueLyser LT	Qiagen
Trans-Blot® Turbo™ Blotting System	Bio-Rad
Vortex system, RS-VA10	PHOENIX Instruments
Shaking Water Bath, Thermolab®, 1083	GFL®

2.1.9 Software

Table 8 contains a list of the used software and its manufacturers.

Table 8: Listing of software and corresponding manufacturers.

Software	Manufacturer
CFX Manager, version 3.1	Bio-Rad
ImageJ	U. S. National Institute of Health
Image Lab™, version 5.2	Bio-Rad
NIS Elements, version 3.22.01	Nikon
Office 2010	Microsoft
SkaniT, version 3.2, research edition for MultiSkani GO	Thermo Scientific
ZEN 2.6 blue edition	Zeiss

2.1.10 Chemicals and reagents

All used chemicals and reagents as well as their manufacturers are listed in table 9.

Table 9: Listing of chemicals, reagents and their suppliers.

Chemical / Reagent	Manufacturer
Agarose NEEO, ROTIGAROSE®	Carl Roth
Ampuwa, sterile water for irrigation	Fresenius Kabi AG
Betaisadona® solution	Mundipharma GmbH
Bio-Rad Protein Assay	Bio-Rad
Carbon tetrachloride	Sigma-Aldrich
Chloroform	J.T. Baker
DEPC-treated water	Ambion
Diethylnitrosamine (DEN)	Sigma Aldrich
Dimethyl sulfoxide (DMSO)	Sigma Aldrich
Direct PCR Tail	Viagen
Direct Red 80	Sigma-Aldrich GmbH
Eosin G, C.I.	Merck KGaA
Ethanol absolute, 99.9%	AppliChem GmbH
Ethanol denatured, 99.9%	AppliChem GmbH
Ethylenediaminetetraacetic acid (EDTA)	Sigma-Aldrich
EZ-Vision® in Gel Solution	Amresco®
Fluoroshield Mounting Medium with DAPI	Abcam
Goat Serum	Sigma-Aldrich
High-fat Paigen diet (HFPD)	Altromin
Hydrochloric acid, 37%	Sigma-Aldrich
Hydrogen peroxide, 30%	Merck
Isoflurane	Piramal Healthcare
Isopropyl alcohol	J.T. Baker
Jacobs Krönung ground coffee	Kraft
Mayers hemalum	Merck KGaA
Paraformaldehyde (PFA)	Sigma-Aldrich
Picric acid moistened with water, $\geq 98\%$	Sigma-Aldrich
Picric acid solution 1.3%	Sigma-Aldrich
Powdered milk	Carl Roth

Protease inhibitor cocktail P8465	Merck
Proteinase K	Qiagen
Roti-Histokitt, resinous medium	Carl Roth
RIPA-Buffer	Sigma-Aldrich
Skin antiseptic	Schülke & Mayr GmbH
Sodium azide $\geq 99,0\%$	Sigma-Aldrich
Sodiumdodecylsulfate (SDS)	Bio-Rad
Tetramethylethylenediamine (TEMED)	AppliChem GmbH
Tri-Sodium citrate 2-hydrate	Roth
TRIzol® Reagent	Invitrogen
Xylene	AppliChem GmbH

2.1.11 Buffers and utility solutions

0.1% sodium azide: 10 g NaN_3 in 100 mL distilled water was diluted 1:100 in distilled water

2x Laemmli buffer: 2% sodium dodecyl sulfate, 62.5 mM Tris-HCl, pH 6.8, 10% glycerol, and 0.001% bromphenol blue

4% paraformaldehyde: 40 g in 1 L distilled water

Buffer for BioTherm Taq DNA Polymerase (Genecraft): 160 mM $(\text{NH}_4)_2\text{SO}_4$, 670 mM

PBS: 137 mM NaCl, 2.7 mM KCl, 8 mM NaH_2PO_4 , 2 mM KH_2PO_4

Sodium citrate buffer pH 6.0: 10 mM sodium citrate, 0.05% Tween 20

Tris-HCl pH 8.8, 15 mM MgCl_2 , 0,1% Tween 20

TAE-Buffer 50x, pH 7.0: 0.8 M Tris Base, 0.2 M Na-Acetate, 20 mM EDTA,

TBS-T pH 7.6: 50 mM Tris, 150 mM NaCl, 0.05% Tween 20

2.1.12 Kits

Clarity Western ECL Substrate Kit (Bio-Rad)

Deoxyribonuclease I, Amplification Grade (Invitrogen)

Nuclear Extraction Kit (Abcam)

OxiSelect™ Hydrogen Peroxide / Peroxidase Assay Kit (Cell Biolabs, INC.)

qPCR MasterMix Plus (Eurogentec)

Superscript™ III First-Strand Synthesis System for RT-PCR (Invitrogen)

TGX Stain-Free™ FastCast™ Acrylamid Kit 10% (Bio-Rad)

Triglyceride Colorimetric Assay Kit (Cayman Chemicals)

2.1.13 High-fat Paigen diet

A variety of lipid-enriched diets have been used to investigate hepatic steatosis and steatohepatitis in different animal models. In this study a modified Paigen diet (also called atherogenic diet) was used. The Paigen diet is characterized by the addition of 1.25% cholesterol and 0.5% sodium cholate and was originally created to study the development of atherosclerotic lesions [199, 200]. The diet applied in this study also contained a raw fat content of 42% in which fat contributes 70% of the total energy requirements. When administered to mice, high-fat Paigen diet (HFPD) induces progressive liver injury leading to steatosis, inflammation and fibrosis within 24 weeks [201, 202]. Furthermore, HFPD is known to cause insulin resistance and hepatocellular ballooning in a time-dependent manner, both features are reliable markers for the diagnosis of human NASH [203]. Since the HFPD causes steatohepatitis without the influence of additional chemical agents, genetic defects or a paucity of nutrients this diet is considered to be an appropriate physiological dietary model closely imitating a typical “Western” food lifestyle.

2.2 Methods

2.2.1 Polymerase chain reaction (PCR) -based genotyping

For genotyping of potentially *UGT1A* transgene-positive mice, a PCR-based amplification of the human *UGT1A3* gene was performed. Therefore, ear samples of each animal were taken and lysed in 100 μ L DirectPCR Lysis reagent (mouse tail; Viagen) containing 1.25 μ L of Proteinase K (VWR). After overnight incubation at 55 $^{\circ}$ C and shaking at 800 rpm, Proteinase K has been subsequently inactivated for 45 min at 85 $^{\circ}$ C and 800 rpm followed by a 5 min centrifugation at 13000 rpm. Next, 0.5 μ L DNA was used for amplification of the specific *UGT1A3* gene sequence.

UGT1A3 PCR-Assay (total volume 25 μ L):

0.5 μ L DNA	~10-100 ng
2.5 μ L Biotherm Reaction Buffer	10x
1.25 μ L Primer Allgen	10 μ M
1.25 μ L Primer GT1A3	10 μ M
1.0 μ L MgCl ₂	50 mM
0.5 μ L dNTPs	10 mM
0.25 μ L Biotherm Taq Polymerase	1 U
17.75 μ L H ₂ O	

Settings for the PCR-based amplification of the *UGT1A3* gene are shown in table 10.

Table 10: Setting for the *UGT1A3* PCR-program.

Temperature	Time	Cycles
94 $^{\circ}$ C	5 min	1
94 $^{\circ}$ C	40 sec	30
56 $^{\circ}$ C	40 sec	
72 $^{\circ}$ C	1 min for 1 kb sequence amplification	
72 $^{\circ}$ C	7 min	1

Amplification products were subsequently mixed with 6x loading dye and loaded onto a 1% agarose gel followed by electrophoretic separation at 120 V for 45 min. Confirmation of the

human *UGT1A3* gene was achieved by the existence of a band at roughly 500 bp. Transgene-positive mice were taken for experiments between 8 and 12 weeks after birth.

2.2.2 Treatment, anesthesia and bile duct ligation of *htgUGT1A* mice

Bile duct ligation (BDL) represents an established experimental model to study the processes relevant for human cholestatic liver fibrosis. Mice of each genotype were divided into four groups of four to eight animals and underwent either 14 days BDL or 14 days sham operation. In addition to BDL or sham surgery, *htgUGT1A*-WT and SNP mice received pre- and co-treatment with coffee provided instead of drinking water 14 days before and after surgical treatment.

For surgical interventions (sham operation and BDL) *htgUGT1A* mice were anesthetized using an isoflurane Vaporizer (VetEquip). Animals were placed in an anesthesia induction chamber and narcotized by inhalation of 4 vol. % isoflurane in 100% oxygen at a flow rate of 4 L/min. After induction of anesthesia, abdominal fur was shaved and mice were placed on a 37 °C heated hotplate covered with a sterile underpad. Due to a missing lid-closing reflex of the eye anesthetized animals received Bepanthen® eye and nose ointment containing 5% dexpanthenol to protect the eyes from drying out. To maintain anesthesia the mouse snout was inserted in a Fluovac mask with 1.5-3 vol. % isoflurane at a flow rate of 1 L/min. After disinfection of the surgical area with Betaisadona® solution, the operation started with a midline laparotomy approximately 1.5 cm in length by simultaneously cutting the *cutis* and the *fascia*. To open the animal's peritoneal cavity the peritoneum was dissected along the *linea alba* and a Colibri retractor (Fine Science Tools) was inserted to spread the operation area. Next, the liver was carefully lifted to expose the bile duct. A micro-serrations forceps was used to separate the common bile duct from the flanking portal vein and hepatic artery (Fig. 12 left picture). Then, the bile duct was obstructed by double ligation using two surgical knots for each ligation (Fig. 12 right picture). In sham-operated mice, the common bile duct has not been ligated. The peritoneal cavity was rinsed with 0.9% NaCl solution and both abdominal layers were closed with separate running sutures. After surgery, animals were allowed to recover under an infrared warming lamp. 14 days after surgery, animals were anesthetized to collect 200 µL of blood and organs, which were immediately shock-frozen in liquid nitrogen and stored at minus 80 °C until use.

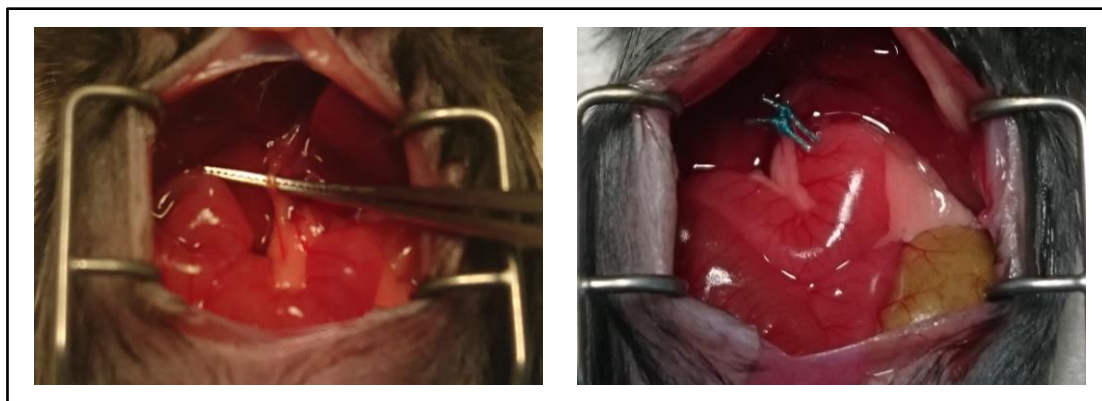


Figure 12: Bile duct ligation of *htgUGT1A* mice. Separation of the common bile duct (left picture) and obstructive cholestasis with double-ligation (right picture).

2.2.3 High-fat Paigen diet treatment of *htgUGT1A* mice

For diet-induced hepatic steatosis, eight-week-old *htgUGT1A*-WT and SNP mice were divided into two groups per genotype. All animals had *ad libitum* access to water and chow and were either fed with normal diet or with HFPD for 24 weeks. Before the HFPD was administered *htgUGT1A* mice need to become accustomed to the change of the dietary components. Therefore, HFPD-treated animals were first given a modified chow for 10 days which includes the same raw nutrient ingredients as the HFPD but does not contain any of the elements believed to be responsible for harmful effects (e.g. high-fat content, cholesterol and sodium cholate). Since a sudden change in eating behavior is often associated with digestive problems initiated by gut microbial disorders [204], the purpose of “acclimatization” diets also aims to allow the intestinal flora to adapt to the environmental change before the obesity-inducing experimental diet is administered. After 24 weeks, animals were killed by cervical dislocation, 200 μ L of blood and organs were collected which were immediately shock-frozen in liquid nitrogen and stored at minus 80 °C until use.

2.2.4 Diethylnitrosamine-induced liver cancer and analysis of liver tumors

The proximate carcinogen DEN was used for chemical induction of liver cancer in *htgUGT1A* mice. Like many other *N*-nitrosoamine compounds, DEN has been reported to exert hepatotoxic and carcinogenic effects. This well-established experimental model is predicted to induce hepatocarcinogenesis after metabolic activation of DEN leading to chemically-caused DNA alternations evoked by alkylating metabolites. Metabolic activation of DEN *via* CYP2E1 biotransformation leads to the generation of α -hydroxy diethylnitrosamine. This intermediate breaks down spontaneously to the alkylating metabolites ethyl diazohydroxide

and ethyl diazonium ion, which cause alkylation of DNA and consequently induce hepatic tumorigenesis [205]. Due to inhibitory effects of estrogens and stimulatory actions of androgens, gender-related differences for DEN-induced HCC incidence in male (up to 100%) and female (around 30%) mice were reported [206, 207]. For that reason, only male mice were used to study the effect of common *UGT1A* polymorphisms on DEN-induced HCC development. A single intraperitoneal DEN injection (20 mg/kg) was administered to 15-day old *htgUGT1A*-WT and SNP mice. Seven days after injection, the mice descendants of each genotype were separated from the mother and further divided into two subgroups either receiving water or coffee until the end of the experiment. 40 weeks after DEN administration, mice were sacrificed to macroscopically determine tumor incidence and size at the liver surface. Visible nodule formations (>1 mm in diameter) were counted and dimensions of tumor nodules were measured. Tumorous tissue was carefully separated from normal (non-tumorous) liver sections and both sample types were immediately snap-frozen in liquid nitrogen and stored at -80°C until use. Serum aminotransferase activities were calculated as described in chapter 2.2.9. To ensure best compatibility between the different groups, all injected animals were treated with same DEN lot number within 5 months.

2.2.5 Preparation of coffee

A stock solution was prepared to represent the preparation mode of commonly used filter coffee. For preparation of coffee, 500 mL water were boiled in a beaker and cooled for 10 seconds. Ten grams of ground coffee powder (Jacobs Krönung) was added and incubated for one minute, followed by filtration through a paper coffee filter (Melitta).

2.2.6 RNA-Isolation

Total RNA was isolated using TRIzol® Reagent (Invitrogen). Therefore, 1 mL TRIzol® reagent together with a stainless bead of 5 mm diameter was added to a reaction tube containing approximately 50 mg shock-frozen liver tissue of sacrificed transgenic mice. After 2 min homogenization in a TissueLyser LT (Qiagen) at an oscillation frequency of 1/50 sec, samples were incubated at room temperature for 5 min followed by addition of 200 µL chloroform and subsequent vortexing for 15 sec. After 15 min incubation at room temperature the homogenate was centrifuged at 4 °C and 12000x g for 15 min and the clear supernatant in the upper phase was transferred into a new reaction tube, mixed with 0.5 mL isopropyl alcohol and again incubated at room temperature for 10 min. Following RNA precipitation an

additional centrifugation step (12000x g, 4 °C for 10 min) and a subsequent washing step with 1 mL of 70% EtOH were performed. After the removal of the supernatant, the RNA pellet was air dried and then solved in 40 - 100 µL of DEPC-treated water.

2.2.7 Reverse transcription polymerase chain reaction (RT-PCR)

The reverse transcription of RNA to cDNA was accomplished by the use of SuperScript® III First-Strand Synthesis System for RT-PCR (Invitrogen). Therefore, 5 µg of RNA was incubated at room temperature with DNase I (Invitrogen) for 15 min.

DNase I digestion (total volume 10 µL):

X µL RNA	5 µg
1 µL DNase I	1 U/µL
1 µL DNase I buffer	10 x
X µL DEPC-treated water	

For subsequent DNase I inactivation 1 µL EDTA was added to each PCR reaction tube and incubated at 65 °C for 10 min. DNase I treated RNA was then used for cDNA synthesis in an oligo(dT)-primed Superscript III reverse transcriptase reaction. First, 1 µL Oligo-dT and 1 µL dNTP-Mix was added to each RT-PCR reaction and incubated at 65 °C for 5 min.

RT-PCR reaction:

10 µL RNA (DNase I treated)	5 µg
1 µL Oligo(dT)	50 µM
1 µL dNTP-Mix	10 mM

Afterwards, RT-PCR reaction was placed on ice and 8 µL of the following master mix were transferred into each reaction tube.

Master mix RT-PCR:

1 µL RT buffer	10 x
4 µL MgCl ₂	25 mM
2 µL DTT	0.1 M
0.5 µL RNaseOUT™	40 U/µL
0.5 µL Superscript® III RT	200 U/µL

RT-PCR was performed at 50 °C for 60 min. In a final step, enzyme activity was inactivated by heating up to 85 °C for 5 min. 1 µL of the synthesized cDNA was used for subsequent TaqMan PCR.

2.2.8 TaqMan PCR

The TaqMan PCR is a modification of the 5'-nuclease PCR assay which was first described by *Holland et al.* in 1991. The principle relies on the 5'-3' exonuclease activity of the DNA Taq polymerase to cleave a probe after hybridization to the complementary target sequence which is localized between forward and reverse primer. In order to avoid the probe from acting as a third primer, the 3'-end is blocked by either a dideoxynucleotide or through a phosphate group [208].

In contrast to the originally radioactive-labeled oligonucleotide, a dual-labeled probe consisting of a covalently attached fluorophore (reporter) at the 5'-end and a quencher molecule at the 3'-end is used. This approach is based on the utilization of the Förster resonance energy transfer (FRET) in which the quencher inhibits the fluorescence signal emitted by the fluorophore as long as both molecules are in close proximity. As soon as the DNA polymerase reaches the probe, during the synthesis of the new DNA strand, the probe gets degraded due to the exonuclease activity and causes the dissociation of the fluorophore molecule from the quencher. The release of the fluorophore increases the distance between reporter and quencher and consequently results in the abrogation of the quenching effect on the reporter fluorescence. The fluorescence of the dissociated fluorophore is now detectable by the qPCR thermal cycler. The emitted signal is directly proportional to the released fluorophore molecules and the amount of cDNA present in the examined sample. On the basis of TaqMan probes it is possible to detect nascent synthesized DNA strands at any time of the reaction. For quantification of gene expression, cDNA concentrations were determined relative to mouse beta-actin.

2.2.9 Biochemical analysis of blood serum

After blood sampling and subsequent centrifugation for 10 min at 4.800x g the blood serum is separated from the coagulum and the supernatant was transferred into a new reaction tube. Serum was stored at -20 °C until measurement of aminotransferase activities and total serum bilirubin levels. In medical diagnosis, increased levels of aspartate aminotransferases (AST) and alanine aminotransferases (ALT) are characteristic indicators for hepatocyte damage and

liver injury [209]. Therefore, elevations of serum AST and ALT enzyme activities can correlate with the extent of liver damage. The biochemical analysis was accomplished using a Fuji DRI-CHEM NX500i (Fujifilm Cooperation, Tokyo, Japan) serum analyzer.

2.2.10 Histological analysis

The right lateral lobe (RLL) of the liver was taken for histological analysis. After organ removal the RLL was carefully separated from the remaining liver and directly transferred into a 4% paraformaldehyde fixation solution, followed by 72 h storage at 4 °C. Then, the liver lobe was placed into Rotilabo® tissue embedding cassettes, sliced lengthways into two halves and conserved in a 0.1% sodium azide solution at 4 °C. For dehydration and paraffin infiltration a spin tissue processor (Microm STP 120, Thermo Scientific) was used. The setup for the dehydration protocol is listed in the table below (Tab. 11).

Table 11: Settings for dehydrogenation protocol of the Microm STP 120.

Chemical	Duration
50% EtOH	90 min
70% EtOH	90 min
80% EtOH	90 min
96% EtOH	90 min
100% EtOH	60 min
100% EtOH	60 min
100% EtOH	60 min
100% Xylene	60 min
100% Xylene	60 min
100% Xylene	60 min
Paraffin	90 min
Paraffin	∞

By the use of a tissue embedding paraffin dispenser (Microm EC 350-1) liver samples were embedded as paraffin blocks. For histological staining, liver paraffin blocks were first trimmed to 2.0 µm-thick sections and placed on microscope slides. Then, sections were dried at room temperature for at least 24 h and are ready for subsequent staining (see 2.2.10.1 and 2.2.10.2).

2.2.10.1 Hematoxylin and Eosin staining

Hematoxylin and eosin (H&E) staining is a commonly used method for microscopic examination of tissues that have been fixed, embedded and sectioned. In H&E-stained tissues, the nucleic acids appear as dark blue in consequence of the binding of hematoxylin to basophilic substances such as negatively charged DNA or RNA [210]. The nuclear staining is followed by counterstaining with a synthetic acidic coloring agent called Eosin which stains acidophilic (or eosinophilic) structures in different shades of pink and red. The H&E procedure has been manually performed in glass cuvettes according to the following protocol (Tab. 12) and specimens were subsequently sealed for long term storage (see 2.2.10.2).

Table 12: Hematoxylin and Eosin staining protocol.

Step	Chemical	Duration	Function
1	100% Xylene	3 min	Deparaffinization
2	100% Xylene	3 min	Deparaffinization
3	100% EtOH	1 min	Rehydration
4	90% EtOH	1 min	Rehydration
5	70% EtOH	1 min	Rehydration
6	Distilled water	30 sec	Rinsing
7	Hemalum	4 min	Staining
8	Tap water	1 min	Rinsing
9	Acid ethanol	10 sec	Rinsing
10	Tap water	3 min	Rinsing
11	Eosin	3 min	Staining
12	Tap water	1 min	Rinsing
13	70% EtOH	30 sec	Dehydration
14	90% EtOH	1 min	Dehydration
15	100% EtOH	1 min	Dehydration
16	100% Xylene	5 min	Dehydration

Acid ethanol: 6 drops concentrated HCl was added to 800 mL 70% EtOH.

2.2.10.2 Sirius red staining

The gold standard method for the histological detection of ECM proteins such as collagen fibers is the Sirius red staining. In this study, Sirius red staining was used for the histological detection and determination of fibrosis. In bright field microscopy, collagen fibers appear red

whereas the cytoplasm and cell nuclei become visible in yellow. After the respective staining process specimens were hermetically sealed for long term storage. Therefore, one drop of Roti-Histokitt coverslipping solution was placed onto the slide and subsequently sealed with a cover slip. Table 13 gives a detailed overview of the Sirius red staining procedure.

Table 13: Sirius red staining protocol.

Step	Chemical	Duration	Function
1	100% Xylene	5 min	Deparaffinization
2	100% Xylene	5 min	Deparaffinization
3	100% EtOH	5 min	Rehydration
4	100% EtOH	5 min	Rehydration
5	95% EtOH	1 min and 10 dips	Rehydration
6	70% EtOH	1 min and 10 dips	Rehydration
7	50% EtOH	30 sec and 5 dips	Rehydration
8	Distilled water	10 dips	Rinsing
9	Sirius red solution with picric acid crystals	12 min	Staining
10	100% EtOH	5 dips	Rinsing
11	100% EtOH	10 dips and 1 min	Dehydration
12	100% Xylene	10 dips	Dehydration
13	100% Xylene	5 dips and ∞	Dehydration

Sirius red solution: 0.5 g Direct red 80, 500 mL 1.3% saturated picric acid solution, 4 teaspoons picric acid crystals moistened in water

2.2.10.3 Immunofluorescence staining

Immunofluorescence staining was performed for evaluation of oxidative stress levels in paraffin embedded tissue samples. For the detection of ROS-caused alternations of macromolecules we used the lipid peroxidation product 4 hydroxynonenal (4-HNE) as an indicator of oxidative liver injury [211]. Table 14 illustrates the protocol applied for the deparaffinization and rehydration before immunofluorescence staining.

Table 14: Immunofluorescence staining protocol.

Step	Chemical	Duration	Function
1	100% Xylene	7 min	Deparaffinization
2	100% Xylene	7 min	Deparaffinization
3	100% EtOH	3 min	Rehydration
4	100% EtOH	3 min	Rehydration
5	100% EtOH	3 min	Rehydration
6	95% EtOH	3 min	Rehydration
7	95% EtOH	3 min	Rehydration
8	80% EtOH	3 min	Rehydration
9	80% EtOH	3 min	Rehydration
10	Distilled water	10 dips and 5 min	Rinsing
11	Distilled water	10 dips and 5 min	Rinsing

After washing twice with distilled water antigen retrieval was performed. Therefore, tissue slides were transformed in stainless steel cuvettes filled with sodium citrate buffer (pH 6.0) and heated for 20 min at 95 – 100 °C. Afterwards, tissue specimens were cooled down in sodium citrate buffer for 40 min until room temperature was reached. Next, tissue slides were washed four times with phosphate-buffered saline (PBS) for 5 min. After that, liver specimens were incubated for 10 min in 3% hydrogen peroxide solution and subsequently washed with PBS for 5 min. The washing step was repeated for another three times followed by 1 h incubation with blocking buffer consisting of 5% goat serum diluted in TBS-T. To remove the blocking buffer from liver tissue, the edge of the microscope slide was carefully blotted against clean paper towels. Rabbit anti-4-HNE antibody (Abcam, ab46545) was added to blocking buffer at a dilution of 1:50 and applied to tissue sample area. In order to be able to determine the fluorescent background signal a negative control was prepared, which was further incubated with blocking buffer. Microscope slides were transferred into a moist chamber and incubated overnight at 4 °C. The next day, 4-HNE antibody solution (or blocking solution respectively) was removed by washing tissue samples three times in TBS-T for 7 min. After 1 h incubation with 1:200 diluted Alexa Fluor® 488 goat-anti-rabbit secondary antibody (Abcam, ab150077) tissue slides were washed three times in the dark with TBS-T for 5 min and subsequently rinsed with distilled water for 10 sec. To preserve fluorescence of tissue, 3-4 drops of Fluoroshield Mounting Medium with DAPI (Abcam) was added directly on the tissue sample and incubated in the dark for 5 min before sealing with a cover slip. To make sure the mounting medium is completely hardened, tissue slides are again

stored for 2 h at 4 °C protected from light. Since the fluorescence signal is retained during prolonged storage, visualization under the microscope was performed at the same day.

2.2.11 Protein isolation

Total protein was isolated by the use of radioimmunoprecipitation assay (RIPA) buffer. 60 mg of shock-frozen liver tissue from a pool of four to eight animals per group was transferred into a 2 mL tube containing stainless beads of 5 mm diameter for the mechanical disruption of cells. Homogenization was performed in 600 µL RIPA extraction buffer (Sigma-Aldrich) containing 1:100 diluted protease inhibitor cocktail (Sigma-Aldrich) with a TissueLyser LT (Qiagen) for 2 min at an oscillation frequency of 1/50 sec. Tissue homogenate was incubated for 1 h on a shaking plate at 4 °C. After centrifugation (13.000 rpm, 10 min, 4 °C) supernatant was transferred into a new vial and protein concentration was photometrically measured by Bradford-assay before performing Western blot analysis.

2.2.12 Nuclear extraction

The process of nuclear extraction is designated to separate nuclear from cytoplasmic cellular fractions. This procedure is used instead of whole total protein isolation protocol where the entire tissue cells are lysed resulting in a protein mixture that incorporates constituents of the nucleus and the cytoplasm. In this study, the following extraction protocol was used to investigate protein expression levels of transcription factors that specifically interact within the nucleus where they bind to regulatory DNA sequences. Chemicals and reagents from the Abcam Nuclear Extraction Kit were used (see 2.1.12).

First, 40 mg frozen liver tissue were placed in a clean Potter-Elvehjem-Type tissue grinder containing 200 µL of DTT Pre-Extraction buffer. Tissue pieces were homogenized with 60 strokes followed by 15 min incubation on ice and subsequent centrifugation for 10 min at 12.000 rpm at 4 °C. Supernatant was discarded and the sample pellet was mixed with 200 µL DTT Extraction buffer comprising a 1:100 diluted protease inhibitor cocktail (Sigma-Aldrich). The tissue extract was incubated on ice for 15 min and every 3 min vortexed for 5 seconds. To increase nuclear protein extraction the extract was further sonicated 3 times for 10 seconds with 20% power. The homogenate was then centrifuged for 10 min at 4 °C and the supernatant was transferred into a new microcentrifuge vial. Protein concentration of nuclear extracts were determined by Bradford-assay and stored at minus 80°C until use.

2.2.13 Western blot analysis

Western blot analysis was used for detection and relative quantification of requested target proteins in purified tissue homogenates. Therefore, 30 µg protein was boiled at 95 °C for 5 min in 2 x Laemmli sample buffer, placed on ice and cooled down for 2 min followed by 10 sec centrifugation at 1.800x g. Denatured protein samples were subsequently separated by 10% SDS-PAGE prior to electrotransfer (1.3 A and 25 V for 8 min) onto a nitrocellulose membrane using the Trans-Blot®-Turbo transfer system (Bio-Rad). Electrophoretic separation was achieved in SDS running buffer after 50 min at 150 V. To prevent non-specific antibody binding the membrane was blocked for 1 h at room temperature with 5% dry milk solubilized in PBS containing 0.1% Tween 20 (PBS-T). Overnight incubation with specific primary antibodies binding to the desired target protein was carried out in 5% dry milk at 4 °C. On the following day, three washing steps of 15 min each with PBS-T were performed to sluice down excess and non-specifically bound antibodies. After 1 h incubation with 1:2000 diluted appropriate HRP-conjugated secondary antibodies and three further washing steps with PBS-T, target protein was visualized by chemoluminescence (Bio-Rad) by use of ChemiDOC MP imaging system (Bio-Rad) and Clarity Western ECL Substrate Kit (Bio-Rad). This kit consists of two components which were mixed in a 1:1 proportion and incubated for 5 min on the nitrocellulose membrane while gently shaking. Staining with secondary GAPDH antibody (Santa cruz, sc-32233) or histone H3 (Abcam, ab12079; for nuclear extracts) was used as loading control.

2.2.14 Peroxidase assay

Modifications in the cell that inhibit antioxidant defense mechanisms or lead to the generation of ROS can result in oxidative injury to hepatocytes and activation of HSCs [212]. To examine potential differences of the variant antioxidative capacity between both mouse lines the Cell Biolabs' OxiSelect™ Hydrogen Peroxide / Peroxidase Assay Kit was used for quantitative colorimetric determination of total peroxidase concentration in the livers of BDL and sham operated *htgUGT1A*-WT and *htgUGT1A*-SNP mice. The assay is based on the principle of color development, which occurs in the presence of peroxidase that reacts with hydrogen peroxide to produce a bright pink colored product. The amount of this generated product can be calculated by comparison with a respective standard curve as absorbance values are proportional to the peroxidase levels within the liver samples. Sample preparation and assay was conducted according to the following protocol. Using the TissueLyser LT

(Qiagen) 100 mg liver tissue were homogenized in 200 μ L assay buffer as described above (see point 2.2.11). Afterwards, tissue homogenate was sonicated on ice and subsequently centrifuged for 10 min at 12.000x g at 4 °C. Supernatant was used to calculate peroxidase concentration. Standard and assay were performed in a 96 well plate according to manufacturer's protocol. Therefore, 50 μ L standard or homogenized liver samples were mixed with 50 μ L peroxidase working solution (50 μ L Colorimetric Probe + 1.14 mL 8.8 mM H₂O₂ + 3.81 mL assay buffer) and incubated for 30 min protected from light. Plate absorbance was analyzed at a wave length of 550 nm using a Multiskan Go Reader (ThermoScientific).

2.2.15 Triglyceride assay

NAFLD is characterized by the excessive accumulation of triglycerides in the liver, which is designated hepatic steatosis. Measurement of the hepatic fat content and especially the proportion of triglycerides is therefore a reliable marker for the experimental determination of steatosis severity, and dyslipidemia. Triglyceride levels were photometrically determined from homogenized snap-frozen liver tissue using the Triglyceride Colorimetric Assay Kit (Cayman Chemical) according to manufacturer's instructions. In this assay, the enzymatic hydrolysis of water-insoluble triglycerides by lipases leads to the production of free fatty acids and glycerol. Following a series of enzymatic reactions, the latter intermediate product is finally transformed into hydrogen peroxide which is further catalyzed by peroxidase and two added co-substrates to a purple colored end product whose absorbance is measured at 540 nm and directly proportional to the initial hepatic fat content of the investigated liver tissue.

2.2.16 Computational histological analysis

Quantification of liver fibrosis was assessed by computational analysis of Sirius red stained areas. For the detection of red colored collagen fibers, liver tissues were stained according to the Sirius red staining procedure mentioned in point 2.2.10.2. The Sirius red positive area was quantified using ImageJ software (U.S. National Institutes of Health; <http://rsb.info.nih.gov/ij/>) and shown as percentage of the total section area. A manually written Java® script was used for ImageJ-based calculation of image stacks (Fig. 44, supplemental data). Images were analyzed from five randomly selected images (magnification 100-fold) of each animal and averaged.

2.2.17 Graphical representations and statistical analysis

Graph generation and the statistical analysis of the results between different experimental groups were carried out by Microsoft Office Excel 2010. Unless otherwise indicated, the following illustrations show the results of three independently performed experiments after organ collection of *htgUGT1A* mice. Data are expressed as mean \pm SD determined by Students *t*-test to determine significance. A pool of four to ten mice (depending on experiment) of each group was analyzed, p values below 0.05 were considered as statistically significant.

3 Results

3.1 Obstructive cholestasis-induced liver fibrosis

Since only limited data exists regarding the transcriptional regulation, activity and functional contribution of UGT1A enzymes during cholestasis-related disease, this study aimed to elucidate the potential role as well as the risk associated with common *UGT1A* polymorphisms for the development of liver fibrosis induced by BDL treatment. Furthermore, the effect of *UGT1A* expression in coffee-based fibrosis protection during obstructive cholestasis was assessed because a significant coffee-mediated induction of human *UGT1A* gene expression in *htgUGT1A* mice has previously been shown by experiments of our laboratory [181]. Therefore, four mice of each transgenic mouse line either underwent sham operation with or without coffee pre- and co-treatment. The BDL-operated groups encompassed six to eight mice per genotype.

3.1.1 Hepatic *UGT1A* expression during cholestatic liver injury in *htgUGT1A* mice

The effect of cholestasis-induced liver injury on hepatic *UGT1A* transcription in *htgUGT1A*-WT and SNP mice is depicted in figure 13 and 14. In sham-operated *htgUGT1A*-WT mice, coffee pre- and co-treatment significantly increased the hepatic expression of all investigated *UGT1A* isoforms (except for *UGT1A7*) compared to the water drinking *UGT1A*-WT group (Fig. 13). As shown in the figure below, 14 days of biliary obstruction induced a significant upregulation of *UGT1A1*-, *UGT1A6*-, *UGT1A7*- and *UGT1A9* mRNA expression. Following coffee + BDL co-treatment, hepatic *UGT1A* mRNA levels were higher as those observed in water drinking BDL *htgUGT1A*-WT mice and reached a considerable induction for *UGT1A1* (7.1-fold), *UGT1A3* (2.3-fold), *UGT1A4* (1.8-fold), *UGT1A6* (4.3-fold), *UGT1A7* (5.9-fold) and *UGT1A9* (3.2-fold).

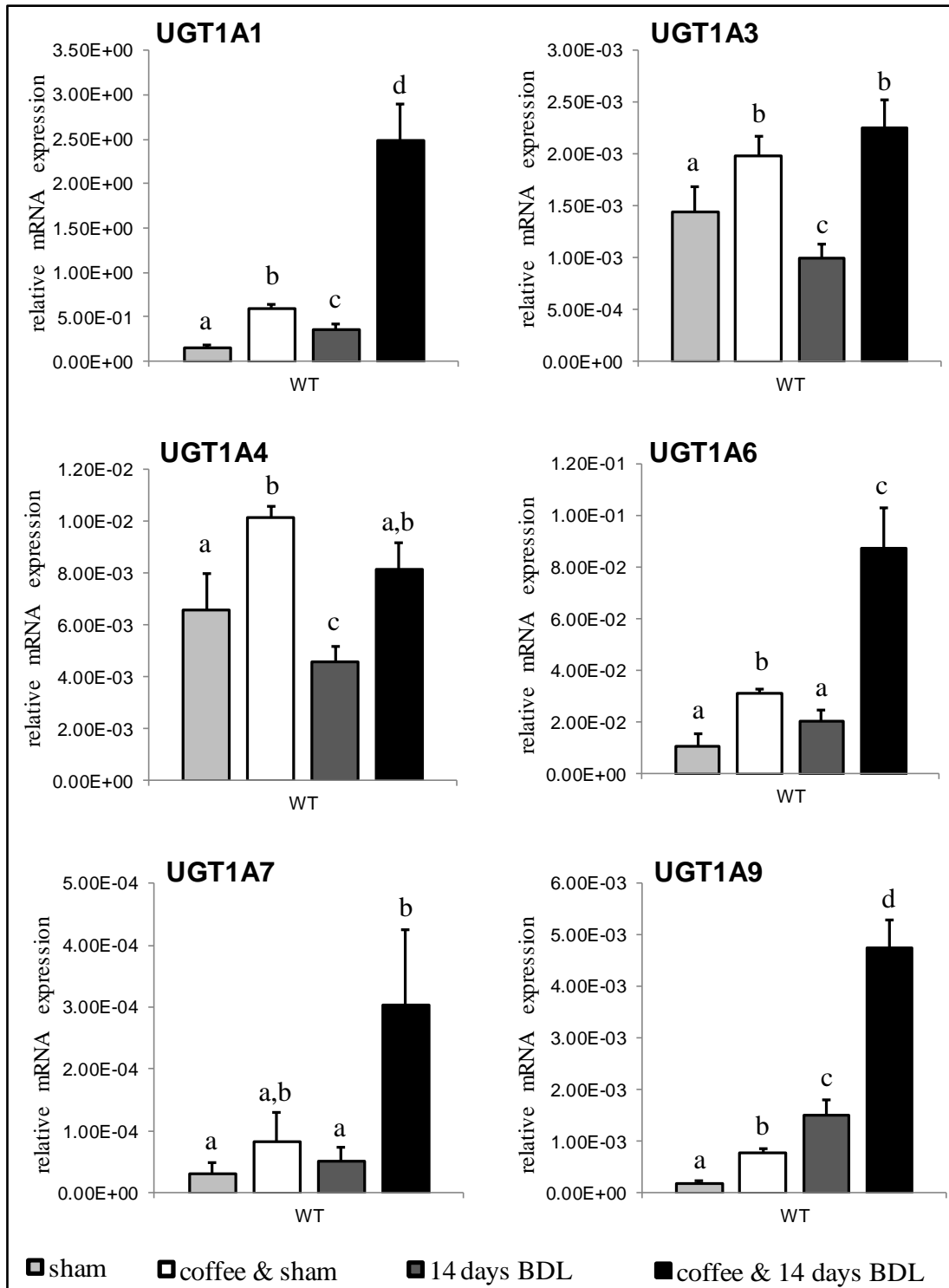


Figure 13: Hepatic UGT1A mRNA expression in *htgUGT1A*-WT mice after sham operation (sham) or 14 days bile duct ligation (BDL) with and without coffee pre- and co-treatment. The panels display the mRNA expression of *UGT1A* genes relative to mouse β -actin. Coffee administration in sham-operated *htgUGT1A*-WT mice led to a considerable transcriptional activation of all investigated *UGT1A* genes compared to the water drinking sham group. BDL led to an upregulation of UGT1A1-, UGT1A6-, UGT1A7- and UGT1A9-mRNA whereby co-treated (coffee + BDL) *htgUGT1A*-WT mice showed significantly increased absolute expression levels and a considerably higher induction compared to water drinking BDL mice. Each column represents the mean \pm SD (n=3). For all variables with the same letter, the difference between the means is not statistically significant. If two variables have different letters, their comparison is statistically significant; $p < 0.05$.

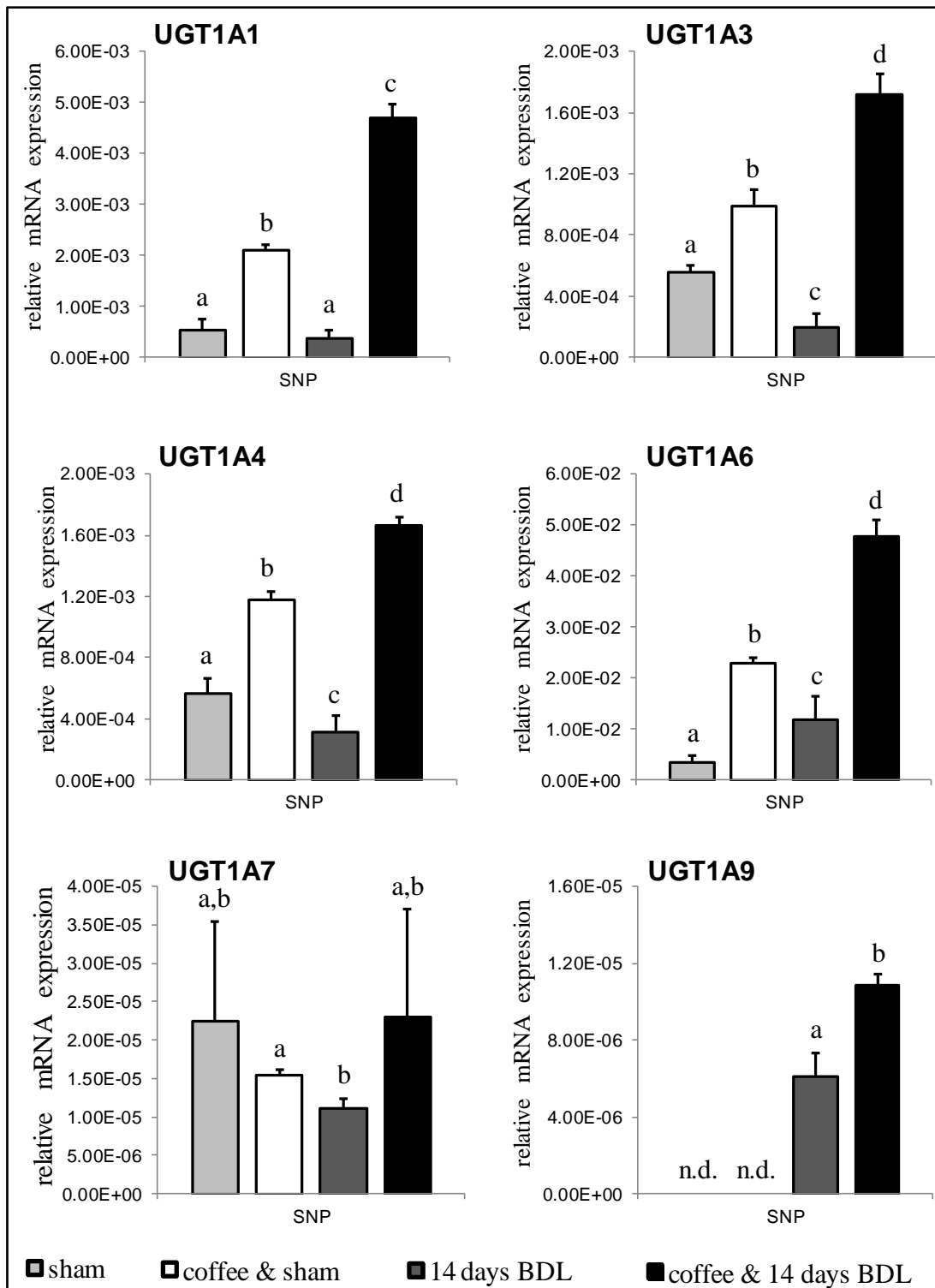


Figure 14: Hepatic UGT1A mRNA expression in *htgUGT1A*-SNP mice after sham operation (sham) or 14 days bile duct ligation (BDL) with and without coffee pre- and co-treatment. The graphs display the mRNA expression of *UGT1A* genes relative to mouse β -actin. In the livers of sham-operated *htgUGT1A*-SNP mice coffee treatment evoked transcriptional *UGT1A* induction of all investigated isoforms (except for UGT1A7). *UGT1A* induction was absent for most isoforms (apart from UGT1A6 and UGT1A9) after BDL, whereas transcriptional activation was detected for every isoform after coffee + BDL co-treatment compared to water drinking BDL mice. Each column represents the mean \pm SD (n=3). Groups without the same letter are significantly different; $p < 0.05$.

In contrast to the results detected in *htgUGT1A*-WT mice, lower absolute expression levels and a reduced responsiveness to coffee were observed in mice carrying the low-activity SNP variant (Fig. 14). Hence, coffee-mediated upregulation in sham-operated *htgUGT1A*-SNP mice was less pronounced as that observed in equivalently treated *htgUGT1A*-WT mice. Furthermore, *UGT1A* induction was reduced (UGT1A6 and UGT1A9) or absent after BDL in *htgUGT1A*-SNP mice. Interestingly, coffee + BDL co-treatment also induced hepatic *UGT1A* gene expression in mice carrying the *UGT1A* SNP haplotype, although absolute expression levels remained far below those observed in *htgUGT1A*-WT mice.

These data indicate that coffee + BDL co-treatment synergistically increases the hepatic expression of *UGT1A* genes in both mouse lines even though the inductive effect is markedly stronger in *htgUGT1A*-WT mice. For UGT1A1 (530-fold), UGT1A3 (1.31-fold), UGT1A4 (4.89-fold), UGT1A6 (1.83-fold), UGT1A7 (13.22-fold) and UGT1A9 (436-fold) a much higher induction compared to coffee + BDL *htgUGT1A*-SNP mice was detected.

3.1.2 Serum bilirubin levels in *htgUGT1A* mice after BDL treatment

As expected, biochemical serum analysis revealed significantly elevated bilirubin levels in both mouse lines after 14 days BDL compared to sham mice (Fig. 15). Interestingly, in comparison with water drinking BDL mice, a significant reduction of total serum bilirubin was detected in both mouse lines after coffee co-treatment. Although not significant, *htgUGT1A*-SNP mice showed slightly higher bilirubin levels after BDL (WT: 23.02 mg/dl and SNP: 25.05 mg/dl) and coffee + BDL co-treatment (WT: 13.67 mg/dl and SNP: 16.12 mg/dl) compared to equivalently treated *htgUGT1A*-WT mice.

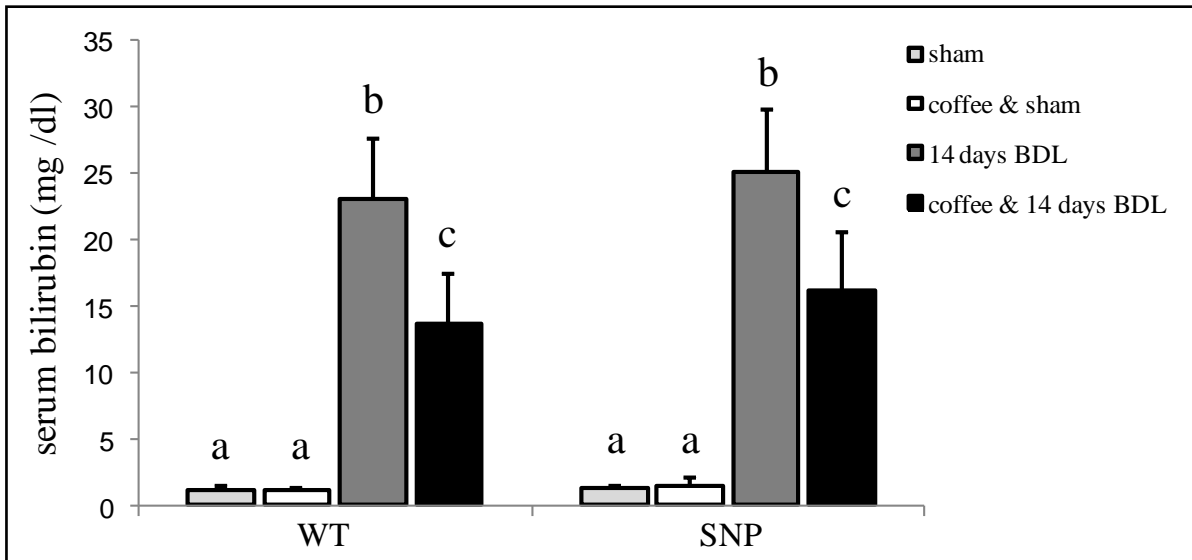


Figure 15: Determination of serum bilirubin levels after 14 days sham or bile duct ligation (BDL) operation in *htgUGT1A*-WT and SNP mice with and without coffee pre- and co-treatment. After 14 days BDL, significantly increased total serum bilirubin levels were detected in *htgUGT1A*-WT and SNP mice. Coffee + BDL co-treatment resulted in decreased but still elevated serum bilirubin levels in both mouse lines. Each column represents the mean \pm SD (n=4 for sham, n=6-8 for BDL). For all variables with the same letter, the difference between the means is not statistically significant. If two variables have different letters, their comparison is statistically significant; $p < 0.05$.

3.1.3 Liver histology of cholestatic *htgUGT1A* mice

Figure 16 illustrates representative sections of Sirius red stained liver areas of *htgUGT1A*-WT mice 14 days after sham or BDL operation with and without coffee pre- and co-treatment. Surgical ligation of the common bile duct led to advanced fibrosis development indicated by a high amount of red stained ECM proteins, mainly concentrated in the area of the fibrously widened portal fields. As obvious from the figures below, a clearly visible reduction of red stained collagen fibers was observed after pre- and co-administration of coffee. In comparison with the Sirius red stained liver section of *htgUGT1A*-WT mice, liver histology of mice carrying the low-function *UGT1A* SNP haplotype revealed aggravated fibrosis development 14 days after BDL (Fig. 17). In addition to a substantial collagen deposition around the portal fields, slightly red stained fibrillary collagen structures between the portal fields are visible. These may be the first signs of bridging fibrosis representing a more severe course of liver fibrosis. Interestingly, coffee co-treatment resulted in reduced hepatic ECM content in *htgUGT1A*-SNP mice as well.

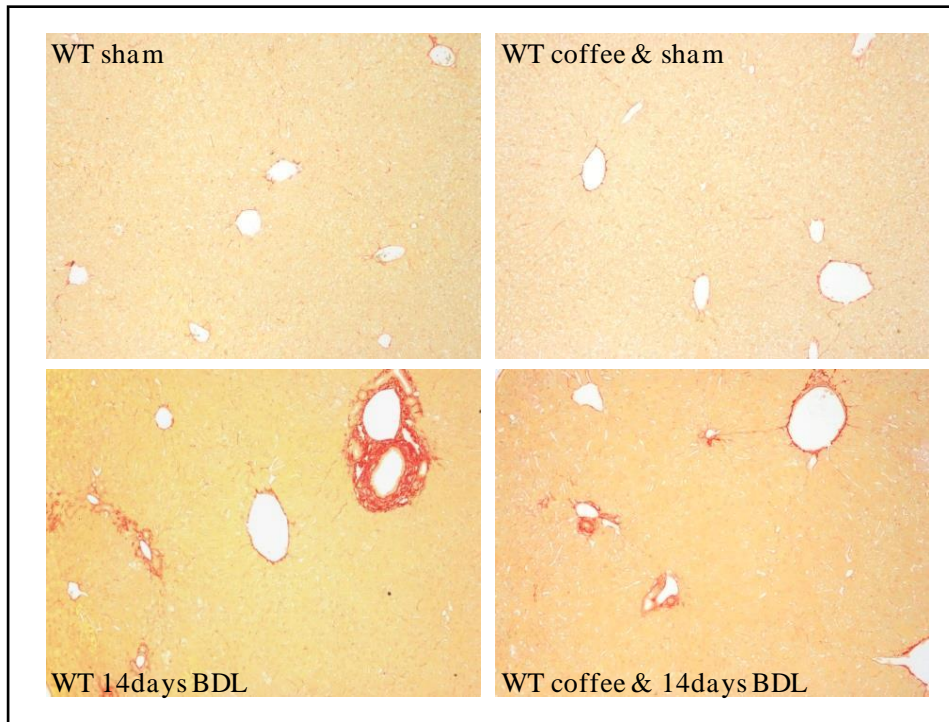


Figure 16: Representative hepatic sections of histological Sirius red staining in *htgUGT1A*-WT mice. Each of the four pictures is shown at 100-fold magnification.

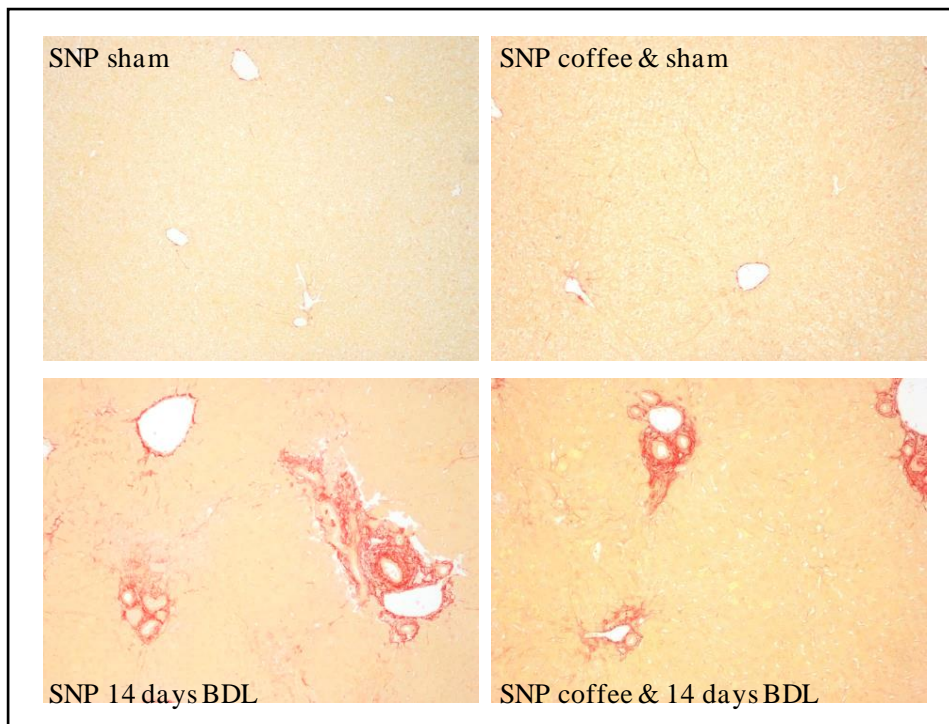


Figure 17: Representative hepatic sections of histological Sirius red staining in *htgUGT1A*-SNP mice. Each of the four pictures is shown 100-fold magnified.

3.1.3.1 Computational analysis of Sirius red stained liver sections of cholestatic *htgUGT1A* mice

Computational quantification of Sirius red positive stained areas supported the visual impression obtained from the histological liver sections (Fig. 18). The direct comparison between *htgUGT1A*-WT and SNP mice chronically-injured by 14 days BDL revealed a significantly higher percentage of red stained ECM proteins in liver tissues of mice carrying the low-activity SNP variant (WT 3.41% and SNP 4.94%). In both mouse lines coffee pre- and co-treatment resulted in lower collagen depositions, although coffee-mediated reduction of fibrillar structures was more prominent in *htgUGT1A*-WT mice. Mice containing multiple genetic *UGT1A* SNP variants showed a reduced but still significantly higher collagen proportion after coffee co-treatment (WT 2.63% and SNP 4.08%).

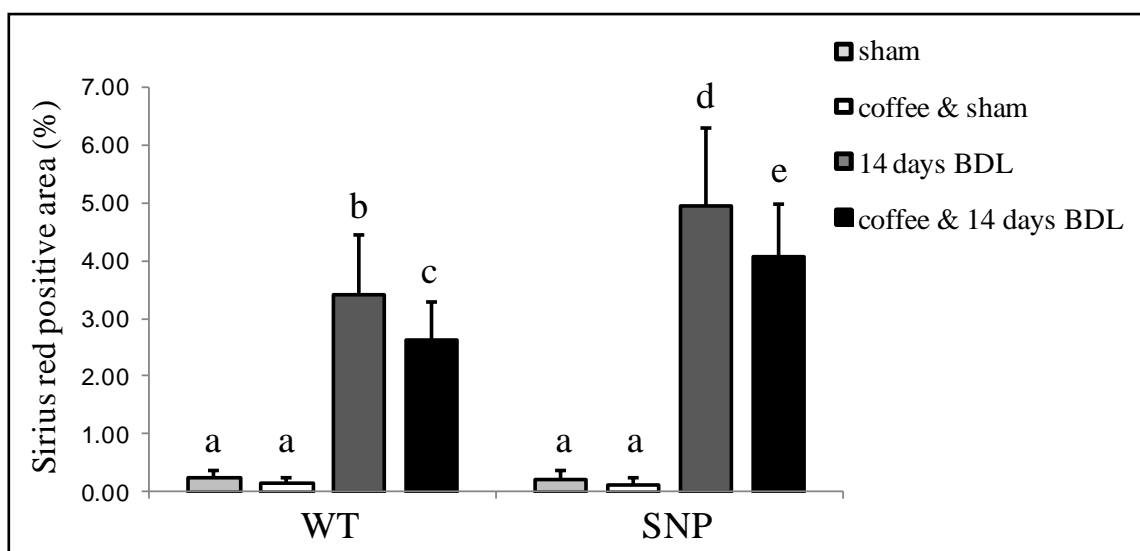


Figure 18: ImageJ-based quantification of Sirius red histological staining in *htgUGT1A*-WT and SNP mice after sham operation (sham) or 14 days bile duct ligation (BDL) with and without coffee pre- and co-treatment. *HtgUGT1A*-SNP mice showed significantly more Sirius red positive staining compared to equivalently treated *htgUGT1A*-WT mice. Each column represents the mean \pm SD of 5 randomly picked pictures per mouse. For all variables with the same letter, the difference between the means is not statistically significant. If two variables have different letters, their comparison is statistically significant; $p < 0.05$.

3.1.3.2 Hepatic collagen expression of *htgUGT1A* mice during cholestatic liver fibrosis

Expression levels of *COL1A1* further supported the results obtained in ImageJ performed computational Sirius red analysis (Fig. 19). Following BDL, transcriptional upregulation of hepatic *COL1A1* expression was measured in both mouse lines. Interestingly, higher mRNA induction was detected in the presence of SNPs (WT 12.4-fold and SNP 22.2-fold). Despite this, a downregulation of *COL1A1* transcription after the simultaneous treatment with coffee and BDL was observed, even though *htgUGT1A*-SNP mice still had higher expression levels

(1.5-fold) compared to their equivalently treated WT counterparts. These data are consistent with the histological and computational analysis and underpin the results on mRNA level.

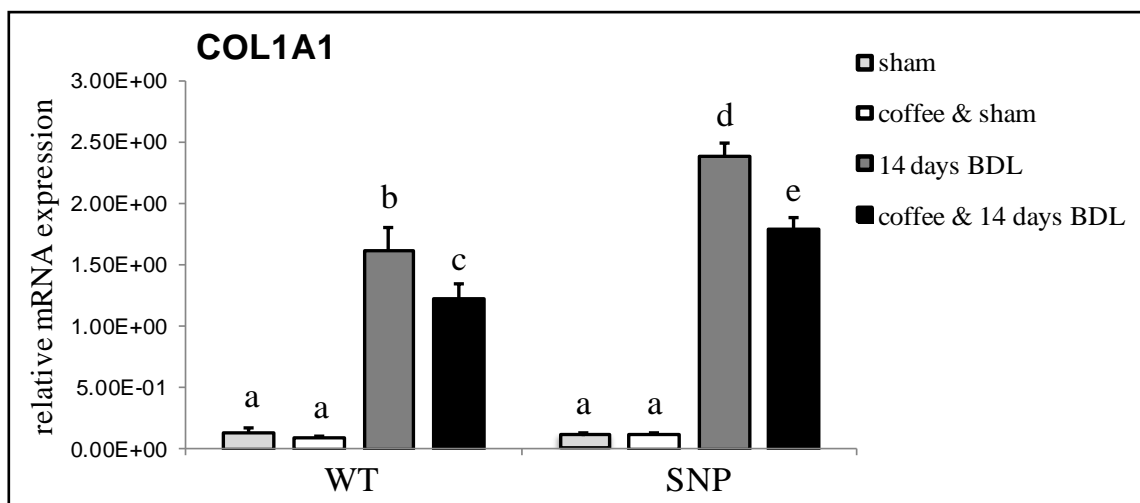


Figure 19: Expression levels of hepatic collagen in *htgUGT1A*-WT and SNP mice after sham operation (sham) or 14 days bile duct ligation (BDL) with and without coffee pre- and co-treatment. The figure shows TaqMan PCR-measured mRNA expression levels of collagen type 1 alpha 1 (*COL1A1*) relative to mouse β -actin. Compared to *htgUGT1A*-WT mice, *COL1A1* expression levels are significantly higher in *htgUGT1A*-SNP mice after BDL. As a result of coffee co-treatment, reduced expression levels were detected in *htgUGT1A*-WT and SNP mice, although last-mentioned still exhibited higher transcriptional *COL1A1* activity. Each column represents the mean \pm SD (n=3). For all variables with the same letter, the difference between the means is not statistically significant. If two variables have different letters, their comparison is statistically significant; $p < 0.05$.

3.1.4 Hepatic expression of profibrotic marker genes in cholestatic *htgUGT1A* mice

To further evaluate differences in the development of liver fibrosis, mRNA levels of key genes related to fibrogenesis were determined (Fig. 20). Compared to sham treatment, absolute expression levels of the profibrotic marker genes ACTA2, CTGF, beta-type platelet-derived growth factor receptor (PDGFRB) and platelet-derived growth factor subunit B (PDGFB) were significantly increased in the livers of BDL-operated *htgUGT1A*-WT and SNP mice. Interestingly, higher absolute expression levels were detected in the presence of the SNP-specific *UGT1A* haplotype, with significant differences for CTGF (1.2-fold) and PDGFRB (2.3-fold). In *htgUGT1A*-WT mice, coffee + BDL co-treatment reduced absolute expression levels of all depicted profibrotic marker genes (except for PDGFRB) compared to the water drinking BDL group. For ACTA2 (0.43-fold), CTGF (0.36-fold), PDGFB (0.84-fold) the downregulation of mRNA expression was significant. Similarly to the results observed in coffee drinking *htgUGT1A*-WT mice simultaneously treated with BDL, significantly decreased transcription levels were detected in equivalent treated *htgUGT1A*-SNP mice. Particularly noteworthy is the fact that the inhibitory influence of coffee pre- and co-treatment on the expression of profibrotic marker genes was less prominent in the presence

of SNPs where higher absolute expression levels for ACTA2 (2.2-fold) and CTGF (2.3-fold) were measured.

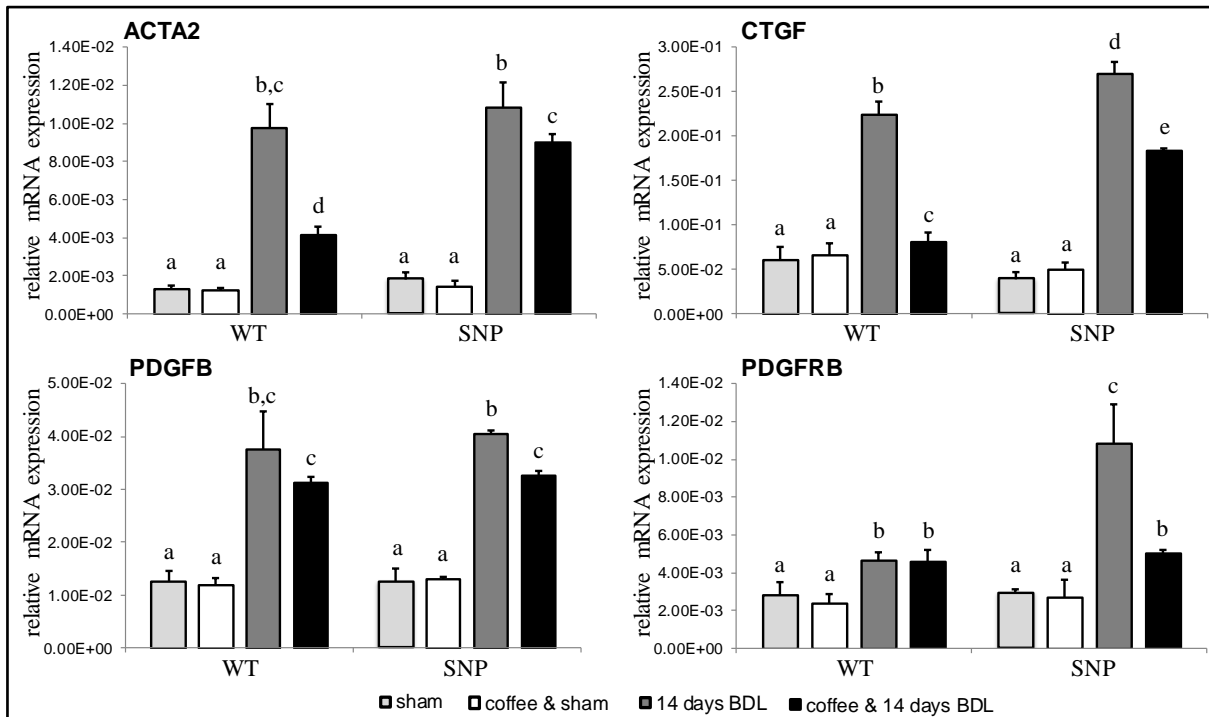


Figure 20: Hepatic expression of marker genes for fibrogenic activity in *htgUGT1A*-WT and SNP mice after sham operation (sham) or 14 days bile duct ligation (BDL) with and without coffee pre- and co-treatment. The graphs display mRNA expression levels of the profibrotic marker genes alpha-actin-2 (ACTA2, α -SMA), connective tissue growth factor (CTGF), platelet-derived growth factor subunit B (PDGFB) and beta-type platelet-derived growth factor receptor subunit B (PDGFRB) relative to mouse β -actin. Both mouse lines show significantly increased transcriptional regulation after BDL, whereas coffee + BDL co-treatment reduced absolute expression levels (except for PDGFRB in *htgUGT1A*-WT mice). Compared to *htgUGT1A*-WT mice, the coffee-mediated downregulation of fibrosis marker genes was less pronounced in mice carrying multiple genetic *UGT1A* SNP variants. As a consequence, *htgUGT1A*-SNP mice showed higher absolute expression levels after 14 days BDL with and without coffee co-treatment. Each column represents the mean \pm SD (n=3). For all variables with the same letter, the difference between the means is not statistically significant. If two variables have different letters, their comparison is statistically significant; $p < 0.05$.

3.1.5 Hepatic expression of proinflammatory marker genes in cholestatic *htgUGT1A* mice

Despite the activation of HSCs and the above shown increase of profibrotic marker genes, the initiation of inflammatory processes such as KC activation, immune cell infiltration, elaboration of chemokines and cytokines as well as an increase of inflammation marker genes is usually observed as a consequence of liver injury. Similar to the mRNA induction detected for the marker genes indicating fibrogenic activity, a significant transcriptional activation of the proinflammatory markers TNF- α and CCL2 was observed in *htgUGT1A*-WT and SNP mice after 14 days of biliary obstruction (Fig. 21). Compared to *htgUGT1A*-WT mice,

absolute expression of TNF- α (1.1-fold) and CCL2 (2.2-fold) was significantly higher in the presence of SNPs. In coffee co-treated *htgUGT1A*-WT mice a considerable downregulation of mRNA expression was detected for TNF- α (0.7-fold) and CCL2 (0.7-fold) compared to the water drinking BDL group. Furthermore, significant downregulation after coffee + BDL co-treatment was also observed in mice carrying multiple genetic *UGT1A* SNP variants, although coffee-mediated reduction of gene expression did not reach the levels measured in animals with normal UGT1A activity. The direct comparison between *htgUGT1A*-WT and SNP mice showed a 1.2-fold higher mRNA induction for TNF- α and 1.6-fold upregulated mRNA expression in case of CCL2.

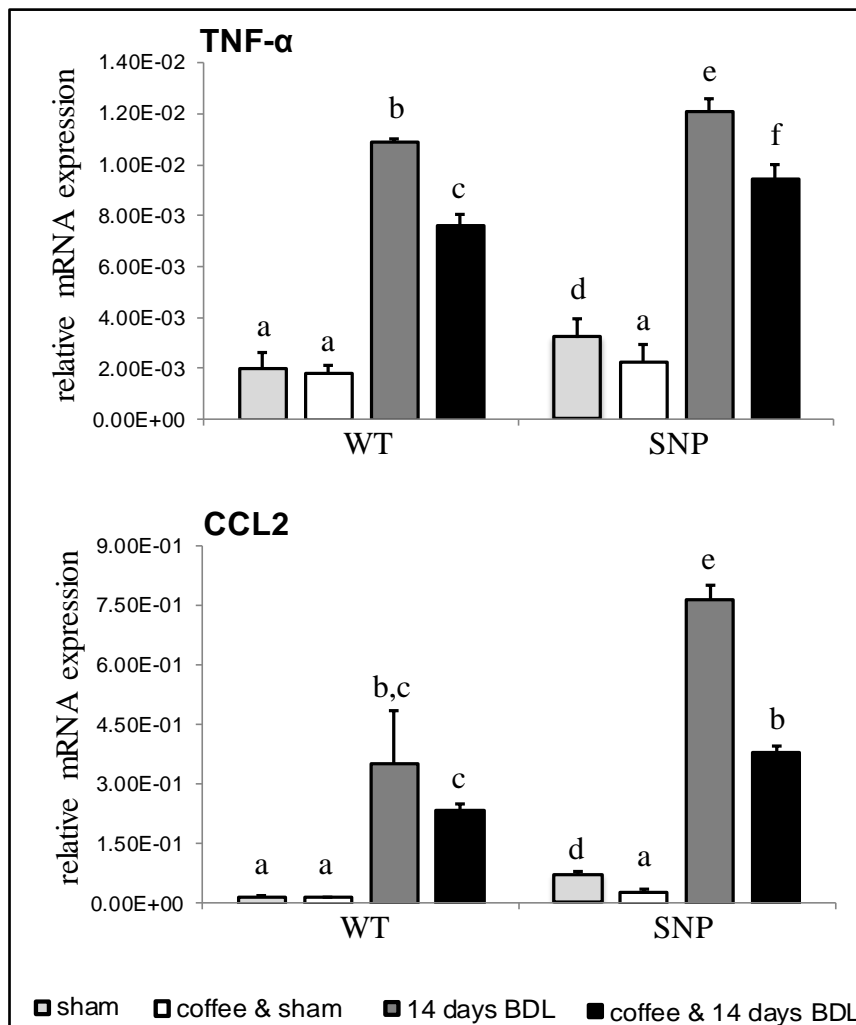


Figure 21: Hepatic expression of proinflammatory marker genes in *htgUGT1A*-WT and SNP mice after sham operation (sham) or 14 days bile duct ligation (BDL) with and without coffee pre- and co-treatment. The graph displays mRNA expression levels of tumor necrosis factor alpha (TNF- α) and C-C chemokine ligand 2 (CCL2) relative to mouse β -actin. 14 days BDL caused a significant upregulation of TNF- α and CCL2 expression in both mouse lines, which was significantly higher in *htgUGT1A*-SNP mice. In contrast, coffee co-treatment induced considerable downregulation in both animal models, although absolute expression levels in *htgUGT1A*-SNP mice remained above those observed in *htgUGT1A*-WT animals. Each column represents the mean \pm SD (n=3). Groups without the same letter are significantly different; $p < 0.05$.

3.1.6 Hepatic oxidative stress levels in cholestatic *htgUGT1A* mice

A key process capable of activating a wide array of profibrotic pathways is oxidative stress. Oxidative injury induced by ROS is a strong inducer of HSC activation which is considered as critical event in liver fibrogenesis [213]. To evaluate differences in the antioxidative capacity based on the ability of UGT1A enzymes to function as indirect antioxidants, and also to analyze the protective effects of coffee on oxidative stress as an initiator of liver fibrogenesis, total hepatic peroxidase concentrations were determined. As indicated in figure 22, coffee administration resulted in an elevation of total peroxidase concentration in the livers of *htgUGT1A*-WT and SNP mice.

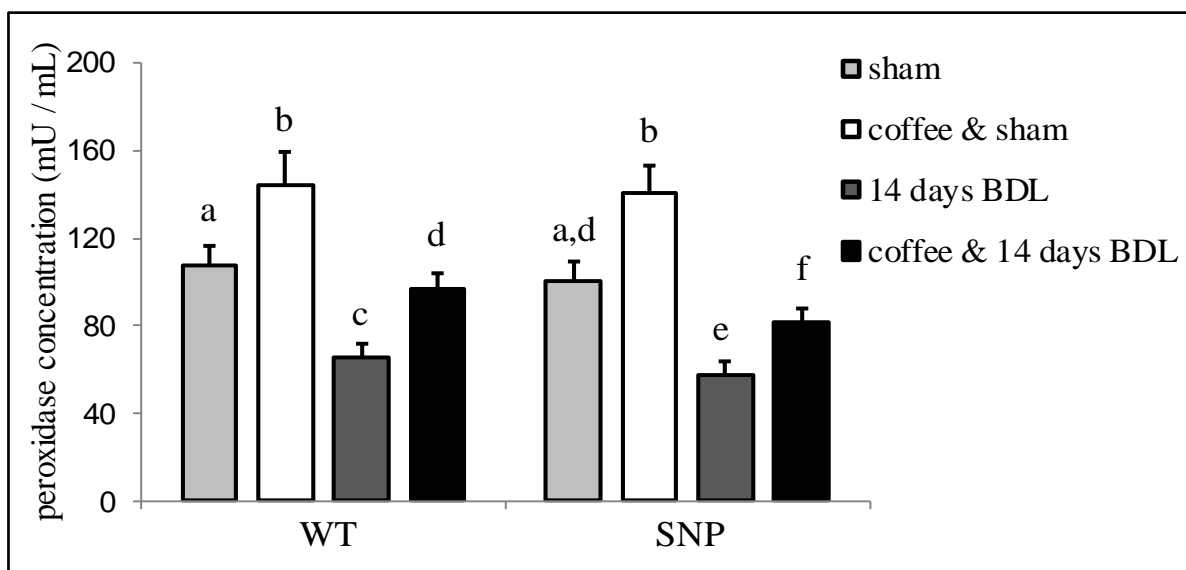


Figure 22: Total hepatic peroxidase concentration of *htgUGT1A*-WT and SNP mice after sham or 14 days bile duct ligation (BDL) operation with and without coffee pre- and co-treatment. Coffee administration caused elevated peroxidase concentrations in both mouse lines compared to water drinking sham mice. After BDL, *htgUGT1A*-WT and SNP mice showed significantly reduced peroxidase concentrations, which were even more decreased in the presence of SNPs. Coffee pre- and co-treatment elevated hepatic peroxidase concentrations in both, *htgUGT1A*-WT and SNP mice, although peroxidase levels in *htgUGT1A*-SNP mice still were significantly lower as those measured in *htgUGT1A*-WT animals. Each column represents the mean \pm SD (n=7). Groups without the same letter are significantly different; $p < 0.05$.

Expectedly, 14 days of surgically-induced cholestasis was accompanied by significantly decreased peroxidase concentrations compared to sham mice. Remarkably, hepatic peroxidase levels were lower in BDL *htgUGT1A*-SNP mice than those measured in mice carrying the human wild type *UGT1A* gene locus (WT 65.5 mU/mL and SNP 57.8 mU/mL). Moreover, coffee + BDL co-treatment significantly attenuated oxidative stress in both animal models, but the comparison of peroxidase concentrations between both mouse lines unveiled significantly higher levels in *htgUGT1A*-WT mice (96.6 mU/mL) as those measured in

htgUGT1A-SNP mice (81.9 mU/mL). These results indicate an altered modification of the metabolic antioxidative balance between the two different *UGT1A* mouse lines which is critically influenced by coffee administration.

4-HNE is a major aldehydic product of lipid peroxidation known to exert cytotoxic effects [214]. 4-HNE immunofluorescence staining was performed for determination of oxidative liver injury resulting from lipid peroxidation (Fig. 23, 100-fold magnification). After BDL, a higher 4-HNE immunofluorescence signal was detected in *htgUGT1A*-SNP mice compared to equivalent treated WT counterparts. Coffee co-administration reduced 4-HNE amount in both mouse lines, although *htgUGT1A*-SNP mice still showed higher levels of the lipid peroxidation product.

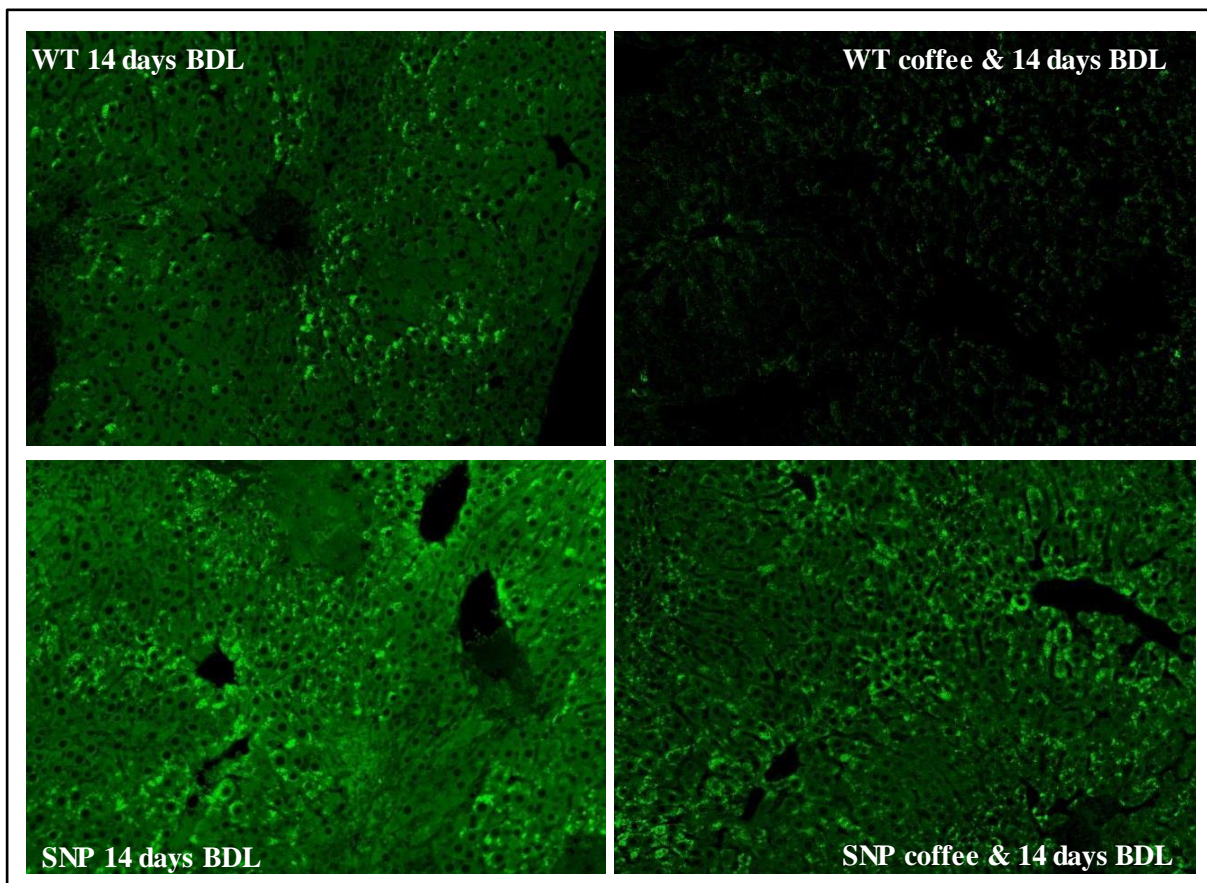


Figure 23: Representative pictures of 4-HNE immunofluorescent stained liver sections of *htgUGT1A*-WT and SNP mice after 14 days bile duct ligation (BDL) with and without coffee pre- and co-treatment. BDL-operated *htgUGT1A*-SNP mice showed higher 4 hydroxynonenal (4-HNE) levels as equivalent treated *htgUGT1A*-WT mice. Coffee + BDL co-treatment visibly reduced oxidative liver injury in both mouse lines, although a stronger 4-HNE antibody fluorescence signal in the presence of SNPs was detected (magnification 100-fold).

3.2 High-fat Paigen diet-induced liver injury

In order to study the effect of hepatic *UGT1A* gene expression on development and progression of diet-induced hepatic steatosis, six mice per genotype received a sodium cholate and cholesterol containing HFPD for 24 weeks. The control group fed with normal chow encompassed 4 animals per genotype.

3.2.1 Hepatic *UGT1A* expression in HFPD-treated *htgUGT1A* mice

The effect of 24 weeks HFPD on transcriptional *UGT1A* expression in *htgUGT1A*-WT and SNP mice is illustrated in figure 24. A significant HFPD-induced mRNA induction in the livers of *htgUGT1A*-WT mice was detected for UGT1A1 (11.8-fold), UGT1A3 (2.9-fold), UGT1A4 (4.1-fold), UGT1A6 (2.6-fold), UGT1A7 (2.6-fold) and UGT1A9 (9.0-fold) compared to mice fed with normal chow. In contrast, UGT1A induction was reduced (UGT1A1, UGT1A7 and UGT1A9) or absent in *htgUGT1A*-SNP mice. As expected, the comparison between both mouse lines revealed significantly lower absolute expression levels of all investigated isoforms (not significant for UGT1A7) in *htgUGT1A*-SNP mice after 24 weeks of HFPD feeding.

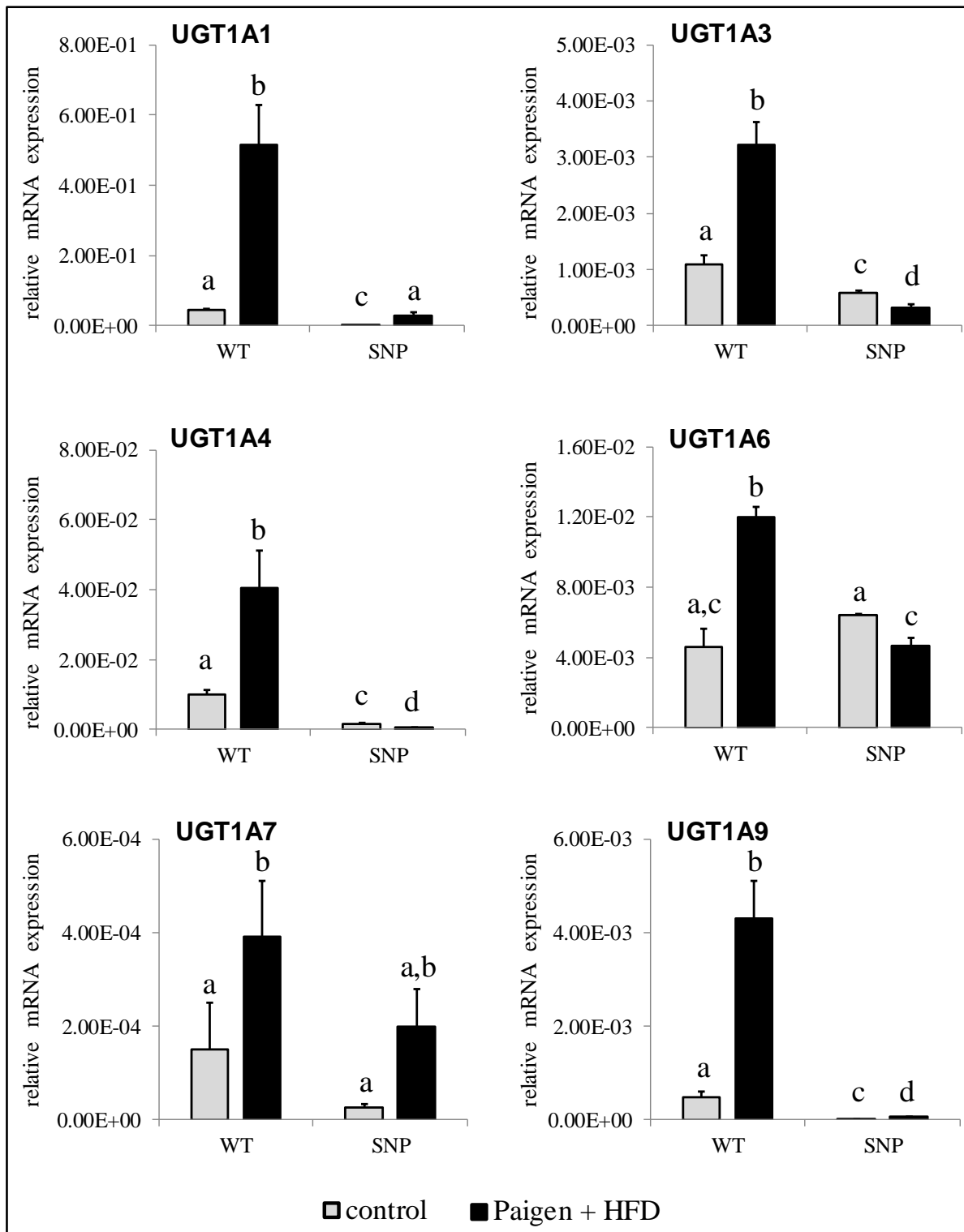


Figure 24: Hepatic UGT1A mRNA expression in *htgUGT1A*-WT and SNP mice after 24 weeks of control or high-fat Paigen diet (HFPD). The graphs illustrate the mRNA expression of *UGT1A* genes relative to mouse β -actin. Compared to *htgUGT1A*-WT mice where significantly increased mRNA expression levels of all investigated *UGT1A* isoforms after HFPD administration were determined, differential induction was observed in *htgUGT1A*-SNP mice. Here, absolute expression levels remained below those observed in mice carrying the human *UGT1A* wild type gene locus. Each column represents the mean \pm SD (n=3). For all variables with the same letter, the difference between the means is not statistically significant. If two variables have different letters, their comparison is statistically significant; $p < 0.05$.

The following figure displays the hepatic UGT1A3 protein expression of control chow and HFPD-fed *htgUGT1A*-WT and SNP mice determined by Western blot analysis (Fig. 25). In the experimental setting of abundant exposure to dietary lipids the UGT1A3 isoform is of higher importance because it's the only isoform in the *UGT1A* gene locus capable of glucuronidating BAs [215]. In line with the findings obtained on mRNA level, UGT1A3 protein quantity was considerably higher after HFPD exposure in *htgUGT1A*-WT mice. Moreover, in comparison to *htgUGT1A*-SNP mice fed with normal chow, UGT1A3 protein expression seems to be reduced in the presence of SNPs after 24 weeks of HFPD.

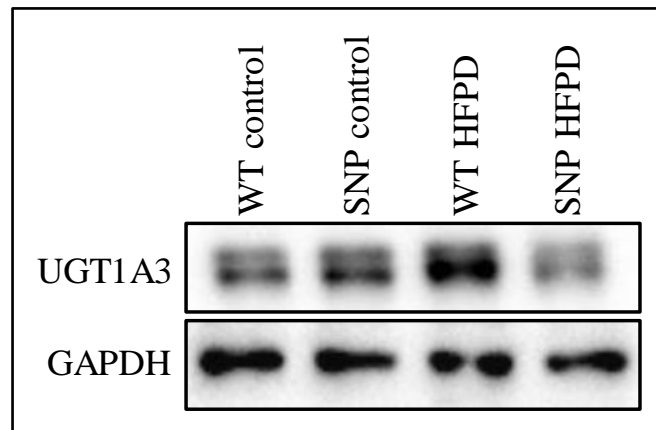


Figure 25: Hepatic UGT1A3 protein expression in *htgUGT1A*-WT and SNP mice after 24 weeks of control or high-fat Paigen diet (HFPD). The livers of HFPD-treated *htgUGT1A*-WT showed a considerable higher amount of UGT1A3 protein as respectively treated SNP animals. Glyceraldehyde 3-phosphate dehydrogenase (GAPDH) was used as loading control.

3.2.2 Serum aminotransferase activities in HFPD-treated *htgUGT1A* mice

Results of the biochemical blood serum analysis of aminotransferase activities are shown in figure 26. Measurement of AST (1.7-fold) and ALT (3.7-fold) levels revealed significant elevations after HFPD feeding in *htgUGT1A*-WT mice, whereas AST (1.3-fold) and ALT (1.3-fold) enzyme activities in *htgUGT1A*-SNP mice were only slightly elevated in comparison with control diet fed mice. Interestingly, HFPD-treated *htgUGT1A*-SNP mice showed significantly lower serum aminotransferase activities as equivalently treated *htgUGT1A*-WT animals (AST: 0.76-fold and ALT: 0.35-fold).

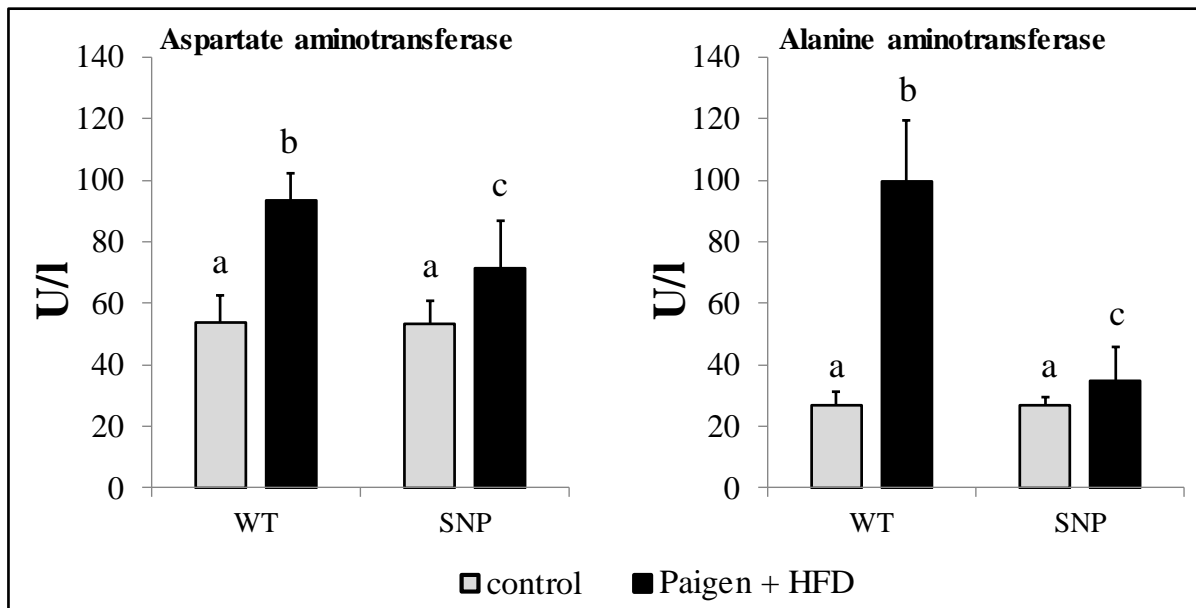


Figure 26: Serum aminotransferase activity levels of high-fat Paigen diet (HFPD)-treated *htgUGT1A*-WT and SNP mice. The diagram illustrates alanine aminotransferase (ALT) and aspartate aminotransferase (AST) levels as units per liter serum. After HFPD, both transaminases were significantly elevated in *htgUGT1A*-WT and SNP mice. Interestingly, lower AST and ALT levels were detected in mice with multiple genetic *UGT1A* gene variants. Each column represents the mean \pm SD (n=4 for control; n=6 for HFPD). For all variables with the same letter, the difference between the means is not statistically significant. If two variables have different letters, their comparison is statistically significant; $p < 0.05$.

3.2.3 Hepatic fat deposition in HFPD-treated *htgUGT1A* mice

Macroscopic examination of the livers unveiled a clearly visible higher fat incorporation in *htgUGT1A*-WT mice compared to their SNP counterparts after exposition to HFPD (Fig. 27). In consistence with these observations, histological assessment of the hepatic fat content by means of light microscopy revealed advanced steatosis (with steatohepatitis) in *htgUGT1A*-WT mice (Fig. 28). H&E stained liver sections of *htgUGT1A*-WT mice showed a high proportion of steatotic hepatocytes, discernible by a mix of small and large lipid droplets within the cytoplasm. Since hepatic lipid accumulation in *htgUGT1A*-SNP mice wasn't spread all over the entire liver section, it can be presumed that SNP carriers developed milder hepatic steatosis as similarly-treated *htgUGT1A*-WT mice.

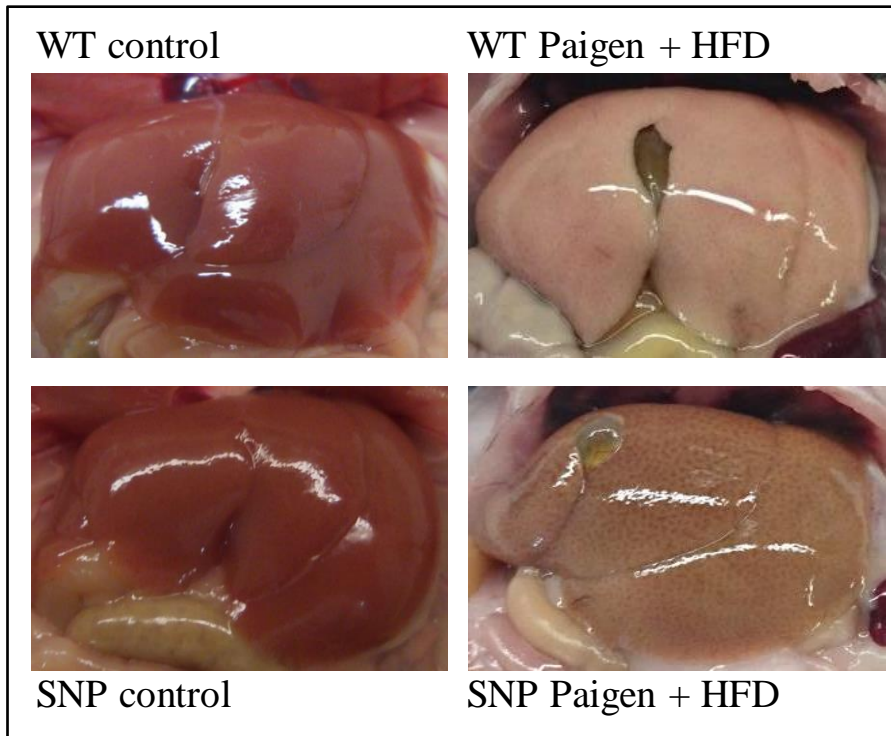


Figure 27: Macroscopic pictures of *htgUGT1A*-WT and SNP mice livers 24 weeks after control or high-fat Paigen diet (HFPD). Reduced lipid incorporation in the livers of *htgUGT1A*-SNP mice compared to *htgUGT1A*-WT mice.

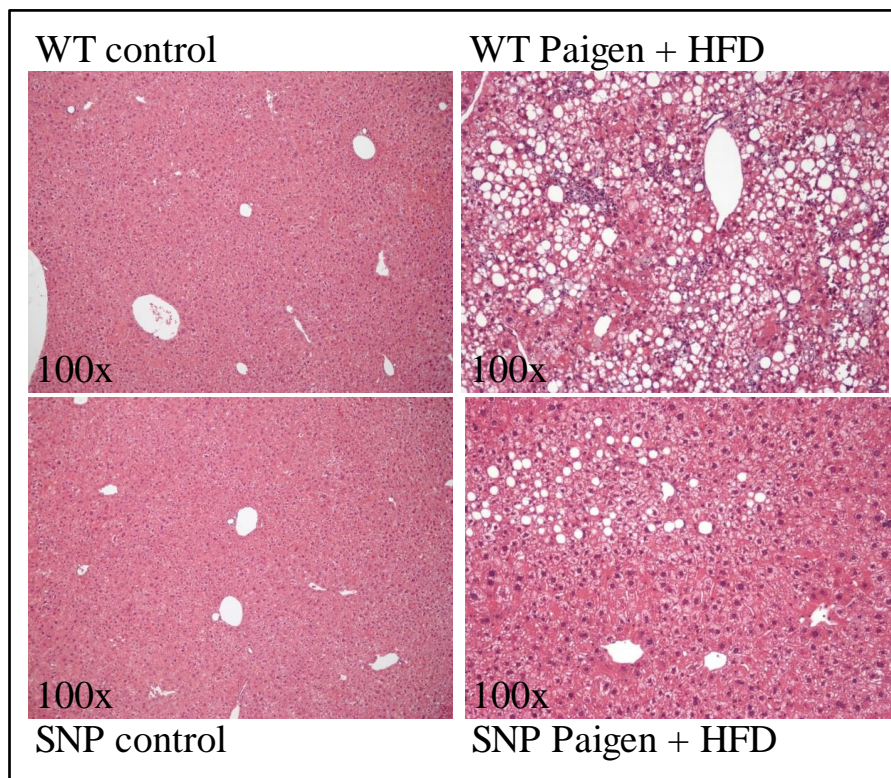


Figure 28: Representative H&E stained liver sections of *htgUGT1A*-WT and SNP mice 24 weeks after control or high-fat Paigen diet (HFPD). Mice with the Gilbert syndrome-associated SNP haplotype showed less steatotic hepatocytes as their equivalently treated *UGT1A*-WT counterparts.

In line with the differential hepatic lipid incorporation, hepatic triglyceride levels significantly differed between *htgUGT1A*-WT and SNP mice (Fig. 29). Although the hepatic content of triglycerides was radically elevated in both mouse lines, *htgUGT1A*-WT (277%) and SNP (191%), significantly lower hepatic triglycerides (31%) were determined in mice containing multiple *UGT1A* SNP variants.

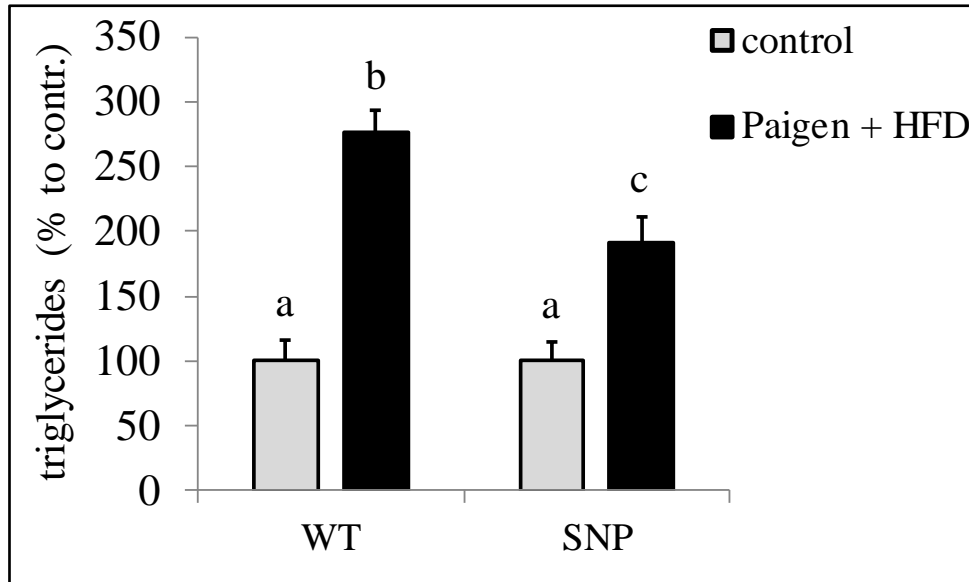


Figure 29: Hepatic triglyceride content of *htgUGT1A*-WT and SNP mice after 24 weeks of control or high-fat Paigen diet (HFPD). The hepatic triglyceride content is expressed as percentage proportion referred to mice fed with normal chow. Both mouse lines showed increased triglyceride levels after 24 weeks of HFPD. Remarkably, compared to *htgUGT1A*-WT mice significantly lower levels were detected in the presence of SNPs. Each column represents the mean \pm SD (n=3). Groups without the same letter are significantly different; $p < 0.05$.

3.2.4 Hepatic inflammation in HFPD-treated *htgUGT1A* mice

The H&E stained liver sections depicted in figure 30 show representative areas of HFPD-treated *htgUGT1A*-WT and SNP mice in 200-fold magnified view. In both mouse lines, the pictures focus on the fatty areas of the respective hepatic section in which the cytoplasm is illustrated in bright pink, cell nuclei are imaged in deep purple and inflammation cells are mapped in dark blue. As the beneath displayed figure implies, there is a differential degree of inflammation cell recruitment in both mouse lines. While the livers of *htgUGT1A*-SNP mice hardly showed any accumulation of infiltrating inflammation cells, an advanced state of liver inflammation, indicated by the massive infiltration of inflammatory cells, was observed in *htgUGT1A*-WT mice suggesting the development of NASH.

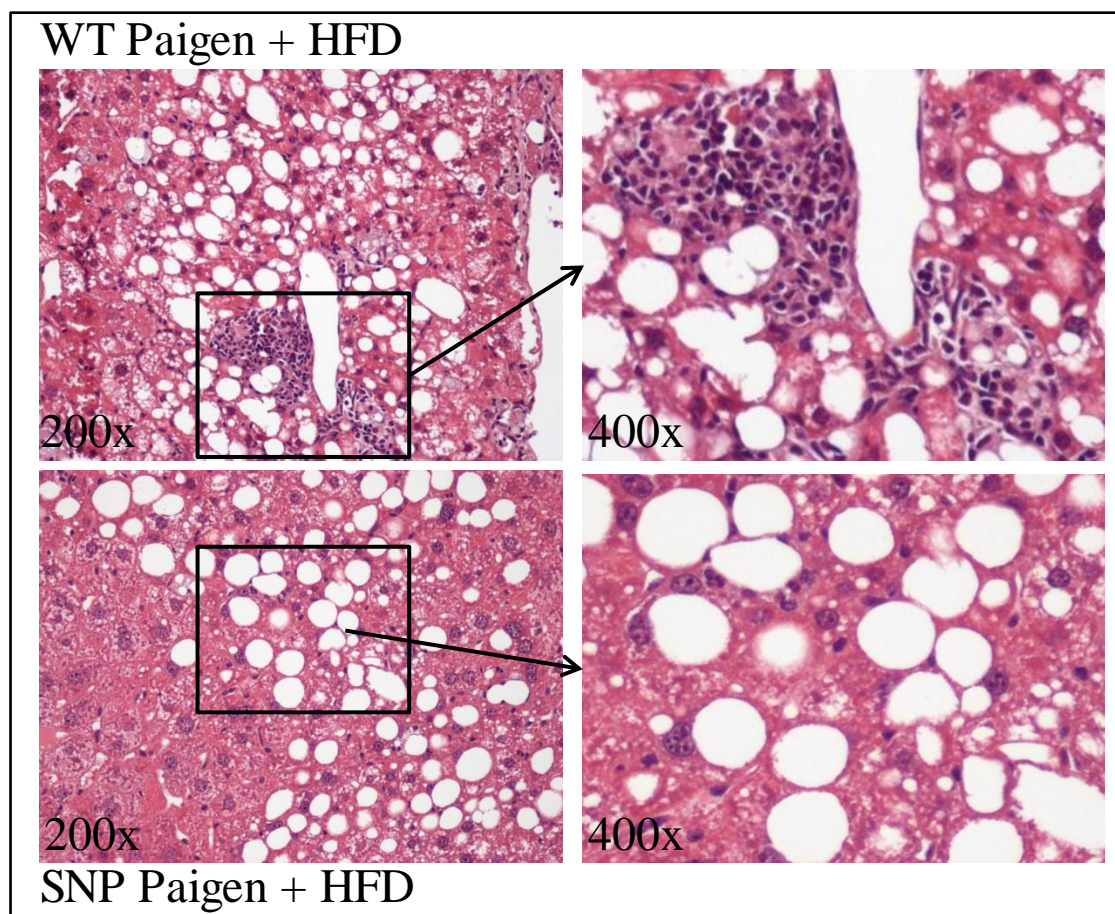


Figure 30: Hematoxylin & Eosin stained liver sections of *htgUGT1A*-WT and SNP mice after 24 weeks of high-fat Paigen diet (HFPD). The figure shows two representative areas of liver tissue from the distinct mouse lines in 200-fold (left) or 400-fold (right) magnified view. Infiltration of inflammation cells (stained in dark blue) was observed to a considerable extent in tissue samples of *htgUGT1A*-WT mice. In contrast, hardly any liver infiltrating inflammatory cells were observed in *htgUGT1A*-SNP mice.

3.2.4.1 Hepatic expression of proinflammatory marker genes in HFPD-treated *htgUGT1A* mice

Apart from the above-mentioned differences in the recruitment of inflammation cells, the microscopic observations were supported by significant differences in transcriptional activation of the proinflammatory marker genes CCL2 and TNF- α (Fig. 31). In mice carrying the human *UGT1A* wild type gene locus, a 17.4-fold CCL2 upregulation and a 10.8-fold TNF- α mRNA induction was detected, whereas the transcriptional activation of CCL2 (6.4-fold) and TNF- α (2.4-fold) was significantly less evident in *htgUGT1A*-SNP mice.

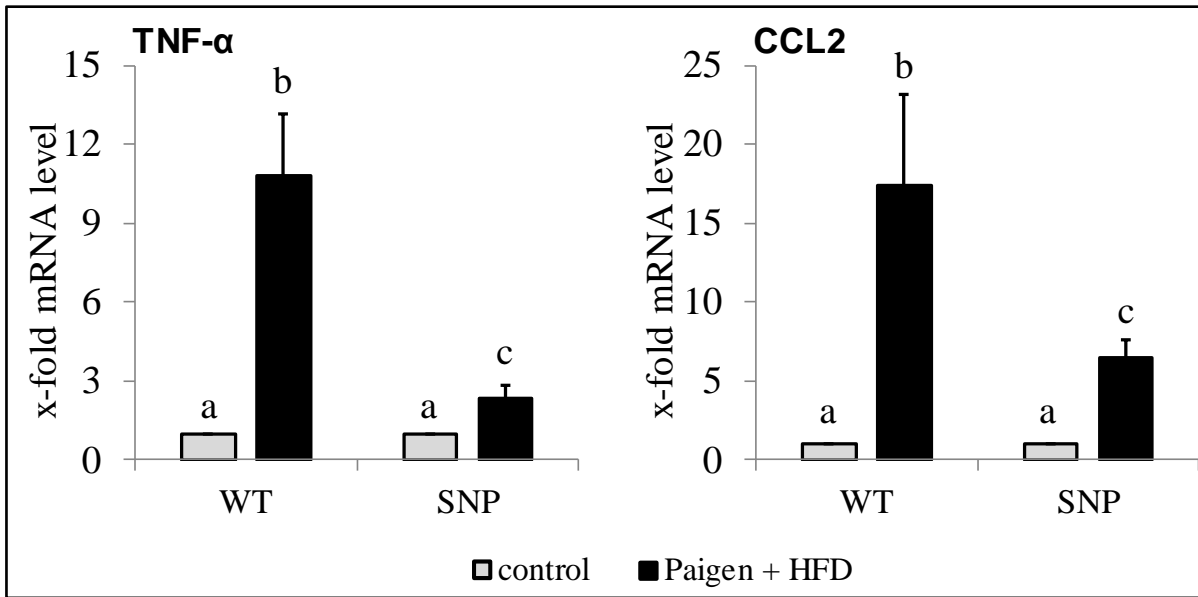


Figure 31: Hepatic expression of proinflammatory marker genes in *htgUGT1A*-WT and SNP mice after 24 weeks of control or high-fat Paigen diet (HFPD). Values are shown as fold induction mRNA expression to control diet fed mice. In both mouse lines a significant increase of tumor necrosis factor alpha (TNF- α) and C-C chemokine ligand 2 (CCL2) mRNA levels was detected. Of note, hepatic mRNA induction of both inflammatory markers was significantly higher in HFPD-treated *htgUGT1A*-WT mice. Each column represents the mean \pm SD (n=3). Groups without the same letter are significantly different; $p < 0.05$.

3.2.5 Quantification of liver fibrosis in HFPD-treated *htgUGT1A* mice

With the intention of determining differences in fibrosis development and hepatic collagen deposition, computational quantification of Sirius red staining and gene expression analysis of profibrotic markers were evaluated. Figure 32 displays representative liver sections of control chow or HFPD fed *htgUGT1A*-WT and SNP mice after Sirius red staining. As this figure implies, no excessive ECM accumulation was detected in control diet fed mice. Histological staining revealed a high proportion of fibrous collagens and the characteristic “chicken wire” pattern in *htgUGT1A*-WT mice after 24 weeks of HFPD feeding. In contrast, less collagen fibers and consequently a milder fibrogenesis process is perceptible in the presence of SNPs.

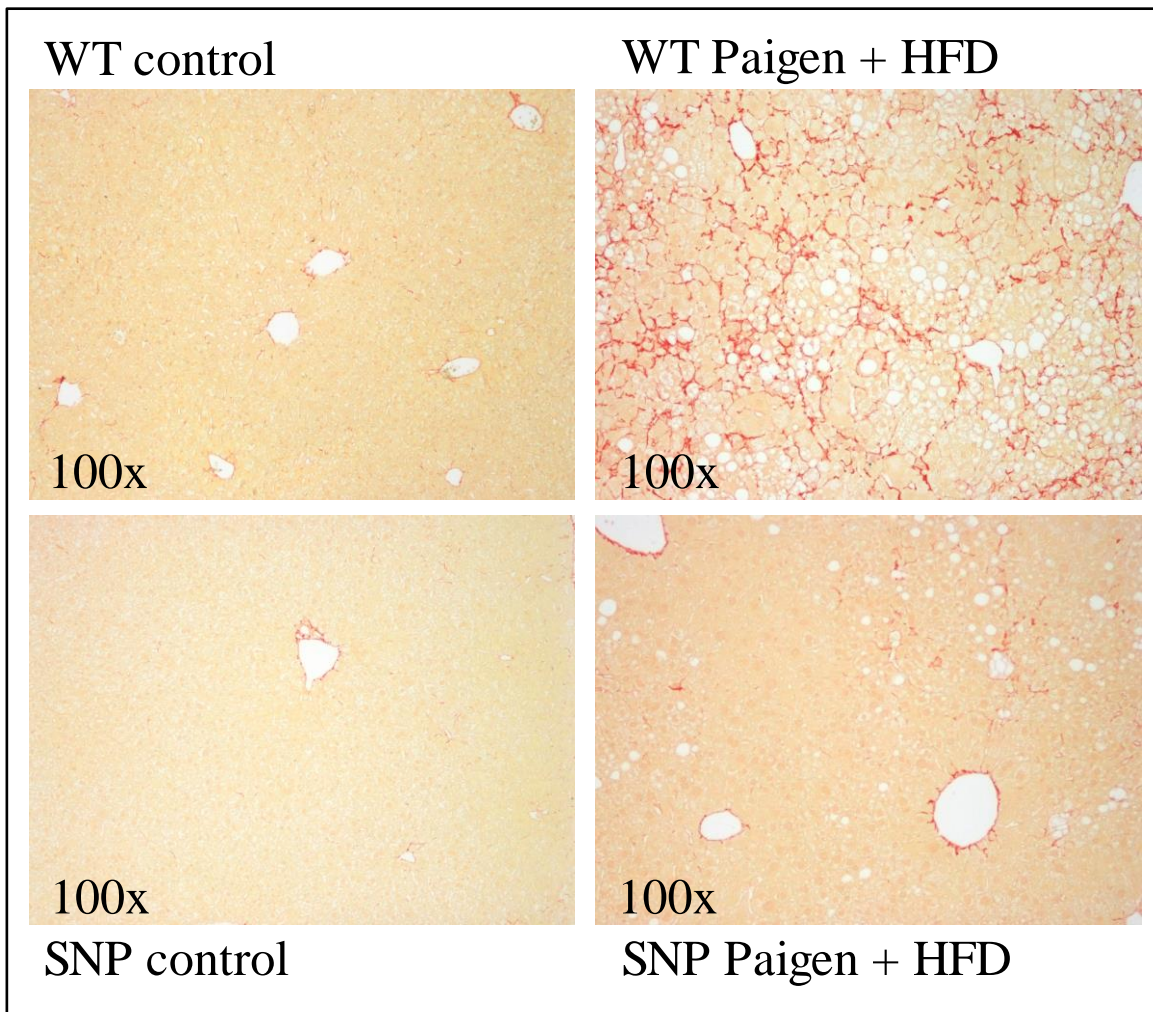


Figure 32: Representative liver sections of Sirius red histological staining of *htgUGT1A*-WT and SNP mice after 24 weeks of control or high-fat Paigen diet (HFPD). Each of the four pictures is shown in 100-fold magnification. As illustrated on the panel in the upper right corner, a high proportion of red stained ECM proteins was detected in HFPD-treated *htgUGT1A*-WT mice whereas only a few collagen fibers can be seen in *htgUGT1A*-SNP mice.

Computational quantification of the Sirius red staining further supported the histological finding of an increased formation of hepatic collagens in HFPD fed *htgUGT1A*-WT mice (Fig. 33, left chart). In fact, the percentage portion of the positive stained area was significantly lower in *htgUGT1A*-SNP mice (1.04%) compared to *htgUGT1A*-WT mice (8.73%). Furthermore, the direct comparison of *COL1A1* expression levels between the two distinct transgenic mouse lines further confirmed the results at a molecular level (fig 33, right chart). Although considerable higher induction of mRNA transcript levels were detected in *htgUGT1A*-WT and SNP mice after 24 weeks of HFPD feeding, the 18.4-fold mRNA induction in *htgUGT1A* -WT mice was significantly higher as the 6.2-fold mRNA induction level measured in mice with altered UGT1A expression and activity.

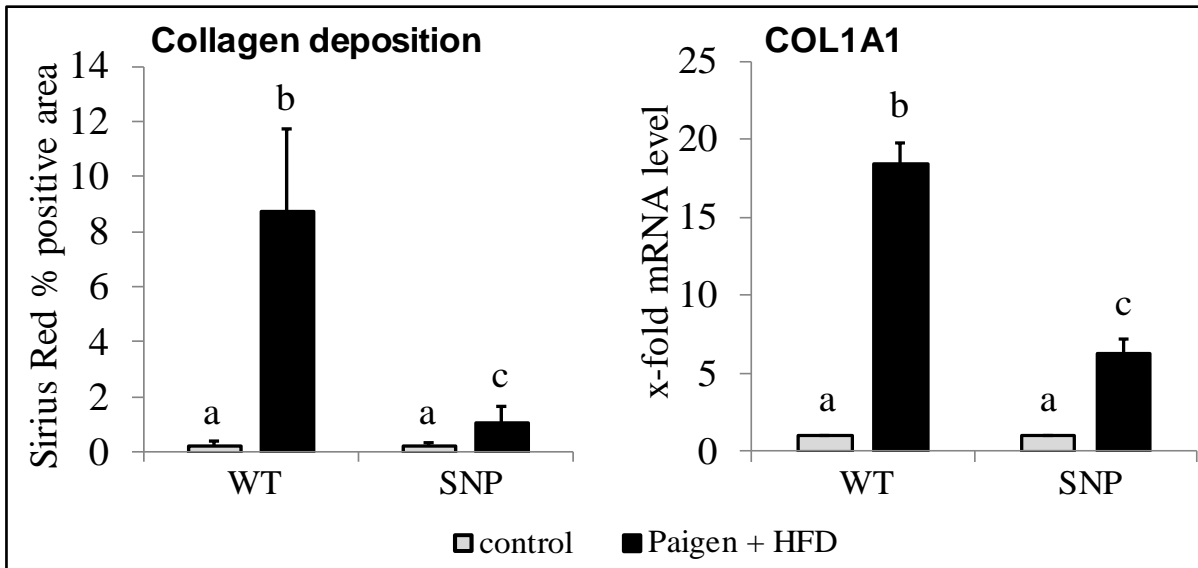


Figure 33: Computational evaluation of Sirius red stained areas and hepatic collagen expression in *htgUGT1A*-WT and SNP mice after 24 weeks of control or high-fat Paigen diet (HFPD). In both mouse lines HFPD administration caused a significant increase in hepatic collagen deposition. The computational analysis detected an average of 8.7% of positive Sirius red staining per area in *htgUGT1A*-WT mice, while in the presence of SNPs only 1.0% of the total area contained red colored collagen (left panel). In line with these findings, hepatic collagen type 1 alpha 1 (COL1A1) expression significantly differed between both mouse lines and revealed a 18.4-fold increased mRNA level in *htgUGT1A*-WT mice compared to a 6.2-fold elevated mRNA level in *htgUGT1A*-SNP mice (right panel). COL1A1 mRNA levels are shown as fold induction compared to control diet fed mice. Each column represents the mean \pm SD (n=3). For all variables with the same letter, the difference between the means is not statistically significant. If two variables have different letters, their comparison is statistically significant; $p < 0.05$.

3.2.5.1 Hepatic expression of profibrotic marker genes in HFPD-treated *htgUGT1A* mice

In addition to the significant hepatic accumulation of ECM proteins, the manifestation of liver fibrosis is usually associated with a considerable increase of cytokines and various key genes that influence fibrogenesis thereby indicating the state of fibrogenic activity. In *htgUGT1A*-WT mice, HFPD administration caused a significant higher transcriptional activation of the profibrotic markers TIMP1 (45.4-fold), CTGF (2.8-fold), PDGFB (9.2-fold) and TGF- β (2.7-fold) as observed in the presence of SNPs. In *htgUGT1A*-SNP mice the mRNA induction was reduced in case of TIMP1 (22.9-fold) and PDGFB (1.6-fold) or almost unaffected for TGF- β and CTGF (Fig. 34). In combination, these data suggest a protective effect of a common low-function Gilbert syndrome-associated SNP haplotype, present in 10% of the white population, resulting in attenuated hepatic fibrosis and inflammation during diet-induced NASH.

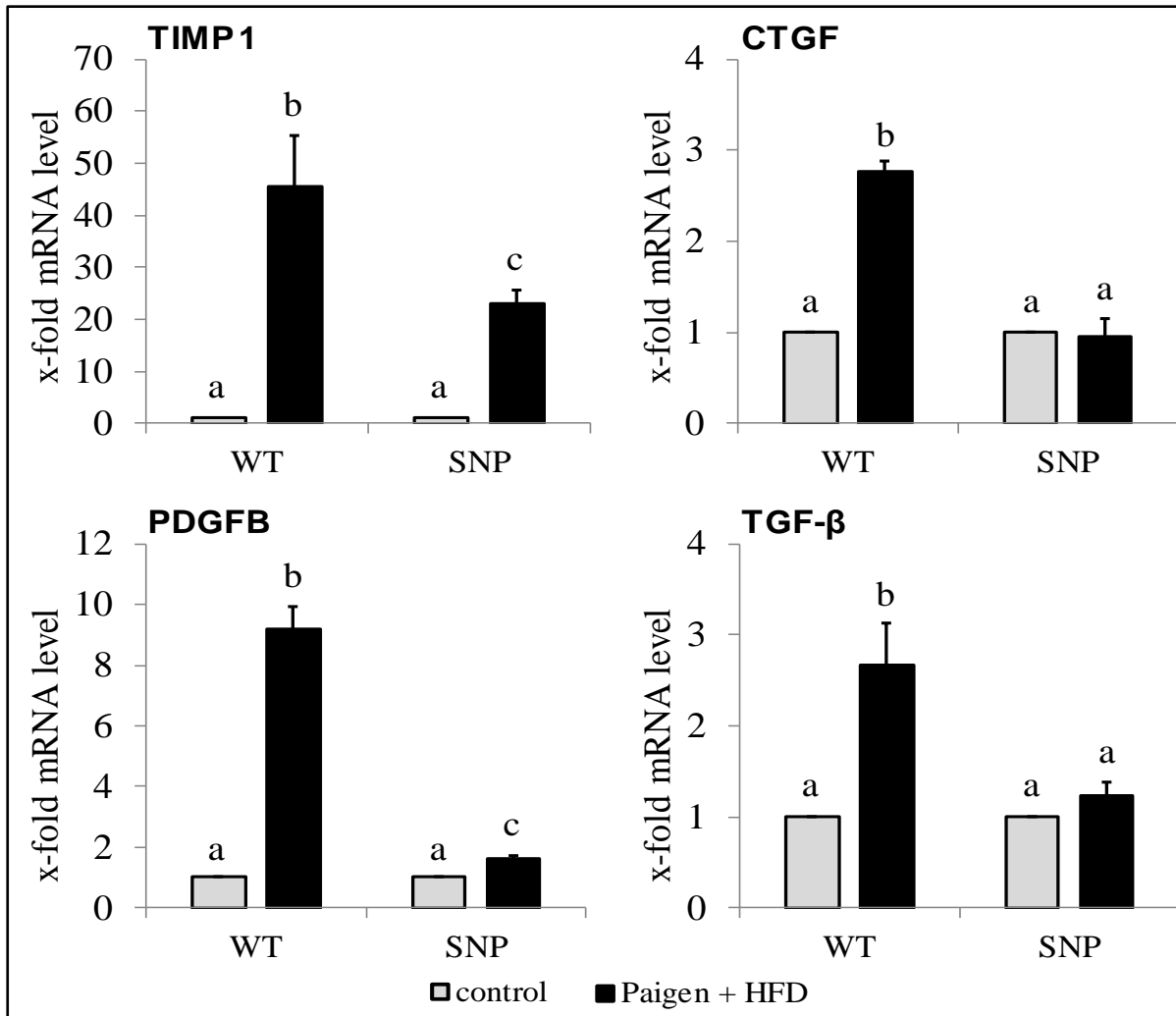


Figure 34: Hepatic expression of fibrosis marker genes in *htgUGT1A*-WT and SNP mice after 24 weeks of control or high-fat Paigen diet (HFPD). The figure shows the expression of the profibrotic marker genes tissue inhibitor metalloprotease 1 (TIMP1), connective tissue growth factor (CTGF), platelet-derived growth factor subunit B (PDGFB) and transforming growth factor beta (TGF- β) expressed as fold value of control diet fed mice. Significant higher expression levels in HFPD-treated *htgUGT1A*-WT compared to analogously treated *htgUGT1A*-SNP mice were measured for all investigated fibrogenic marker genes. Each column represents the mean \pm SD (n=3). For all variables with the same letter, the difference between the means is not statistically significant. If two variables have different letters, their comparison is statistically significant; $p < 0.05$.

3.2.6 Hepatic expression of nuclear receptors in HFPD-treated *htgUGT1A* mice

Nuclear receptors, especially FXR and PPAR α , have been identified as promising therapeutic targets for the treatment of NASH [216]. To elucidate potential differences in activation of molecular mechanisms involving FXR or PPAR α signaling, mRNA expression and nuclear protein levels were determined in *htgUGT1A*-WT and SNP mice (Fig. 35). FXR is a key mediator of BA-dependent effects during NAFLD. After diet-induced liver injury evoked by HFPD administration, a significant downregulation of FXR expression was detected in both

mouse lines (Fig. 35, left panel). Interestingly, the degree of inhibition reached 58% in *htgUGT1A*-WT mice, compared to only 36% detected in *htgUGT1A*-SNP mice.

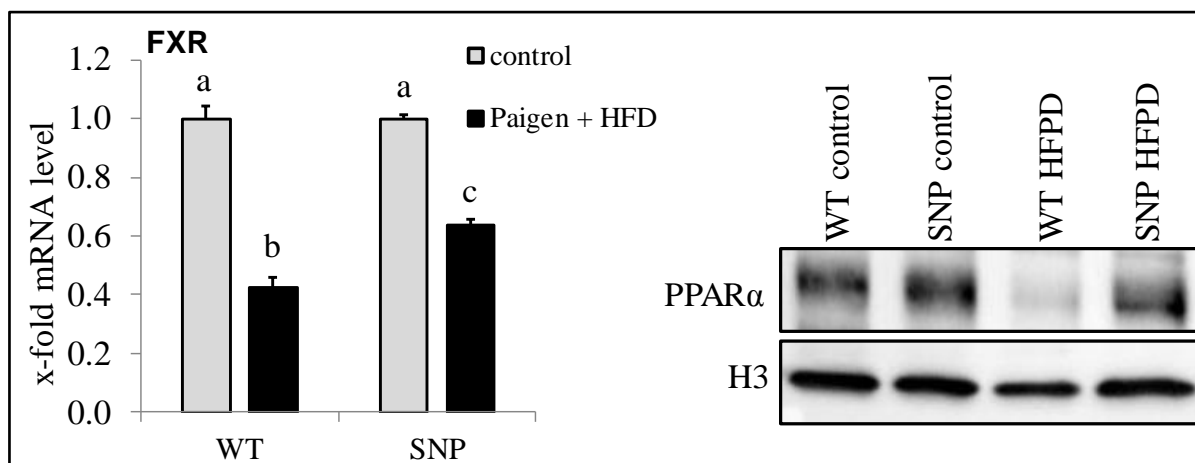


Figure 35: Hepatic mRNA expression and nuclear protein of nuclear receptors in *htgUGT1A*-WT and SNP mice after 24 weeks of control or high-fat Paigen diet (HFPD). The left panel shows the expression of farnesoid X receptor (FXR) expressed as fold value of control diet receiving mice. Enhanced inhibition of FXR mRNA expression was detected in *htgUGT1A*-WT mice (58%) compared to *htgUGT1A*-SNP mice (36%). Western blot analysis revealed significantly reduced nuclear peroxisome proliferator-activated receptor alpha (PPAR α) protein levels in HFPD-treated *htgUGT1A*-WT in contrast to unchanged levels in the presence of SNPs (right panel). Histone H3 (H3) was used as loading control. Each column represents the mean \pm SD (n=3). For all variables with the same letter, the difference between the means is not statistically significant. If two variables have different letters, their comparison is statistically significant; $p < 0.05$.

Furthermore, nuclear translocation of FXR downstream target PPAR α , which is known to mediate hepatic fatty acid oxidation, was downregulated in HFPD fed *htgUGT1A*-WT mice (Fig. 36, right panel). As shown by Western blot analysis, PPAR α protein quantity of nuclear extracts remained unchanged in mice carrying the *UGT1A* SNP haplotype. As expected, no differences in the nuclear protein quantity of the FXR downstream target gene PPAR α was detected in control chow exposed mice.

3.3 DEN-induced carcinogenic liver injury

Given the special importance of *UGT1A* enzymes in detoxification of environmental toxins and carcinogens, the effect of common *UGT1A* polymorphisms on HCC development was investigated using DEN-injected *htgUGT1A* mice. Hepatocarcinogenesis was chemically-induced by a single intraperitoneal DEN injection in male mice 15 days after birth. 21-day old DEN-treated mice of each genotype were then further divided in two subgroups either receiving water (n=9) or coffee co-treatment (WT: n=11; SNP n=10) for the following 39 weeks.

3.3.1 Incidence and size of HCC-like tumor formations in DEN-treated *htgUGT1A* mice

40 weeks after DEN injection considerable differences in tumorigenesis between both mouse lines and within the two subgroups (water or coffee co-treatment) were observed. Representative pictures of tumor bearing livers after abdominal opening are shown in the upper four images of figure 36. The respective liver lobes, which exhibit tumorous transformations, are depicted in the lower panels (black scale bar: 10 mm).

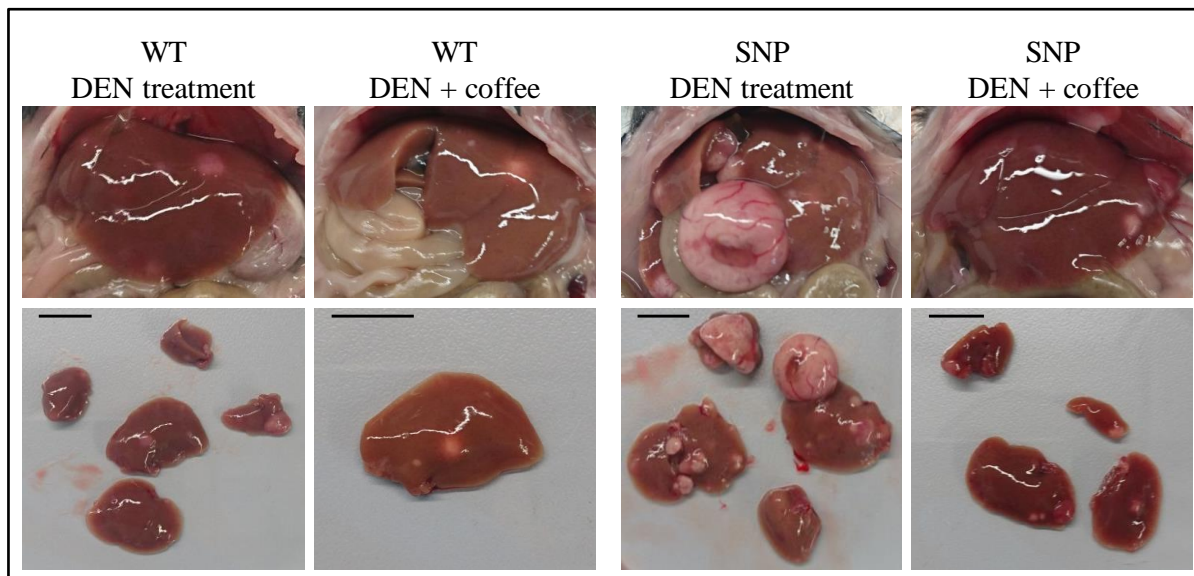


Figure 36: Representative liver images of *htgUGT1A*-WT and SNP mice 40 weeks after diethylnitrosamine (DEN) injection with and without coffee co-treatment. The upper four panels show the outcome of HCC-like tumor development immediately after laparotomy. Lobes affected by tumor nodules are separately shown in the lower 4 panels (black scale bar: 10 mm).

In DEN-treated *htgUGT1A*-SNP mice a total of 62 macroscopically visible tumor formations with a total cumulative diameter of 231 mm developed, whereas in *htgUGT1A*-WT mice only 44 tumors (86 mm in diameter) were observed (Fig. 37). After DEN + coffee co-treatment, the number of perceptible tumors markedly decreased in both mouse lines, but was still higher in mice carrying the *UGT1A* SNP haplotype. Accordingly, 48 nodules measuring a total diameter of 97 mm were spotted in *htgUGT1A*-SNP mice, in contrast to only 11 nodules / 23 mm in diameter detected in *htgUGT1A*-WT mice. Moreover, the average tumor size per mouse as well as the proportion of animals that developed extraordinary large HCC-like tumor formations differed noticeably between both mouse lines. Nodule formations > 5 mm in diameter were observed in approximately 20% of DEN-treated and 10% of DEN + coffee co-treated *htgUGT1A*-WT mice. In the presence of SNPs, the percentage of animals bearing large tumors was markedly higher (water: 78%, coffee: 30%).

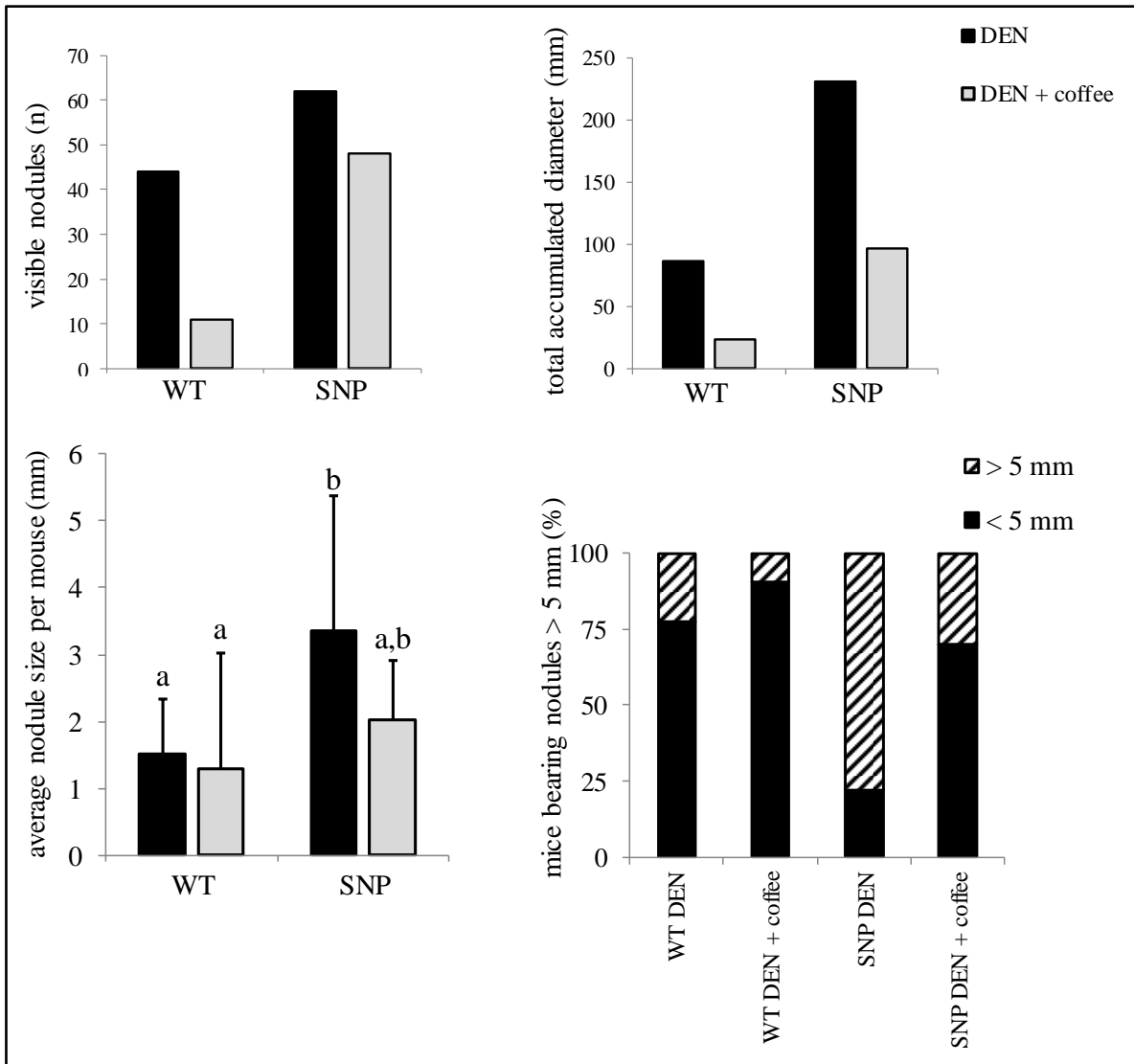


Figure 37: Characterization of all visible liver nodules in *htgUGT1A*-WT and SNP mice 40 weeks after diethylnitrosamine (DEN) injection with and without coffee co-treatment. In the presence of SNPs, incidence, size, average nodule size per mouse and the proportion of mice with big tumor formations (> 5 mm) was markedly higher. DEN + coffee co-treatment decreased HCC-like tumor outcome and growth in both mouse lines, but absolute values for nodule incidence and progression were still higher in *htgUGT1A*-SNP mice. For all variables with the same letter, the difference between the means is not statistically significant. If two variables have different letters, their comparison is statistically significant; $p < 0.05$.

Figure 38 gives a detailed overview of nodule incidence, size and susceptibility of the differently treated groups separately listed for each mouse (every animal is represented by one spot). All DEN-injected *htgUGT1A*-SNP mice developed macroscopically detectable neoplasia formations within 40 weeks. Interestingly, animals without nodules were only observed in mice carrying the human *UGT1A* WT gene locus. Accordingly, no nodules were detected in one water drinking and five coffee co-treated *htgUGT1A*-WT mice. In line with the results shown in figure 37, average nodule incidence and growth was highest in *htgUGT1A*-SNP mice drinking water and lowest in *htgUGT1A*-WT mice with coffee co-

administration. Comparable nodule incidences were observed between the water receiving *htgUGT1A*-WT mice and coffee drinking *htgUGT1A*-SNP animals, although considerable differences among the individual mice within one group were detected.

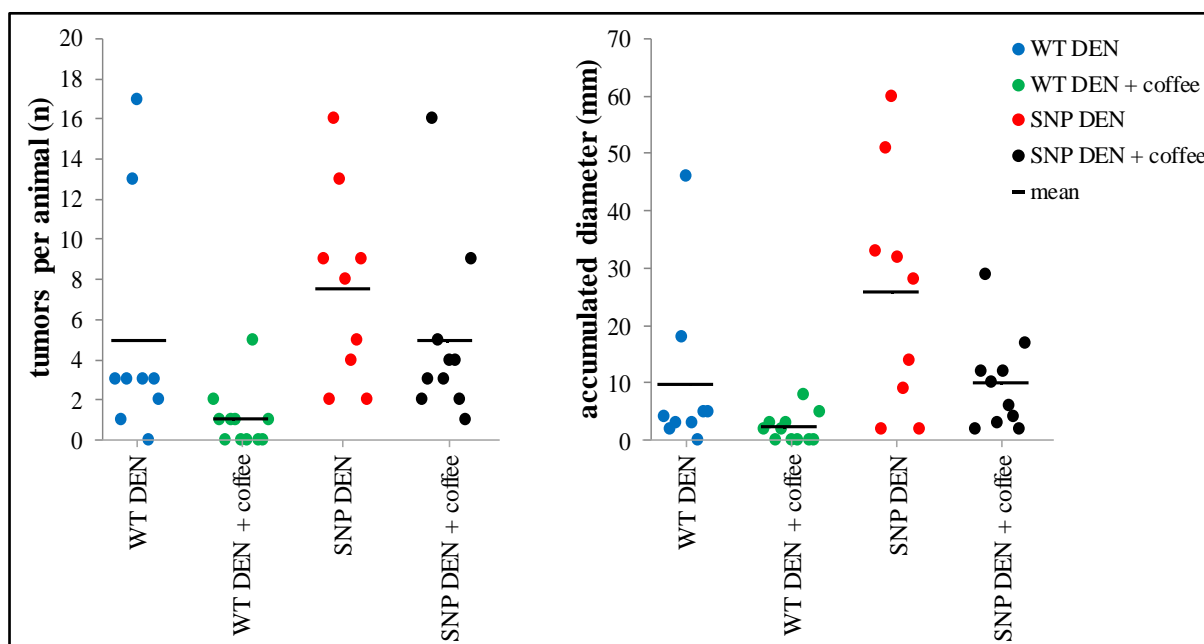


Figure 38: Detailed overview of tumor susceptibility in *htgUGT1A*-WT and SNP mice 40 weeks after diethylnitrosamine (DEN)-induced hepatocarcinogenesis. Each dot represents the total number of visible nodules (left panel) or the cumulative diameter of these liver nodules (right panel) of a single mouse. The average values of the various groups are indicated by the black line. Both, the total number of HCC-like tumor formations and the accumulated diameter were highest in DEN-injected *htgUGT1A*-SNP and lowest in coffee co-treated *htgUGT1A*-WT mice. The two remaining groups (DEN-treated *htgUGT1A*-WT mice and coffee co-treated *htgUGT1A*-SNP) exhibited a comparable tumor outcome and development. Intriguingly, only in mice carrying the human wild-type *UGT1A* gene locus no liver nodules were detected (in five mice drinking coffee and in one mouse that received water).

3.3.2 Serum aminotransferase activities in DEN-treated *htgUGT1A* mice

Elevated blood levels of aminotransferase activities are an indicator for hepatocellular damage and liver injury. Since high serum AST levels have been measured in sera of HCC patients [217], liver enzyme concentrations were determined in both mouse lines 40 weeks after DEN-induced carcinogenic liver injury (Fig. 39). As expected, significantly higher AST and ALT levels were measured in *htgUGT1A*-SNP mice (AST: 107.4 U/l and ALT: 186.1 U/l) compared to only slightly elevated levels observed in *htgUGT1A*-WT animals (AST: 62.2 U/l and ALT: 59.0 U/l). Coffee + DEN co-treatment lowered AST and ALT values in both mouse lines, but ALT levels remained slightly, but insignificantly higher as those measured in the respective control group.

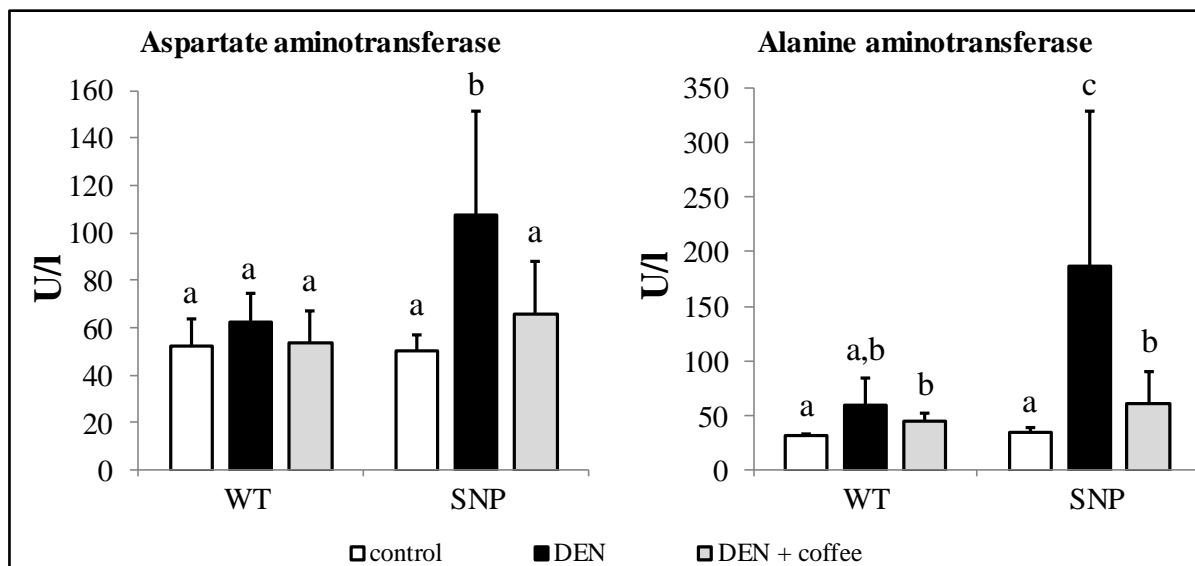


Figure 39: Serum aminotransferase activities of *htgUGT1A*-WT and SNP mice 40 weeks after diethylnitrosamine (DEN)-induced hepatocarcinogenesis. The diagram shows alanine aminotransferase (ALT) and aspartate aminotransferase (AST) levels as units per liter serum. Values of both enzymes were significantly increased in DEN-treated *htgUGT1A*-SNP mice but only moderately elevated in *htgUGT1A*-WT mice. Moreover, coffee co-treatment decreased AST and ALT levels in both mouse lines but remained slightly elevated in the presence of SNPs. Each column represents the mean \pm SD. For all variables with the same letter, the difference between the means is not statistically significant. If two variables have different letters, their comparison is statistically significant; $p < 0.05$.

3.3.3 Hepatic *UGT1A* expression in DEN-treated *htgUGT1A* mice

40 weeks after DEN injection, hepatic *UGT1A* expression was determined in healthy (normal) liver tissue and within tumor nodules of both mouse lines either receiving water or coffee co-treatment (Fig. 40 and 41, values of *htgUGT1A*-WT mice refer to the left y-axis, those of *htgUGT1A*-SNP mice refer to the right y-axis). Compared to control mice, the single DEN-injection caused a significant upregulation of all *UGT1A* isoforms in normal (non-tumorous) liver tissue of water drinking *htgUGT1A*-WT mice, whereas lower expression levels were detected within HCC-like tumor transformations. Interestingly, no transcriptional *UGT1A* induction was observed in *htgUGT1A*-WT and SNP mice after coffee co-treatment. Moreover, absolute expression levels were lower inside tumor-like liver tissues of DEN + coffee co-treated *htgUGT1A*-WT animals compared to those measured inside the nodule formations of *htgUGT1A*-WT mice receiving water. A comparable expression profile was determined in equivalently treated *htgUGT1A*-SNP mice, although absolute expression levels remained far below those measured in mice carrying the *UGT1A* WT gene locus. Of note, only *UGT1A1* and *UGT1A6* showed a different expression pattern with elevated mRNA levels within HCC-like liver tumors of *htgUGT1A*-SNP animals co-treated with coffee.

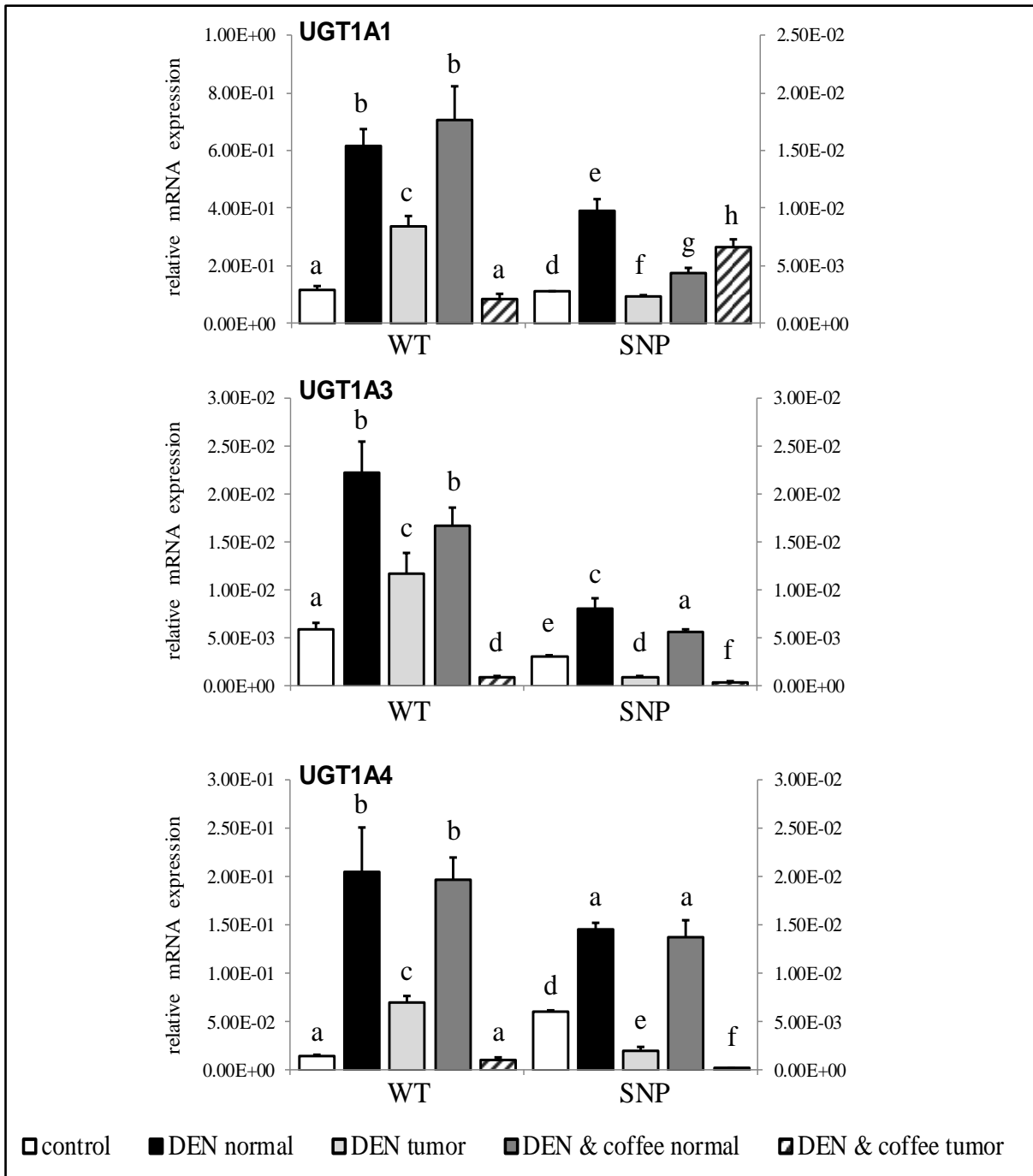


Figure 40: Hepatic expression of UGT1A1, UGT1A3 and UGT1A4 in *htgUGT1A*-WT and SNP mice after 40 weeks of diethylnitrosamine (DEN)-induced hepatocarcinogenesis. The graphs illustrate the mRNA expression of *UGT1A* genes relative to mouse β -actin measured in normal or tumorous liver tissue. Values for *htgUGT1A*-WT mice refer to the left y-axis, those of *htgUGT1A*-SNP mice refer to the right y-axis. A transcriptional upregulation of the depicted *UGT1A* genes was observed in normal liver tissue after DEN + water treatment in both mouse lines. Significantly higher absolute expression levels were detected in *htgUGT1A*-WT mice. No further *UGT1A* induction was measured in normal liver tissue after DEN + coffee co-treatment. Except for *UGT1A1* expression in *htgUGT1A*-SNP mice, lower transcriptional activation was detected within tumorous liver tissue. Each column represents the mean \pm SD (n=3). For all variables with the same letter, the difference between the means is not statistically significant. If two variables have different letters, their comparison is statistically significant; $p < 0.05$.

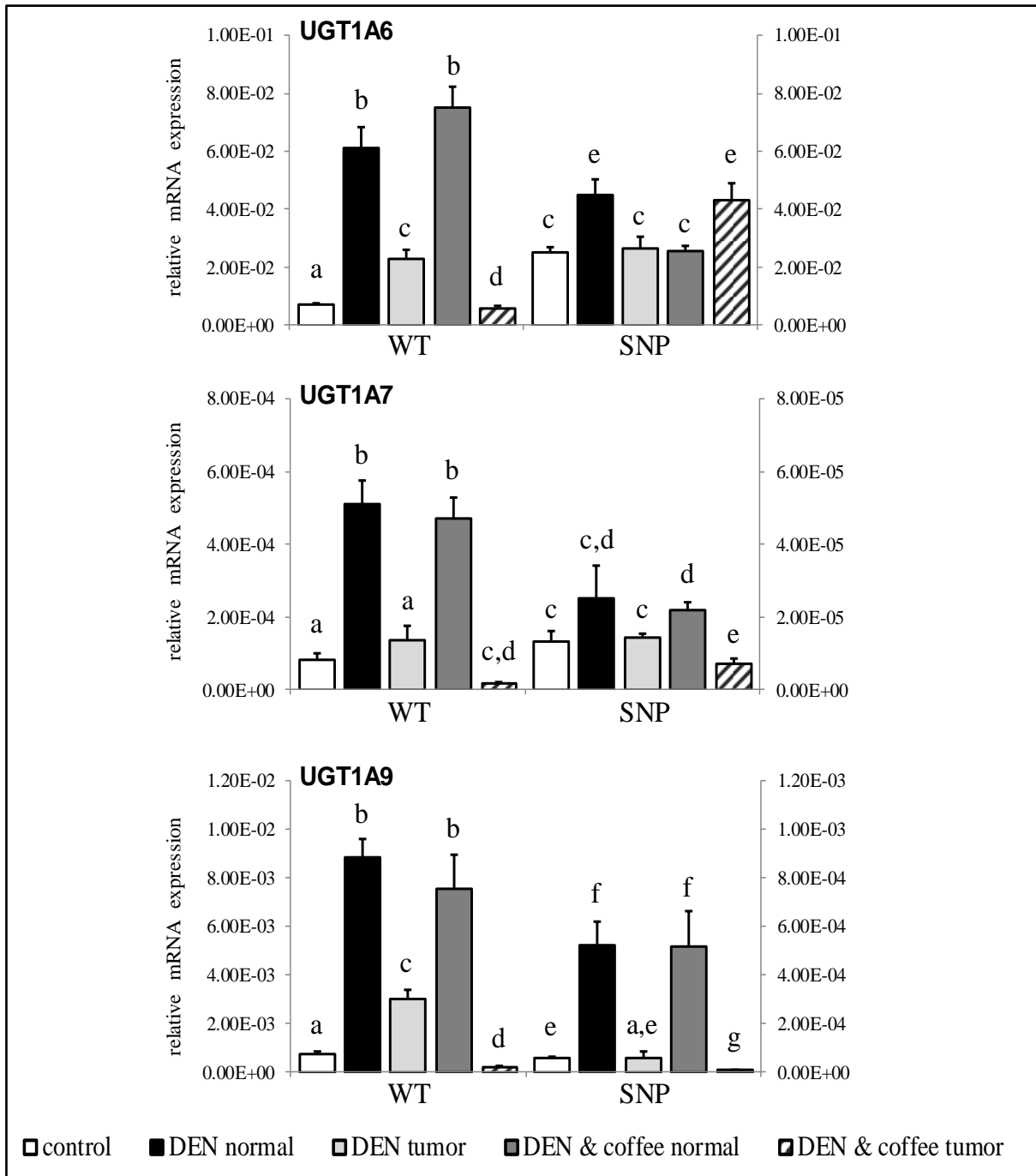


Figure 41: Hepatic expression of UGT1A6, UGT1A7 and UGT1A9 isoforms in *htgUGT1A*-WT and SNP mice after 40 weeks of diethylnitrosamine (DEN)-induced hepatocarcinogenesis. The panels illustrate the mRNA expression of *UGT1A* genes relative to mouse β -actin measured in normal or tumorous liver tissue. Values for *htgUGT1A*-WT mice refer to the left y-axis, those of *htgUGT1A*-SNP mice refer to the right y-axis. In normal liver tissue, an upregulation of *UGT1A* gene expression was measured in both mouse lines after DEN + water treatment, whereby significantly higher absolute expression levels were detected in *htgUGT1A*-WT mice. No further *UGT1A* induction was measured in nodule-unaffected liver sections after DEN + coffee co-treatment. Except for *UGT1A6* expression in *htgUGT1A*-SNP mice, lower transcriptional activation was observed within tumor nodules. Each column represents the mean \pm SD (n=3). For all variables with the same letter, the difference between the means is not statistically significant. If two variables have different letters, their comparison is statistically significant; $p < 0.05$.

4 Discussion

4.1 BDL-induced liver fibrosis

4.1.1 Differential hepatic *UGT1A* expression during cholestatic liver fibrosis in *htgUGT1A*-WT and SNP mice with and without coffee pre- and co-treatment

Cholestasis-related diseases are among the most common causes of liver fibrosis in patients with chronic liver diseases. The hepatic accumulation of toxic BAs as well as increased hepatocellular oxidative stress levels are well-defined pathological features in cholestasis representing critical effectors for the initiation of hepatocyte damage and subsequent fibrogenesis. Both, BAs and ROS, are implicated in the transcriptional stimulation of cytoprotective *UGT1A* genes *via* activation of their corresponding transcription factors FXR and Nrf2. In order to investigate the primary hypothesis of the present study, the (negative) impact of *UGT1A* polymorphisms on inflammation and progression of liver fibrosis, the influence of BDL-induced obstructive cholestasis on hepatic expression of antioxidative *UGT1A* genes was examined. The study demonstrates a significant isoform-specific activation of *UGT1A1*, *UGT1A6*, *UGT1A7* and *UGT1A9* mRNA expression in BDL-operated *htgUGT1A*-WT mice, in contrast to lower absolute expression levels observed in the presence of SNPs (Fig. 13 and 14). These results basically correspond to the findings of earlier studies conducted by the *Strassburg* laboratory showing a reduced transcriptional activation of *UGT1A* genes in the presence of commonly occurring *UGT1A* polymorphisms. As described previously, cholestasis-induced fibrosis is *inter alia* characterized by elevated oxidative stress levels [218]. Since AREs have been identified in the respective promoter regions of *UGT1A1*, *UGT1A6* and *UGT1A7*, the detected upregulation of these isoforms is likely the result of an Nrf2-mediated transcriptional activation due to elevated oxidative stress. As an enhancement of defensive mechanisms is required under this particular pathological condition, it is not surprising that the expression of other isoforms (e.g. *UGT1A9*) is also upregulated, although none of the typical *UGT1A9* inducers (PPAR α or AhR) appear to play a role under cholestatic conditions. This probably indicates the contribution of this isoform to protect the organism against additional, so far unknown, internal insults arising in the setting of cholestasis.

Considering the special importance of *UGT1A3* in BA metabolism, it is surprising that BDL failed to induce the hepatic expression of this isoform. Since higher hepatic BA concentrations are expected with incremental duration of bile flow blockage, the resultant BA-mediated FXR stimulation is expected to increase the transcriptional activation of

UGT1A3. The absent induction is possibly the result of a negative feedback loop involving the *UGT1A3*-mediated glucuronidation of CDCA to generate chenodeoxycholic acid 24-glucuronide (CDCA-24G), which in turn has been suggested to exert inhibitory effects on CDCA-mediated activation of FXR and consequently on *UGT1A3* [163, 165].

These findings were expanded by studying the effects of coffee exposure. Coffee is a potent inducer of the Nrf2 and AhR signaling pathways and has earlier been reported to exhibit beneficial effects in chronic liver diseases [219, 220]. Coffee was found to further increase human *UGT1A* gene expression in BDL animals resulting in a significant decrease of total serum bilirubin levels (Fig. 15). In agreement with our hypothesis, expression levels in *htgUGT1A*-SNP mice were lower and induction by coffee did not reach the levels measured in *htgUGT1A*-WT mice. The fact that coffee also induced the hepatic *UGT1A* expression in the presence of SNPs is of significant importance for patients carrying the Gilbert syndrome-associated SNP haplotype, as these, according to the generated results, should be able to compensate their genetically reduced *UGT1A* transcription by coffee consumption which is potentially leading to protective effects in cholestasis (discussed in the section below, point 4.1.2). Although no significant differences in serum bilirubin levels were detected between *htgUGT1A*-WT and SNP mice, the slightly higher bilirubin concentrations in mice carrying the *UGT1A* SNP haplotype indicate a reduced enzymatic activity of the bilirubin-conjugating *UGT1A1* isoform as well as an impaired responsiveness towards coffee as a consequence of the *UGT1A1**28 promoter polymorphism. To determine whether and to which extent the elevated proportion of indirect (unconjugated) bilirubin is responsible for the insignificant higher total bilirubin content measured in *htgUGT1A*-SNP mice, an additional analysis that quantifies the amount of conjugated bilirubin is required.

In conclusion, a common *UGT1A* haplotype, observed in 10% of the white population, significantly impairs the physiological responsiveness towards coffee, oxidative stress as well as cytotoxic BAs and therefore represents a potential risk factor for the onset and development of hepatic fibrosis in cholestasis-related liver diseases.

4.1.2 Differential effect on hepatic fibrogenesis in *htgUGT1A*-WT and SNP mice during cholestasis and coffee-dependent modulation of UGT1A-mediated hepatoprotection

With the intention of examining the functional contribution of *UGT1A* gene expression in the development of liver fibrosis, pathohistological analysis of the livers was performed. Comparison of the hepatic deposition of ECM proteins between water drinking BDL-treated *htgUGT1A*-WT and SNP mice revealed a higher content of collagen fibers in mice with genetically reduced *UGT1A* expression (Fig. 16 and 17). The computational analysis of Sirius red stained liver sections (Fig. 18) substantiated this observation and confirmed a more severe process of liver fibrosis in *htgUGT1A*-SNP mice by detecting a significantly higher proportion of Sirius red stained areas. Since the only difference between both animal models is the expression of *UGT1A* genes, the lower degree of fibrosis in *htgUGT1A*-WT compared to SNP mice suggests a protective role of UGT1A enzymes for hepatic fibrogenesis in this pathological situation. This is likely the result of the higher capacity of *UGT1A*-WT animals to more effectively detoxify cytotoxic BAs as their SNP counterparts. As the hepatic retention of BAs leads to severe cellular and tissue damage [162], any factors that favor or disfavor the detoxification of the amphipathic molecules may be an important determinant capable to affect disease progression and subsequent fibrogenesis. In conditions of severe cholestasis, glucuronidation reduces the exposition of hepatocytes to toxic BAs by increasing the proportion of hydrophilic and therefore less toxic BA glucuronides. Glucuronidated BAs were shown to be effectively excreted *via* urine by means of MRP3 transporters localized in the basolateral membrane of hepatocytes. This was suggested to be of particular importance during biliary obstruction as increased urinary elimination of BA glucuronides has been detected in patients with cholestasis [221]. Therefore, the unaffected functionality of BA detoxifying enzymes, including UGT1As, is likely to influence the susceptibility of cholestasis-induced liver fibrosis. As part of a haplotype consisting of 10 common occurring polymorphisms, the variant *UGT1A3* gene (W11R/ V47A/ -66T>C) is included in the human *UGT1A* gene locus of the *htgUGT1A*-SNP mouse line. The associated reduced *UGT1A3* basal expression as well as the decreased inducibility of substrates (e.g. CDCA) provides a possible explanation for potentially higher levels of cytotoxic BAs and the associated increased BA-induced hepatotoxicity in *htgUGT1A*-SNP mice. Determination of BA glucuronide concentrations in both animal models could provide direct evidence for differences on UGT1A-mediated BA detoxification and the proposed attenuated hepatocyte damage in *htgUGT1A*-WT mice.

To dissect the role of UGT1A enzymes in hepatoprotection by exposure to coffee, fibrosis development, collagen deposition and mRNA expression of profibrotic genes were determined after BDL + coffee pre- and co-treatment. The antifibrotic potential of coffee in a wide-ranging spectrum of chronic liver diseases has been previously described [222]. In this respect an inverse association between coffee intake and fibrosis progression has been shown in a recently conducted study [223]. In line with these data, coffee co-treatment reduced hepatic ECM deposition and transcriptional *COL1A1* activation in both mouse lines (Fig. 18 and 19). Of note, mice carrying the *UGT1A* haplotype with multiple genetic variants still showed significantly more fibrous collagens and higher expression levels of *COL1A1* compared to *htgUGT1A*-WT mice. These results were accompanied by comparable expression patterns of key genes related to fibrosis (*CCL2*, *TNF- α* , *PDGFRB* and *CTGF*) which were found to be higher in the presence of SNPs (Fig. 20 and 21). In this context, the expression levels of *PDGFRB* and *CCL2* reflect some special characteristics. Following chronic liver injury, the transition of quiescent into activated HSCs is associated with an upregulation of *PDGFRB* representing a reliable marker for increased stellated cell numbers [224, 225]. Comparing transcriptional activation between both mouse lines, *PDGFRB* has been the most changed parameter. The fact that *PDGFRB* expression is only slightly elevated in BDL *htgUGT1A*-WT mice compared to a considerable induction in the presence of SNPs indicates a putative effect of UGT1As on activation of the *PDGFRB* signaling cascade within HSCs. As the transcriptional *PDGFRB* induction was only slightly elevated in *htgUGT1A*-WT mice after BDL, the co-treatment with coffee could not further reduce hepatic *PDGFRB* expression. In contrast, the administration of coffee significantly downregulated *PDGFRB* transcription in *htgUGT1A*-SNP mice, thus reflecting an remarkable coffee-mediated antifibrotic effect as the *PDGFB* / *PDGFRB* signaling axis is considered to be one of the most potent mitogenic pathways for HSC activation and proliferation [226]. The possibility that this difference might arise due to varying levels of *PDGFB* may be excluded due to more or less identical *PDGFB* expression patterns in both mouse lines. Moreover, *CCL2* seems to be more responsive to coffee in *htgUGT1A*-SNP mice compared to the *UGT1A* wild type group. As such, there appears to be a differential response to coffee when comparing *htgUGT1A*-WT and SNP mice. This could reflect the consequence of an UGT1A independent coffee-mediated hepatoprotective effect which is better perceivable in case of more severe liver injury (e.g. in *htgUGT1A*-SNP mice) compared to moderate liver damage in *htgUGT1A*-WT animals. A detailed elucidation of the underlying mechanisms accountable for these observations certainly requires greater study.

However, these data support the hypothesis of coffee-induced hepatoprotective effect mediated by differences in coffee-dependent *UGT1A* induction. An attenuated protective effect of coffee in BDL co-treated *htgUGT1A*-SNP mice further corroborates that the coffee-mediated protection against hepatic fibrosis is to a substantial extent attributable to the ability of inducing UGT1A enzymes. The protective effects of coffee could therefore serve as a potential medical strategy to therapeutically activate *UGT1A* transcription also in SNP carriers.

Oxidative stress is a crucial factor for the initiation and perpetuation of hepatic injury and has found to be associated with liver fibrosis and cirrhosis development. Recently published data suggests that antioxidative properties of coffee leading to reduced oxidative stress in bile duct ligated Wistar rats can attenuate hepatic fibrogenesis [227]. As progressive fibrosis is often associated with a decrease in antioxidative defense mechanisms [46], increased antioxidative UGT1A activity was hypothesized to exert protective effects in liver fibrosis. By sensing lipid peroxidation with 4-HNE antibody the study demonstrated that UGT1A function and inducibility significantly affects the antioxidative protective effect of coffee during cholestasis resulting in a lower amount of ROS-caused alternations of macromolecules and oxidative injury (Fig. 23). These findings provide direct evidence for hepatic protection against oxidative cell damage linked to the transcriptional activation of antioxidative *UGT1A* genes by coffee. As a consequence, the mechanism of action behind the coffee-mediated hepatoprotective effects is closely related to the coffee-induced enhancement of the antioxidative defense system in which UGT1As constitute a major player. Intracellular ROS generation has been proposed to be an early event in BA-induced hepatocyte injury [44]. Thus, the transcriptional regulation of *UGT1A* genes may represent an important initial process controlling the subsequent activation of profibrotic mechanisms leading to a milder scarring response of the liver. Consequently, in addition to the already mentioned impaired BA detoxification process, the reduced cellular protection against oxidative stress in *htgUGT1A*-SNP mice is likely to represent another crucial factor for enhanced fibrosis development during cholestasis. Moreover, these results suggest potential involvement of *UGT1A* genes in every diseases in which enhanced antioxidative defense mechanisms are required to uphold cytoprotection and counteract disease progression.

In conclusion the study demonstrated that coffee consumption leads to protection against cholestasis-initiated liver fibrosis during BDL treatment, which involves the induction of *UGT1A* genes. The significant activation of human *UGT1A* expression is probably also associated with coffee exposure-mediated protective properties in other chronic liver diseases

e.g. alcoholic liver disease or HCC [228]. A detailed examination of UGT1A enzymes paired with the identification of the relevant key constituents in coffee responsible for *UGT1A* activation could provide significant benefits for risk assessment of low-activity variants and for the evaluation of UGT1A enzymes as new therapeutic targets and additional option in the medical treatment of cholestatic liver diseases in *UGT1A*-WT and SNP carriers.

4.2 HFPD-induced liver fibrosis

4.2.1 Differential outcome of hepatic fibrosis in *htgUGT1A*-WT and SNP mice

Arising from rather uncomplicated steatosis, NASH is a well-recognized cause of liver cirrhosis and has been increasingly associated with the development of HCC. Previous studies have shown that the presence of NAFLD is almost invariably associated with a deregulation of phase I and II enzymes [229, 230]. These include *UGT1A* gene products which catalyze the glucuronidation of various compounds involved in lipid homeostasis (e.g. BAs, hormones, fatty acids and other eicosanoids derivatives) [70, 103]. Although variations of *UGT1A* expression levels have previously been detected in human liver samples during various stages of NAFLD [231], their physiological role in NAFLD progression is yet to be clarified. Steatosis-induced changes of *UGT1A* gene expression have the potential to not only impair the efficiency of therapeutic drugs, but also to influence the detoxification of environmental xenobiotics and the clearance of toxic endobiotic by-products from the body. In respect of NAFLD, the presence of polymorphisms affecting *UGT1A* gene expression and function was hypothesized to reduce antioxidative effects and the modulation of UGT1A-mediated cytoprotection. Accordingly, a higher degree of hepatic steatosis, NASH progression and liver fibrosis was expected to evolve in low-activity *htgUGT1A*-SNP mice during this study. Therefore, the present work aimed to experimentally analyze the effects of altered UGT1A activity on the pathogenesis of NAFLD and the associated consequences for the pathology of the liver.

Contrary to the initial hypothesis and expectations, the results clearly indicate that increased *UGT1A* expression does not exert protection against hepatic steatosis and NASH in a humanized UGT1A mouse model of NAFLD. In contrast, the opposite effect occurred suggesting a protective effect of a low-function Gilbert syndrome-associated SNP haplotype in the experimental setting of NAFLD/NASH. In comparison with *htgUGT1A*-WT mice, lower AST and ALT levels (Fig. 26) and milder hepatic steatosis (Fig. 27) characterized by significantly lower levels of hepatic triglycerides (Fig. 29) were observed in *htgUGT1A*-SNP

mice. In addition, a reduced deposition of fibrillar ECM proteins and decreased expression levels of fibrosis-related marker genes underline the attenuated degree of fibrogenesis in mice carrying the *UGT1A* SNP variant (Fig. 31, 33 and 34). The advanced process of liver fibrosis in *htgUGT1A*-WT mice was accompanied by a significant upregulation of *UGT1A* expression, compared to a reduced or absent induction in the presence of *UGT1A* SNPs (Fig. 24). Although the role of distinct UGT1As is difficult to delineate, a potential SNP-associated protective mechanism is depicted in figure 42 and may involve the specific UGT1A3 isoform, which is the major enzyme in the *UGT1A* gene locus capable to catalyze the glucuronidation of CDCA to generate CDCA-24G [163]. CDCA has shown to be elevated in patients with NASH [232] and is a potent inducer of FXR [233], whereas CDCA-24G was hypothesized to inhibit the ability of CDCA to act as an FXR activator [165]. Due to higher *UGT1A3* expression in *htgUGT1A*-WT animals potentially leading to higher levels of CDCA-24G, increased UGT1A3 activity is hypothesized to enhance the inhibition of FXR in *htgUGT1A*-WT mice *via* improved CDCA-24G generation. This was demonstrated by a significant higher degree of inhibition of FXR expression in *htgUGT1A*-WT mice compared to mice carrying the low-function *UGT1A* SNP haplotype (Fig. 35).

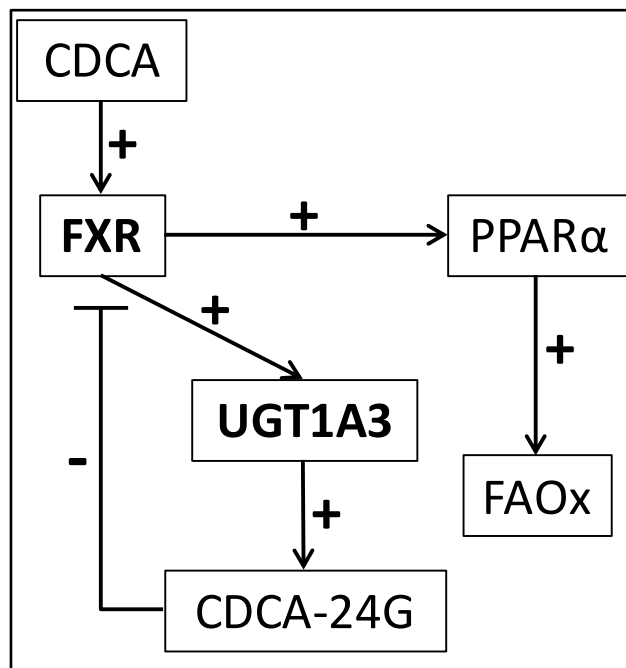


Figure 42: Schematic illustration of a putative mechanism of action involving the reduced expression of UGT1A3 due to the presence of SNPs. Higher UGT1A3 activity in *htgUGT1A*-WT mice is proposed to be associated with an increased generation of chenodeoxycholic acid 24-glucuronide (CDCA-24G) leading to enhanced inhibition of farnesoid X receptor (FXR)-induced peroxisome proliferator-activated receptor alpha (PPAR α)-mediated fatty acid oxidation (FAOx) and consequently to more severe hepatic steatosis in *htgUGT1A*-WT mice.

Consequently, *htgUGT1A*-SNP mice possibly experience a protective effect during hepatic steatosis as a result of improved stimulation of FXR-induced PPAR α -mediated fatty acid oxidation. Lower levels of nuclear PPAR α protein in *htgUGT1A*-WT mice underline this hypothesis (Fig. 35) and lead to the conclusion that the differential regulation of both nuclear receptors is likely to be directly linked to the differential *UGT1A* gene expression and may be accountable for the observed protection in *htgUGT1A*-SNP mice. In addition, the FXR downstream targets SHP and PPAR α have previously been shown to initiate the downregulation of the lipogenic master regulator sterol regulatory element-binding protein 1c (SREBP-1c, Fig. 43) [234, 235].

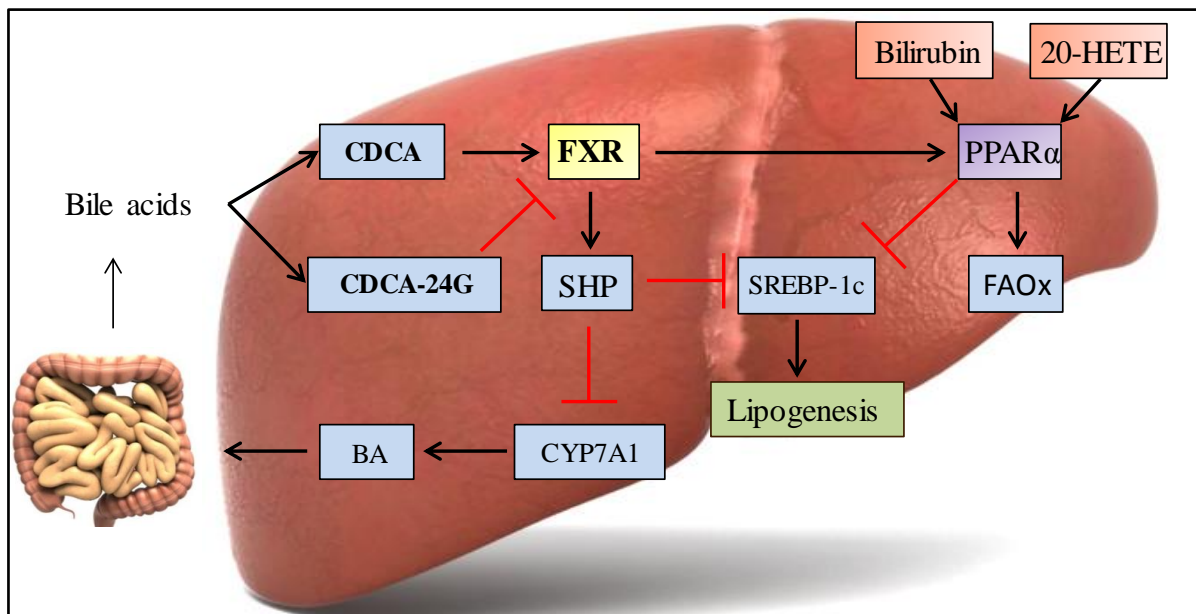


Figure 43: Graphical overview of potential factors possibly contributing to the protective effects of *htgUGT1A*-SNP mice in non-alcoholic fatty liver disease. Increased generation of chenodeoxycholic acid 24-glucuronide (CDCA-24G) in *htgUGT1A*-WT mice (due to higher *UGT1A3* activity) can cause a more pronounced inhibition of farnesoid X receptor (FXR) leading to a limited induction small heterodimer partner (SHP) and peroxisome proliferator-activated receptor alpha (PPAR α) and consequently to a less effective suppression of the sterol regulatory element-binding protein 1c (SREBP-1c)-mediated *de novo* lipogenesis. In contrast, the higher levels of chenodeoxycholic acid (CDCA) in *htgUGT1A*-SNP mice (due to lower *UGT1A3* activity) may result in a reduced FXR inhibition and consequently in enhanced SHP- and PPAR α activation leading to limited *de novo* lipogenesis. Elevated levels of further PPAR α ligands (e.g. bilirubin or 20 hydroxyeicosatetraenoic acid (20-HETE)) may also contribute to the documented protection of individuals carrying the investigated Gilbert syndrome-associated SNP haplotype. (BA) bile acid, (CYP7A1) cytochrome P450 7A1, (FAOx) fatty acid oxidation [58, modified].

Therefore, the improved activation of FXR in *htgUGT1A*-SNP mice, may also lead to an enhanced stimulation of SHP and consequently to an improved SHP- and PPAR α -dependent repression of SREBP-1c. This, in turn, could result in decreased *de novo* lipogenesis thereby reducing the degree of hepatic steatosis and may contribute to the observed hepatoprotection in the presence of SNPs. Although glucuronidation of CDCA and other bile acids has

previously been demonstrated in mice [236], it is important to note that CDCA glucuronidation constitutes a relevant BA detoxification pathway in humans. In mice, however, it is predominantly converted into muricholic acid by *cyp2c70* and only minute amounts are present [237, 238]. Nevertheless, the proposed physiological role of this conjugation reaction is likely, even if the relative occurrence of this pathway is minor compared to other BA conjugation pathways. Moreover, it is difficult to assume that only a single *UGT1A* variant, or one specific ligand (here CDCA-24G) is responsible for the protective effect in *htgUGT1A*-SNP mice. It is more likely the result of a combined effect of multiple genetic *UGT1A* polymorphisms that work in concert to less effectively glucuronidate potential FXR or PPAR α ligands. In line with this, accumulating evidence suggests the involvement of fatty acids in the modulation of signaling pathways [65]. As UGT1A-mediated glucuronidation of dietary fatty acids that act as ligands for PPAR α was demonstrated *in vitro* [239-241], this provides a functional link between UGT1A enzymes and fatty acid-dependent signaling. Because glucuronidation modulates the biological properties of signaling molecules such as dietary fatty acids, increased UGT1A function may have profound consequences on the maintenance of the nuclear receptor-mediated biological effects. In this context, *Little et al.* concluded that UGT1A enzymes may function as modulators for the availability of fatty acids that function as ligands for nuclear receptors. With regard to this, the improved UGT1A-mediated clearance of PPAR α ligands in *htgUGT1A*-WT animals probably causes significant impairments of the fatty acid-dependent PPAR α activation and further aggravates the reduction of fatty acid oxidation leading to the higher degree of hepatic steatosis in animals with normal UGT1A activity. A specific example is the glucuronidation of arachidonic acids and its metabolites 20-hydroxyeicosatetraenoic acid (20-HETE) and leucotriene B₄ (LTB₄). Both have been identified as potent activators of PPAR α [242] and as UGT1A substrates [243]. During NAFLD, the UGT1A1- and UGT1A9-mediated 20-HETE inactivation possibly contributes to impairments of hepatic fatty acid oxidation, due to limited PPAR α activation, and hence exacerbates the condition of steatosis (Fig. 43).

This scenario is potentially possible for each UGT1A substrate which is also a ligand for FXR and/or PPAR α . Further putative candidates include the dietary fatty acids phytanic acid and docosahexaenoic acid. Both are effectively glucuronidated by human liver microsomes while being also potent ligands for PPAR α or its dimerization partner RXR within the cell [239, 244]. Since western blot analysis revealed no differences in nuclear RXR protein amount between HFPD-treated *htgUGT1A*-WT and SNP mice (Fig. 45, supplemental data), the

possibility of a glucuronidated RXR ligand conferring the observed protective effect is rather unlikely. The recently identified novel role of bilirubin as PPAR α activator [245] may also contribute to the lower degree of liver damage in *htgUGT1A-SNP* mice (Fig.43). In light of this, *in vivo* experiments by *Stec* and colleagues demonstrated lower hepatic lipid accumulation as a consequence of direct binding of bilirubin to activate PPAR α . Even if the bilirubin-mediated activation of PPAR α may not seem to play a significant role in the present animal model, it again highlights the fact that many different *UGT1A* SNP-associated factors are likely to exert the protective effects during NAFLD. However, polymorphisms in *UGT1A* genes may ultimately lead to various metabolic changes and large-scale OMICS analysis might be necessary to get a full picture of the transcriptomic/proteomic alterations associated with this common *UGT1A*-SNP genotype.

To date, several studies have reported an association between the presence of *UGT1A* SNPs and various diseases. An increased risk for the development of different cancers [109, 114, 246], an elevated potential for drug toxicity [247] as well as a more severe fibrosis development in patients with hepatitis B and C have been observed [117]. On the other hand, beneficial effects of *UGT1A1**28 individuals have also been reported. These contain protective effects in cardiovascular and Crohn's disease [248, 249], a reduced risk for diabetes mellitus [250] and a lower prevalence for the metabolic syndrome [251]. With this study, another protective effect of a Gilbert syndrome-associated SNP haplotype was discovered resulting in milder hepatic steatosis and attenuated progression to NASH with less hepatic fibrosis. In contrast, mice with normal *UGT1A* expression developed more severe NASH, which is contrary to the initial hypothesis. In agreement with this study, a low-activity *UGT1A1* gene variant was reported to be associated with a decreased risk of pediatric NAFLD in 234 obese Taiwanese children [252]. Moreover, a case-control study with 641 adult patients suspected to have NAFLD reported an inverse association between unconjugated hyperbilirubinemia and the histopathological severity of liver damage in NASH [253].

In conclusion, this is the first study reporting a protective effect of a common low-function *UGT1A* SNP haplotype present in approximately 10% of the white population leading to milder hepatic steatosis during the development of NASH. With a special significance for *UGT1A3*, the proposed mechanisms include several *UGT1A* polymorphisms which are suggested to work in concert to contribute to the SNP-associated protective effects as a consequence of higher intracellular levels of ligands involved in nuclear receptor activation. This in turn raises the question if a moderate inhibition of *UGT1A* genes may represent a new

medical strategy to decelerate NAFLD progression and might be a useful tool to combat obesity-related liver injury and NASH.

4.3 DEN-induced liver cancer

4.3.1 Differential incidence of HCC-like tumor formations in *htgUGT1A*-WT and SNP mice

The human body is continuously exposed to a large number of environmental xenobiotics and potentially carcinogenic substances. The capacity of *UGT1A* gene products to conjugate mutagenic compounds has linked glucuronidation to the risk of cancer development and progression. For that reason, numerous case-control studies have assessed the association between low-activity *UGT1A* variants and the individual disposition to develop a variety of different cancers. Most of these studies hypothesized that the reduced clearance of cancer-promoting molecules as a result of either decreased *UGT1A* expression or lower enzymatic activity is likely to represent an important reason for the individual genetic disposition towards a certain type of cancer. Long before the first case-control studies identified *UGT1A* polymorphisms as risk factors for cancer development, a genoprotective role of *UGT1A* enzymes was suggested capable to influence an individual's toxicological susceptibility and carcinogenic initiation [254, 255]. In view of that, the study aimed to experimentally analyze the effects of *UGT1A* polymorphisms on HCC outcome and development in *htgUGT1A* mouse models of DEN-induced liver cancer. Since the investigated SNP haplotype is present in nearly 10% of the white population, the study further intended to evaluate the risk for genetic HCC disposition in a large proportion of the human population.

In accordance with the hypothesis, the data indicate a critical impact of reduced *UGT1A* expression on DEN-induced hepatocarcinogenesis. This was clearly observably by a higher number of HCC-like tumor formations, bigger nodule sizes and a more pronounced increase of AST and ALT levels in *htgUGT1A*-SNP mice (Fig. 36 - 39). *UGT1A*-based protection was corroborated by higher *UGT1A* expression levels in *htgUGT1A*-WT mice compared to lower transcriptional activity observed in mice carrying the *UGT1A* SNP variant (Fig. 40 and 41). Therefore, the correlation of nodule formation with the presence of *UGT1A* polymorphisms is the likely result of a SNP-associated reduction in glucuronidation activity. Particular isoforms, such as *UGT1A1*, *UGT1A4* or *UGT1A7*, play an extremely important role in the detoxification of carcinogens and case-control studies with individuals carrying the investigated *UGT1A7* promoter polymorphism in combination with the exon-derived

polymorphisms (*UGT1A7*3*) reported an increased risk for HCC development [111]. Since glucuronidation of DEN has earlier been demonstrated *in vivo* [256], the increased incidence of tumor nodules in *htgUGT1A*-SNP mice is expected to be directly attributable to the impaired capacity for detoxification of cancerogenic DEN intermediates. Especially the lower expression levels of *UGT1A4*, which are capable of glucuronidating carcinogenic food-borne primary amines and nitrosamines such as the nicotine-derived tobacco-specific 4-(methylnitrosamino)-1-(3-pyridyl)-1-butatone (NNAL) carcinogen [257, 258], are a likely explanation for an increase of carcinogenesis in *htgUGT1A*-SNP animals. Intriguingly, *UGT1A4* mRNA expression is decreased in *htgUGT1A*-SNP mice although the investigated haplotype does not contain polymorphisms in this isoform. The lower expression level is possibly the consequence of the capability of individual SNPs in specific *UGT1A* genes to affect the activities of other *UGT1A* genes [68].

Interestingly, lower *UGT1A* expression levels were measured inside tumorous nodules compared to the non-tumorous (normal) liver tissue. This is consistent with previous observations by *Strassburg et al.* detecting lower *UGT1A* mRNA and protein levels within tumors of patients with HCC compared to normal liver tissue of the same livers [259]. The measured downregulation of *UGT1A* transcription inside tumor nodules may represent an early event in tumorigenesis that reduces the *UGT1A*-dependent genoprotection and intracellular defense thereby limiting the ability of hepatocytes to eliminate carcinogens and other reactive molecules (e.g. ROS). As a consequence, the cell is exposed to increased levels of cancer-promoting substances which may cause carcinogen-induced genetic instability thereby affecting the predisposition of hepatocytes for neoplastic transformation and/or favoring the conditions of tumor growth. Significantly enlarged average nodule sizes and a higher proportion of *htgUGT1A*-SNP mice bearing nodules larger than 5 mm support this suggestion (Fig. 37, lower panels). To clarify whether the different diameters of HCC-like tumors are either the result of an earlier initiated tumorigenesis or rather the consequence of faster tumor growth, or a combination of both, the experiment would have to be repeated in a time-dependent manner. Importantly, this data now provide direct experimental evidence, that the regulation of *UGT1A* genes directly modulates the risk for neoplastic mutational events and hence confirms case-control studies investigating the association of HCC incidence and the presence *UGT1A* SNPs.

The study was expanded by investigating the effect of DEN + coffee co-treatment on tumor outcome and progression. Coffee consumption has been shown to induce *UGT1A* expression and is epidemiologically linked to a lower incidence of fibrosis, cirrhosis and HCC [260].

Administration of coffee was found to reduce the development of tumor formations in both mouse lines. Of note, coffee co-treated *htgUGT1A*-WT mice experienced a higher degree of protection as water drinking animals of the same genotype, although comparable *UGT1A* expression levels were measured in both groups when samples were tested at the end of the experimental period (Fig. 40 and 41). This could either indicate that the protective effect of coffee on nodule development is mediated independently of UGT1As, or, that no inductive effect was detectable after 40 weeks of coffee consumption. Regarding the different frequencies of nodule formations between coffee co-treated *htgUGT1A*-WT and SNP mice, the second possibility seems to be more likely. The timing of the measurement is a likely explanation for this finding. The measured transcription levels only specify the expression of UGT1A enzymes at the specific time point after 40 weeks, but not whether induction was present at the beginning or throughout the experimental period. Due to the high cellular replication rate and the associated base mispairing and error-prone repair mechanism in the presence of carcinogen action, young animals are more susceptible to DEN-induced carcinogenesis [261]. A potent coffee-mediated *UGT1A* activation immediately or shortly after DEN administration may have been a potential coffee-associated protective mechanism which is no longer detectable after 40 weeks. Therefore, the degree of activation of carcinogen detoxifying mechanisms, including UGT1A-mediated conjugation with glucuronic acid, probably constitutes an important factor capable of influencing disease progression especially in early phases of hepatocarcinogenesis.

Another surprising observation are the lower absolute expression levels within the nodules of coffee co-treated compared to water drinking animals (except for UGT1A1 and UGT1A6 in *htgUGT1A*-SNP mice). The neoplastic transformation of normal cells into cancer cells is characterized by genetic changes leading to abnormal cell proliferation and further genome instability promoting additional mutations in many different alleles [262, 263]. Therefore, a tumor-specific analysis is necessary to determine whether the measured *UGT1A* expression pattern is a general feature of all tumor formations evolved during coffee co-treatment, or, as suggested, a specific characteristic of a single investigated nodule as a consequence of cellular processes such as differentiation or DNA-methylation leading to *UGT1A* downregulation. The opposite situation, a gene-activating mutation during tumorigenesis, may explain the elevated expression levels of *UGT1A1* and *UGT1A6* inside the tumor nodules compared to normal liver tissue in coffee co-treated *htgUGT1A*-SNP mice.

In conclusion, the present work provides direct experimental evidence of low-function *UGT1A* SNPs to be associated with an increased tumor development, which can be

protectively modified by coffee. The presence of *UGT1A* polymorphisms is thus likely to represent a relevant risk factor for individual cancer disposition and could serve as genetic indicator contributing to the prediction of HCC susceptibility and progression. Accordingly, *UGT1A* enzymes may represent attractive candidates to function as therapeutic targets for preventive strategies that intend to increase *UGT1A* expression and reduce the risk of carcinogen-induced hepatocarcinogenesis in susceptible individuals.

References

1. Tortora, G.J. and B.H. Derrickson, *Principles of Anatomy and Physiology*. 2008: John Wiley & Sons. ISBN: 978-0-470-08471-7
2. Abu Rmilah, A., et al., *Understanding the marvels behind liver regeneration*. Wiley Interdiscip Rev Dev Biol, 2019. **8**(3): p. e340.
3. Abdel-Misih, S.R. and M. Bloomston, *Liver anatomy*. Surg Clin North Am, 2010. **90**(4): p. 643-53.
4. Baumgärtner, W., *Pathohistologie für die Tiermedizin*. 2007: Enke Verlag. ISBN: 978-3-8304-1144-4
5. Malarkey, D.E., et al., *New insights into functional aspects of liver morphology*. Toxicol Pathol, 2005. **33**(1): p. 27-34.
6. Hernandez-Gea, V. and S.L. Friedman, *Pathogenesis of liver fibrosis*. Annu Rev Pathol, 2011. **6**: p. 425-56.
7. Saxena, R. and N. Theise, *Canals of Hering: recent insights and current knowledge*. Semin Liver Dis, 2004. **24**(1): p. 43-8.
8. Lee, U.E. and S.L. Friedman, *Mechanisms of hepatic fibrogenesis*. Best Pract Res Clin Gastroenterol, 2011. **25**(2): p. 195-206.
9. Wynn, T.A. and T.R. Ramalingam, *Mechanisms of fibrosis: therapeutic translation for fibrotic disease*. Nat Med, 2013. **18**(7): p. 1028-40.
10. Bataller, R. and D.A. Brenner, *Liver fibrosis*. J Clin Invest, 2005. **115**(2): p. 209-18.
11. Han, Y.P., et al., *Essential role of matrix metalloproteinases in interleukin-1-induced myofibroblastic activation of hepatic stellate cell in collagen*. J Biol Chem, 2004. **279**(6): p. 4820-8.
12. Tsukada, S., C.J. Parsons, and R.A. Rippe, *Mechanisms of liver fibrosis*. Clin Chim Acta, 2006. **364**(1-2): p. 33-60.
13. Seki, E. and R.F. Schwabe, *Hepatic inflammation and fibrosis: functional links and key pathways*. Hepatology, 2015. **61**(3): p. 1066-79.
14. Theocharis, A.D., et al., *Extracellular matrix structure*. Adv Drug Deliv Rev, 2016. **97**: p. 4-27.
15. Brunt, E.M., et al., *Pathology of the liver sinusoids*. Histopathology, 2014. **64**(7): p. 907-20.
16. Liu, T., et al., *Molecular serum markers of liver fibrosis*. Biomark Insights, 2012. **7**: p. 105-17.
17. Derynck, R. and Y.E. Zhang, *Smad-dependent and Smad-independent pathways in TGF-beta family signalling*. Nature, 2003. **425**(6958): p. 577-84.
18. Solis Herruzo, J.A., et al., *Molecular targets in the design of antifibrotic therapy in chronic liver disease*. Rev Esp Enferm Dig, 2011. **103**(6): p. 310-23.
19. Niu, T., et al., *Discovery of Matrinic Thiadiazole Derivatives as a Novel Family of Anti-Liver Fibrosis Agents via Repression of the TGFbeta/Smad Pathway*. Molecules, 2018. **23**(7).
20. Shi, C., et al., *Role of CTGF gene promoter methylation in the development of hepatic fibrosis*. Am J Transl Res, 2016. **8**(1): p. 125-32.
21. Murphy, F.R., et al., *Inhibition of apoptosis of activated hepatic stellate cells by tissue inhibitor of metalloproteinase-1 is mediated via effects on matrix metalloproteinase inhibition: implications for reversibility of liver fibrosis*. J Biol Chem, 2002. **277**(13): p. 11069-76.
22. Moreno, M. and R. Bataller, *Cytokines and renin-angiotensin system signaling in hepatic fibrosis*. Clin Liver Dis, 2008. **12**(4): p. 825-52, ix.
23. Marra, F. and F. Tacke, *Roles for chemokines in liver disease*. Gastroenterology, 2014. **147**(3): p. 577-594 e1.
24. Dela Pena, A., et al., *NF-kappaB activation, rather than TNF, mediates hepatic inflammation in a murine dietary model of steatohepatitis*. Gastroenterology, 2005. **129**(5): p. 1663-74.
25. Marra, F., et al., *Molecular basis and mechanisms of progression of non-alcoholic steatohepatitis*. Trends Mol Med, 2008. **14**(2): p. 72-81.

26. Karlmark, K.R., et al., *Hepatic recruitment of the inflammatory Gr1+ monocyte subset upon liver injury promotes hepatic fibrosis*. Hepatology, 2009. **50**(1): p. 261-74.
27. Nakatani, T., et al., *Effects of decorin on the expression of alpha-smooth muscle actin in a human myofibroblast cell line*. Mol Cell Biochem, 2008. **308**(1-2): p. 201-7.
28. Liedtke, C., et al., *Experimental liver fibrosis research: update on animal models, legal issues and translational aspects*. Fibrogenesis Tissue Repair, 2013. **6**(1): p. 19.
29. Krawczyk, M., et al., *Genome-wide association studies and genetic risk assessment of liver diseases*. Nat Rev Gastroenterol Hepatol, 2010. **7**(12): p. 669-81.
30. Hirschfield, H., D. Adams, and E. Liaskou, *Biliary Disease: From Science to Clinic*. 2017: Springer. ISBN: 978-3-319-50166-6
31. Gourgiotis, S., et al., *Gallbladder cancer*. Am J Surg, 2008. **196**(2): p. 252-64.
32. Lammert, F. and T. Sauerbruch, *Mechanisms of disease: the genetic epidemiology of gallbladder stones*. Nat Clin Pract Gastroenterol Hepatol, 2005. **2**(9): p. 423-33.
33. Zhu, Y., et al., *Obstructive jaundice due to a blood clot after ERCP: a case report and review of the literature*. BMC Gastroenterol, 2018. **18**(1): p. 163.
34. Shah, R. and S. John, *Cholestatic Jaundice (Cholestasis, Cholestatic Hepatitis)*. 2019.
35. Santiago, P., A.R. Scheinberg, and C. Levy, *Cholestatic liver diseases: new targets, new therapies*. Therap Adv Gastroenterol, 2018. **11**: p. 1756284818787400.
36. Abshagen, K., et al., *Pathobiochemical signatures of cholestatic liver disease in bile duct ligated mice*. BMC Syst Biol, 2015. **9**: p. 83.
37. Russell, D.W., *The enzymes, regulation, and genetics of bile acid synthesis*. Annu Rev Biochem, 2003. **72**: p. 137-74.
38. Garcia, M., et al., *Nuclear Receptor Metabolism of Bile Acids and Xenobiotics: A Coordinated Detoxification System with Impact on Health and Diseases*. Int J Mol Sci, 2018. **19**(11).
39. Claudel, T., B. Staels, and F. Kuipers, *The Farnesoid X receptor: a molecular link between bile acid and lipid and glucose metabolism*. Arterioscler Thromb Vasc Biol, 2005. **25**(10): p. 2020-30.
40. Fiorucci, S., et al., *Targeting farnesoid X receptor for liver and metabolic disorders*. Trends Mol Med, 2007. **13**(7): p. 298-309.
41. Trauner, M., P.J. Meier, and J.L. Boyer, *Molecular pathogenesis of cholestasis*. N Engl J Med, 1998. **339**(17): p. 1217-27.
42. Woolbright, B.L., et al., *Bile acid-induced necrosis in primary human hepatocytes and in patients with obstructive cholestasis*. Toxicol Appl Pharmacol, 2015. **283**(3): p. 168-77.
43. Billington, D., et al., *Effects of bile salts on the plasma membranes of isolated rat hepatocytes*. Biochem J, 1980. **188**(2): p. 321-7.
44. Perez, M.J. and O. Briz, *Bile-acid-induced cell injury and protection*. World J Gastroenterol, 2009. **15**(14): p. 1677-89.
45. Pisoschi, A.M. and A. Pop, *The role of antioxidants in the chemistry of oxidative stress: A review*. Eur J Med Chem, 2015. **97**: p. 55-74.
46. Mormone, E., J. George, and N. Nieto, *Molecular pathogenesis of hepatic fibrosis and current therapeutic approaches*. Chem Biol Interact, 2011. **193**(3): p. 225-31.
47. Paumgartner, G. and U. Beuers, *Ursodeoxycholic acid in cholestatic liver disease: mechanisms of action and therapeutic use revisited*. Hepatology, 2002. **36**(3): p. 525-31.
48. McCullough, A.J., *Epidemiology of the metabolic syndrome in the USA*. J Dig Dis, 2011. **12**(5): p. 333-40.
49. Younossi, Z.M., et al., *Global epidemiology of nonalcoholic fatty liver disease-Meta-analytic assessment of prevalence, incidence, and outcomes*. Hepatology, 2016. **64**(1): p. 73-84.
50. Flegal, K.M., et al., *Prevalence of obesity and trends in the distribution of body mass index among US adults, 1999-2010*. Jama, 2012. **307**(5): p. 491-7.
51. Perumpail, B.J., et al., *Clinical epidemiology and disease burden of nonalcoholic fatty liver disease*. World J Gastroenterol, 2017. **23**(47): p. 8263-8276.
52. Sanyal, A.J., *NASH: A global health problem*. Hepatol Res, 2011. **41**(7): p. 670-4.
53. Tiniakos, D.G., M.B. Vos, and E.M. Brunt, *Nonalcoholic fatty liver disease: pathology and pathogenesis*. Annu Rev Pathol, 2010. **5**: p. 145-71.
54. Kleiner, D.E. and H.R. Makhlof, *Histology of Nonalcoholic Fatty Liver Disease and Nonalcoholic Steatohepatitis in Adults and Children*. Clin Liver Dis, 2016. **20**(2): p. 293-312.

55. Charlton, M.R., et al., *Frequency and outcomes of liver transplantation for nonalcoholic steatohepatitis in the United States*. Gastroenterology, 2011. **141**(4): p. 1249-53.
56. Loomba, R. and N. Chalasani, *The Hierarchical Model of NAFLD: Prognostic Significance of Histologic Features in NASH*. Gastroenterology, 2016. **149**(2): p. 278-81.
57. Trayhurn, P., *Hypoxia and adipose tissue function and dysfunction in obesity*. Physiol Rev, 2013. **93**(1): p. 1-21.
58. Chalasani, N. and G. Szabo, *Alcoholic and Non-Alcoholic Fatty Liver Disease: Bench to Bedside*. 1 ed. 2016: Springer. ISBN: 978-3-319-20537-3
59. Kazantzis, M. and A. Stahl, *Fatty acid transport proteins, implications in physiology and disease*. Biochim Biophys Acta, 2012. **1821**(5): p. 852-7.
60. Ipsen, D.H., J. Lykkesfeldt, and P. Tveden-Nyborg, *Molecular mechanisms of hepatic lipid accumulation in non-alcoholic fatty liver disease*. Cell Mol Life Sci, 2018. **75**(18): p. 3313-3327.
61. Schierwagen, R., et al., *Seven weeks of Western diet in apolipoprotein-E-deficient mice induce metabolic syndrome and non-alcoholic steatohepatitis with liver fibrosis*. Sci Rep, 2015. **5**: p. 12931.
62. Angulo, P., et al., *Liver Fibrosis, but No Other Histologic Features, Is Associated With Long-term Outcomes of Patients With Nonalcoholic Fatty Liver Disease*. Gastroenterology, 2015. **149**(2): p. 389-97 e10.
63. Hagstrom, H., et al., *Overweight in late adolescence predicts development of severe liver disease later in life: A 39years follow-up study*. J Hepatol, 2016. **65**(2): p. 363-8.
64. Bechmann, L.P., et al., *The interaction of hepatic lipid and glucose metabolism in liver diseases*. J Hepatol, 2012. **56**(4): p. 952-64.
65. Hwang, D. and S.H. Rhee, *Receptor-mediated signaling pathways: potential targets of modulation by dietary fatty acids*. Am J Clin Nutr, 1999. **70**(4): p. 545-56.
66. Cobbina, E. and F. Akhlaghi, *Non-alcoholic fatty liver disease (NAFLD) - pathogenesis, classification, and effect on drug metabolizing enzymes and transporters*. Drug Metab Rev, 2017. **49**(2): p. 197-211.
67. Hu, D.G., et al., *Transcriptional regulation of human UDP-glucuronosyltransferase genes*. Drug Metab Rev, 2014. **46**(4): p. 421-58.
68. Strassburg, C.P., S. Kalthoff, and U. Ehmer, *Variability and function of family 1 uridine-5'-diphosphate glucuronosyltransferases (UGT1A)*. Crit Rev Clin Lab Sci, 2008. **45**(6): p. 485-530.
69. Strassburg, C.P., et al., *Polymorphic expression of the UDP-glucuronosyltransferase UGT1A gene locus in human gastric epithelium*. Mol Pharmacol, 1998. **54**(4): p. 647-54.
70. Bock, K.W., *Functions and transcriptional regulation of adult human hepatic UDP-glucuronosyl-transferases (UGTs): mechanisms responsible for interindividual variation of UGT levels*. Biochem Pharmacol, 2010. **80**(6): p. 771-7.
71. Mojarrabi, B. and P.I. Mackenzie, *Characterization of two UDP glucuronosyltransferases that are predominantly expressed in human colon*. Biochem Biophys Res Commun, 1998. **247**(3): p. 704-9.
72. Strassburg, C.P., M.P. Manns, and R.H. Tukey, *Expression of the UDP-glucuronosyltransferase 1A locus in human colon. Identification and characterization of the novel extrahepatic UGT1A8*. J Biol Chem, 1998. **273**(15): p. 8719-26.
73. Wells, P.G., et al., *Glucuronidation and the UDP-glucuronosyltransferases in health and disease*. Drug Metab Dispos, 2004. **32**(3): p. 281-90.
74. Jancova, P., P. Anzenbacher, and E. Anzenbacherova, *Phase II drug metabolizing enzymes*. Biomed Pap Med Fac Univ Palacky Olomouc Czech Repub, 2010. **154**(2): p. 103-16.
75. Ehmer, U., *Genetics and metabolism: characterization of individual genetic variation of UDP-glucuronosyltransferase regulation in a humanized mouse model*. 2009, Hannover Medical School.
76. Guillemette, C., *Pharmacogenomics of human UDP-glucuronosyltransferase enzymes*. Pharmacogenomics J, 2003. **3**(3): p. 136-58.
77. Buckley, D.B. and C.D. Klaassen, *Induction of mouse UDP-glucuronosyltransferase mRNA expression in liver and intestine by activators of aryl-hydrocarbon receptor, constitutive*

- androstane receptor, pregnane X receptor, peroxisome proliferator-activated receptor alpha, and nuclear factor erythroid 2-related factor 2*. *Drug Metab Dispos*, 2009. **37**(4): p. 847-56.
78. Tukey, R.H. and C.P. Strassburg, *Human UDP-glucuronosyltransferases: metabolism, expression, and disease*. *Annu Rev Pharmacol Toxicol*, 2000. **40**: p. 581-616.
79. Fujiwara, R., T. Yokoi, and M. Nakajima, *Structure and Protein-Protein Interactions of Human UDP-Glucuronosyltransferases*. *Front Pharmacol*, 2016. **7**: p. 388.
80. Court, M.H., et al., *Quantitative distribution of mRNAs encoding the 19 human UDP-glucuronosyltransferase enzymes in 26 adult and 3 fetal tissues*. *Xenobiotica*, 2012. **42**(3): p. 266-77.
81. Mackenzie, P.I., et al., *Nomenclature update for the mammalian UDP glycosyltransferase (UGT) gene superfamily*. *Pharmacogenet Genomics*, 2005. **15**(10): p. 677-85.
82. Mackenzie, P., J.M. Little, and A. Radomska-Pandya, *Glucosidation of hyodeoxycholic acid by UDP-glucuronosyltransferase 2B7*. *Biochem Pharmacol*, 2003. **65**(3): p. 417-21.
83. Meech, R., et al., *The UDP-Glycosyltransferase (UGT) Superfamily: New Members, New Functions, and Novel Paradigms*. *Physiol Rev*, 2019. **99**(2): p. 1153-1222.
84. Dutton, G.J., *Glucuronidation of drugs and other compounds*. 1980, Boca Raton, FL: CRC Boca Raton Press. 3-268.
85. Chen, S., et al., *Tissue-specific, inducible, and hormonal control of the human UDP-glucuronosyltransferase-1 (UGT1) locus*. *J Biol Chem*, 2005. **280**(45): p. 37547-57.
86. Gong, Q.H., et al., *Thirteen UDPglucuronosyltransferase genes are encoded at the human UGT1 gene complex locus*. *Pharmacogenetics*, 2001. **11**(4): p. 357-68.
87. Radomska-Pandya, A., et al., *Structure of UDP-glucuronosyltransferases in membranes*. *Methods Enzymol*, 2005. **400**: p. 116-47.
88. Ohno, S. and S. Nakajin, *Determination of mRNA expression of human UDP-glucuronosyltransferases and application for localization in various human tissues by real-time reverse transcriptase-polymerase chain reaction*. *Drug Metab Dispos*, 2009. **37**(1): p. 32-40.
89. Rowland, A., J.O. Miners, and P.I. Mackenzie, *The UDP-glucuronosyltransferases: their role in drug metabolism and detoxification*. *Int J Biochem Cell Biol*, 2013. **45**(6): p. 1121-32.
90. Meech, R. and P.I. Mackenzie, *Structure and function of uridine diphosphate glucuronosyltransferases*. *Clin Exp Pharmacol Physiol*, 1997. **24**(12): p. 907-15.
91. Uchaipichat, V., et al., *Human udp-glucuronosyltransferases: isoform selectivity and kinetics of 4-methylumbelliferone and 1-naphthol glucuronidation, effects of organic solvents, and inhibition by diclofenac and probenecid*. *Drug Metab Dispos*, 2004. **32**(4): p. 413-23.
92. Fang, J.L. and P. Lazarus, *Correlation between the UDP-glucuronosyltransferase (UGT1A1) TATAA box polymorphism and carcinogen detoxification phenotype: significantly decreased glucuronidating activity against benzo(a)pyrene-7,8-dihydrodiol(-) in liver microsomes from subjects with the UGT1A1*28 variant*. *Cancer Epidemiol Biomarkers Prev*, 2004. **13**(1): p. 102-9.
93. Strassburg, C.P., et al., *Regulation and function of family 1 and family 2 UDP-glucuronosyltransferase genes (UGT1A, UGT2B) in human oesophagus*. *Biochem J*, 1999. **338**(Pt 2): p. 489-498.
94. Strassburg, C.P., et al., *Polymorphic gene expression and interindividual variation of UDP-glucuronosyltransferase activity in human small intestine*. *J Biol Chem*, 2000. **275**: p. 36164-36171.
95. Strassburg, C.P., et al., *Differential expression of the UGT1A locus in human liver, biliary, and gastric tissue: identification of UGT1A7 and UGT1A10 transcripts in extrahepatic tissue*. *Mol Pharmacol*, 1997. **52**(2): p. 212-20.
96. Strassburg, C.P., et al., *UDP-glucuronosyltransferase activity in human liver and colon*. *Gastroenterology*, 1999. **116**(1): p. 149-60.
97. Strassburg, C.P., *Gilbert-Meulengracht's syndrome and pharmacogenetics: is jaundice just the tip of the iceberg?* *Drug Metab Rev*, 2010. **42**(1): p. 162-75.
98. Burchell, B., et al., *Drug-mediated toxicity caused by genetic deficiency of UDP-glucuronosyltransferases*. *Toxicol Lett*, 2000. **112-113**: p. 333-40.

99. Mackenzie, P.I., D.G. Hu, and D.A. Gardner-Stephen, *The regulation of UDP-glucuronosyltransferase genes by tissue-specific and ligand-activated transcription factors*. Drug Metab Rev, 2010. **42**(1): p. 99-109.
100. Maghzal, G.J., et al., *Limited role for the bilirubin-biliverdin redox amplification cycle in the cellular antioxidant protection by biliverdin reductase*. J Biol Chem, 2009. **284**(43): p. 29251-9.
101. Bosma, P.J., et al., *Bilirubin UDP-glucuronosyltransferase 1 is the only relevant bilirubin glucuronidating isoform in man [published erratum appears in J Biol Chem 1994 Oct 14;269(41):2542]*. J Biol Chem, 1994. **269**(27): p. 17960-4.
102. Barbarino, J.M., et al., *PharmGKB summary: very important pharmacogene information for UGT1A1*. Pharmacogenet Genomics, 2014. **24**(3): p. 177-83.
103. Strassburg, C.P., *Pharmacogenetics of Gilbert's syndrome*. Pharmacogenomics, 2008. **9**(6): p. 703-15.
104. Bosma, P.J., et al., *The genetic basis of the reduced expression of bilirubin UDP-glucuronosyltransferase 1 in Gilbert's syndrome*. N Engl J Med, 1995. **333**(18): p. 1171-5.
105. Beutler, E., T. Gelbart, and A. Demina, *Racial variability in the UDP-glucuronosyltransferase 1 (UGT1A1) promoter: a balanced polymorphism for regulation of bilirubin metabolism?* Proc Natl Acad Sci U S A, 1998. **95**(14): p. 8170-4.
106. Ritter, J.K., et al., *Identification of a genetic alteration in the code for bilirubin UDP-glucuronosyltransferase in the UGT1 gene complex of a Crigler-Najjar type I patient*. J Clin Invest, 1992. **90**(1): p. 150-5.
107. Dhawan, A., et al., *Disease burden of Crigler-Najjar syndrome: Systematic review and future perspectives*. J Gastroenterol Hepatol, 2019.
108. Lankisch, T.O., et al., *Identification and characterization of a functional TATA box polymorphism of the UDP glucuronosyltransferase 1A7 gene*. Mol Pharmacol, 2005. **67**(5): p. 1732-9.
109. Vogel, A., et al., *Genetic link of hepatocellular carcinoma with polymorphisms of the UDP-Glucuronosyltransferase UGT1A7 gene*. Gastroenterology, 2001. **121**: p. 1136-1144.
110. Wang, Y., et al., *UDP-glucuronosyltransferase 1A7 genetic polymorphisms are associated with hepatocellular carcinoma in japanese patients with hepatitis C virus infection*. Clin Cancer Res, 2004. **10**(7): p. 2441-6.
111. Tseng, C.S., et al., *UDP-glucuronosyltransferase 1A7 genetic polymorphisms are associated with hepatocellular carcinoma risk and onset age*. Am J Gastroenterol, 2005. **100**(8): p. 1758-63.
112. Stucker, I., et al., *UDP-glucuronosyltransferase UGT1A7 genetic polymorphisms in hepatocellular carcinoma: a differential impact according to seropositivity of HBV or HCV markers?* BMC Cancer, 2007. **7**: p. 214.
113. Guillemette, C., et al., *Structural heterogeneity at the UDP-glucuronosyltransferase 1 locus: functional consequences of three novel missense mutations in the human UGT1A7 gene*. Pharmacogenetics, 2000. **10**(7): p. 629-44.
114. Strassburg, C.P., et al., *Polymorphisms of the UDP-glucuronosyltransferase (UGT) 1A7 gene in colorectal cancer*. Gut, 2002. **50**: p. 851-856.
115. Malfatti, M.A. and J.S. Felton, *Human UDP-glucuronosyltransferase 1A1 is the primary enzyme responsible for the N-glucuronidation of N-hydroxy-PhIP in vitro*. Chem Res Toxicol, 2004. **17**(8): p. 1137-44.
116. Mojarrabi, B., R. Butler, and P.I. Mackenzie, *cDNA cloning and characterization of the human UDP glucuronosyltransferase, UGT1A3*. Biochem Biophys Res Commun, 1996. **225**(3): p. 785-90.
117. Tang, K.S., et al., *UDP-glucuronosyltransferase 1A7 polymorphisms are associated with liver cirrhosis*. Biochem Biophys Res Commun, 2008. **366**(3): p. 643-8.
118. Tang, K.S., et al., *Link between colorectal cancer and polymorphisms in the uridine-diphosphoglucuronosyltransferase 1A7 and 1A1 genes*. World J Gastroenterol, 2005. **11**(21): p. 3250-4.
119. Guillemette, C., A. Belanger, and J. Lepine, *Metabolic inactivation of estrogens in breast tissue by UDP-glucuronosyltransferase enzymes: an overview*. Breast Cancer Res, 2004. **6**(6): p. 246-54.

120. Shatalova, E.G., et al., [Association of polymorphisms in *SULT1A1* and *UGT1A1* Genes with breast cancer risk and phenotypes in Russian women]. *Mol Biol (Mosk)*, 2006. **40**(2): p. 263-70.
121. Szanyi, I., et al., *Effects of cytochrome P450 1A1 and uridine-diphosphate-glucuronosyltransferase 1A1 allelic polymorphisms on the risk of development and the prognosis of head and neck cancers*. *Eur J Cancer Prev*, 2012. **21**(6): p. 560-8.
122. Hu, D.G., et al., *Genetic polymorphisms of human UDP-glucuronosyltransferase (UGT) genes and cancer risk*. *Drug Metab Rev*, 2016. **48**(1): p. 47-69.
123. Oda, S., et al., *Epigenetic regulation of the tissue-specific expression of human UDP-glucuronosyltransferase (UGT) 1A10*. *Biochem Pharmacol*, 2014. **87**(4): p. 660-7.
124. Guillemette, C., et al., *UGT genomic diversity: beyond gene duplication*. *Drug Metab Rev*, 2010. **42**(1): p. 24-44.
125. Buckley, D.B. and C.D. Klaassen, *Tissue- and gender-specific mRNA expression of UDP-glucuronosyltransferases (UGTs) in mice*. *Drug Metab Dispos*, 2007. **35**(1): p. 121-7.
126. Basu, N.K., et al., *The major chemical-detoxifying system of UDP-glucuronosyltransferases requires regulated phosphorylation supported by protein kinase C*. *J Biol Chem*, 2008. **283**(34): p. 23048-61.
127. Chen, H., et al., *Up-regulation of UDP-glucuronosyltransferase (UGT) 1A4 by 17beta-estradiol: a potential mechanism of increased lamotrigine elimination in pregnancy*. *Drug Metab Dispos*, 2009. **37**(9): p. 1841-7.
128. Belanger, A.S., et al., *Regulation of UGT1A1 and HNF1 transcription factor gene expression by DNA methylation in colon cancer cells*. *BMC Mol Biol*, 2010. **11**: p. 9.
129. Hu, D.G., et al., *A novel polymorphism in a forkhead box A1 (FOXA1) binding site of the human UDP glucuronosyltransferase 2B17 gene modulates promoter activity and is associated with altered levels of circulating androstane-3alpha,17beta-diol glucuronide*. *Mol Pharmacol*, 2010. **78**(4): p. 714-22.
130. Lu, H., F.J. Gonzalez, and C. Klaassen, *Alterations in hepatic mRNA expression of phase II enzymes and xenobiotic transporters after targeted disruption of hepatocyte nuclear factor 4 alpha*. *Toxicol Sci*, 2010. **118**(2): p. 380-90.
131. Gardner-Stephen, D.A. and P.I. Mackenzie, *Liver-enriched transcription factors and their role in regulating UDP glucuronosyltransferase gene expression*. *Curr Drug Metab*, 2008. **9**(5): p. 439-52.
132. Kandel, B.A., et al., *Genomewide comparison of the inducible transcriptomes of nuclear receptors CAR, PXR and PPARalpha in primary human hepatocytes*. *Biochim Biophys Acta*, 2016. **1859**(9): p. 1218-1227.
133. Prakash, C., et al., *Nuclear Receptors in Drug Metabolism, Drug Response and Drug Interactions*. *Nucl Receptor Res*, 2015. **2**.
134. Senekeo-Effenberger, K., et al., *Expression of the human UGT1 locus in transgenic mice by 4-chloro-6-(2,3-xylidino)-2-pyrimidinylthioacetic acid (WY-14643) and implications on drug metabolism through peroxisome proliferator-activated receptor alpha activation*. *Drug Metab Dispos*, 2007. **35**(3): p. 419-27.
135. Verreault, M., et al., *Regulation of endobiotics glucuronidation by ligand-activated transcription factors: physiological function and therapeutic potential*. *Drug Metab Rev*, 2010. **42**(1): p. 110-22.
136. Sugatani, J., et al., *The induction of human UDP-glucuronosyltransferase 1A1 mediated through a distal enhancer module by flavonoids and xenobiotics*. *Biochem Pharmacol*, 2004. **67**(5): p. 989-1000.
137. Yueh, M.F. and R.H. Tukey, *Nrf2-Keap1 signaling pathway regulates human UGT1A1 expression in vitro and in transgenic UGT1 mice*. *J Biol Chem*, 2007. **282**(12): p. 8749-58.
138. Mangelsdorf, D.J., et al., *The nuclear receptor superfamily: the second decade*. *Cell*, 1995. **83**(6): p. 835-9.
139. Lee, F.Y., et al., *FXR, a multipurpose nuclear receptor*. *Trends Biochem Sci*, 2006. **31**(10): p. 572-80.
140. Makishima, M., et al., *Identification of a nuclear receptor for bile acids*. *Science*, 1999. **284**(5418): p. 1362-5.

141. Yuan, Z.Q. and K.W. Li, *Role of farnesoid X receptor in cholestasis*. J Dig Dis, 2016. **17**(8): p. 501-509.
142. Degirolamo, C., C. Sabba, and A. Moschetta, *Intestinal nuclear receptors in HDL cholesterol metabolism*. J Lipid Res, 2015. **56**(7): p. 1262-70.
143. Hiebl, V., et al., *Natural products as modulators of the nuclear receptors and metabolic sensors LXR, FXR and RXR*. Biotechnol Adv, 2018. **36**(6): p. 1657-1698.
144. Dawson, P.A., T. Lan, and A. Rao, *Bile acid transporters*. J Lipid Res, 2009. **50**(12): p. 2340-57.
145. Hegade, V.S., et al., *Novel bile acid therapeutics for the treatment of chronic liver diseases*. Therap Adv Gastroenterol, 2016. **9**(3): p. 376-91.
146. Trauner, M. and E. Halilbasic, *Nuclear receptors as new perspective for the management of liver diseases*. Gastroenterology, 2011. **140**(4): p. 1120-1125 e1-12.
147. Hoeke, M.O., et al., *Human FXR regulates SHP expression through direct binding to an LRH-1 binding site, independent of an IR-1 and LRH-1*. PLoS One, 2014. **9**(2): p. e88011.
148. Modica, S., R.M. Gadaleta, and A. Moschetta, *Deciphering the nuclear bile acid receptor FXR paradigm*. Nucl Recept Signal, 2010. **8**: p. e005.
149. Kong, B., et al., *Mechanism of tissue-specific farnesoid X receptor in suppressing the expression of genes in bile-acid synthesis in mice*. Hepatology, 2012. **56**(3): p. 1034-43.
150. Cicione, C., C. Degirolamo, and A. Moschetta, *Emerging role of fibroblast growth factors 15/19 and 21 as metabolic integrators in the liver*. Hepatology, 2012. **56**(6): p. 2404-11.
151. Taoka, H., et al., *Role of bile acids in the regulation of the metabolic pathways*. World J Diabetes, 2016. **7**(13): p. 260-70.
152. Trauner, M. and J.L. Boyer, *Bile salt transporters: molecular characterization, function, and regulation*. Physiol Rev, 2003. **83**(2): p. 633-71.
153. Wahlstrom, A., et al., *Intestinal Crosstalk between Bile Acids and Microbiota and Its Impact on Host Metabolism*. Cell Metab, 2016. **24**(1): p. 41-50.
154. Chiang, J.Y.L., *Bile acid metabolism and signaling in liver disease and therapy*. Liver Res, 2017. **1**(1): p. 3-9.
155. Goodwin, B., et al., *A regulatory cascade of the nuclear receptors FXR, SHP-1, and LRH-1 represses bile acid biosynthesis*. Mol Cell, 2000. **6**(3): p. 517-26.
156. Lu, T.T., et al., *Molecular basis for feedback regulation of bile acid synthesis by nuclear receptors*. Mol Cell, 2000. **6**(3): p. 507-15.
157. Gall, W.E., et al., *Differential glucuronidation of bile acids, androgens and estrogens by human UGT1A3 and 2B7*. J Steroid Biochem Mol Biol, 1999. **70**(1-3): p. 101-8.
158. Gnerre, C., et al., *Regulation of CYP3A4 by the bile acid receptor FXR: evidence for functional binding sites in the CYP3A4 gene*. Pharmacogenetics, 2004. **14**(10): p. 635-45.
159. Takikawa, H., et al., *Serum concentrations of bile acid glucuronides in hepatobiliary diseases*. Digestion, 1983. **27**(4): p. 189-95.
160. Belanger, A., et al., *Inactivation of androgens by UDP-glucuronosyltransferase enzymes in humans*. Trends Endocrinol Metab, 2003. **14**(10): p. 473-9.
161. Barbier, O., et al., *FXR induces the UGT2B4 enzyme in hepatocytes: a potential mechanism of negative feedback control of FXR activity*. Gastroenterology, 2003. **124**(7): p. 1926-40.
162. Perreault, M., et al., *Urinary Elimination of Bile Acid Glucuronides under Severe Cholestatic Situations: Contribution of Hepatic and Renal Glucuronidation Reactions*. Can J Gastroenterol Hepatol, 2018. **2018**: p. 8096314.
163. Erichsen, T.J., et al., *Regulation of the human bile acid UDP-glucuronosyltransferase 1A3 by the farnesoid X receptor and bile acids*. J Hepatol, 2010. **52**(4): p. 570-8.
164. Trubetskoy, O.V., et al., *High throughput screening assay for UDP-glucuronosyltransferase 1A1 glucuronidation profiling*. Assay Drug Dev Technol, 2007. **5**(3): p. 343-54.
165. Trottier, J., et al., *Human UDP-glucuronosyltransferase (UGT)1A3 enzyme conjugates chenodeoxycholic acid in the liver*. Hepatology, 2006. **44**(5): p. 1158-70.
166. Hofmann, A.F., *Why bile acid glucuronidation is a minor pathway for conjugation of endogenous bile acids in man*. Hepatology, 2007. **45**(4): p. 1083-4; author reply 1084-5.
167. Hylemon, P.B., et al., *Bile acids as regulatory molecules*. J Lipid Res, 2009. **50**(8): p. 1509-20.

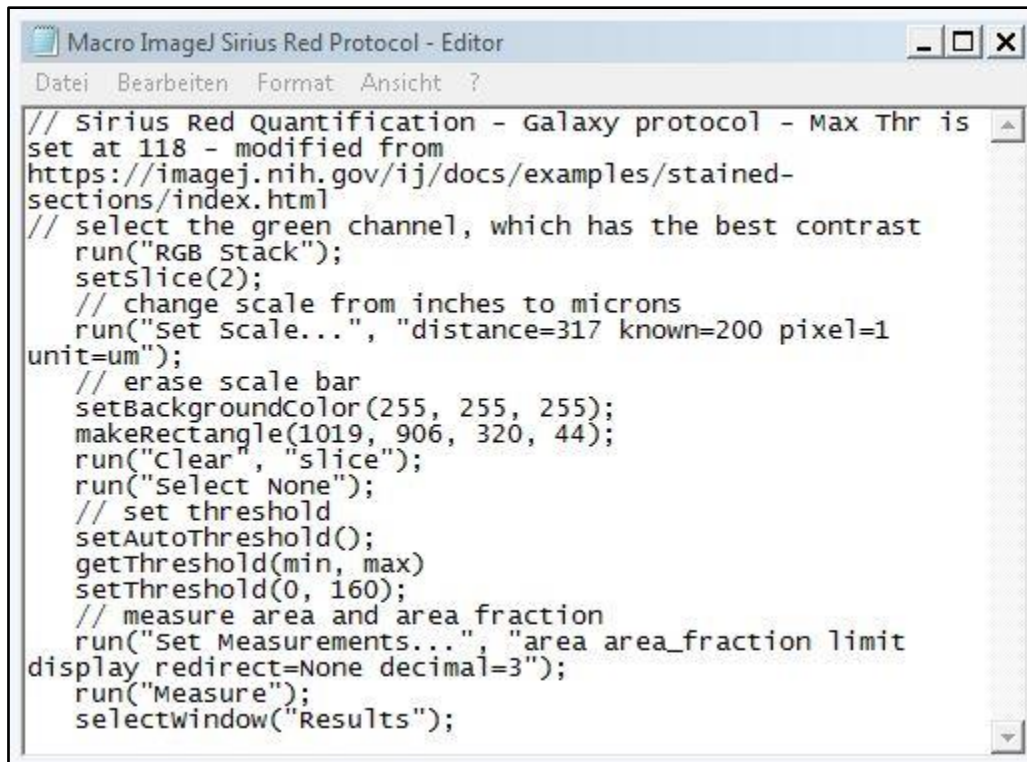
168. Sinal, C.J., et al., *Targeted disruption of the nuclear receptor FXR/BAR impairs bile acid and lipid homeostasis*. Cell, 2000. **102**(6): p. 731-44.
169. Halilbasic, E., T. Claudel, and M. Trauner, *Bile acid transporters and regulatory nuclear receptors in the liver and beyond*. J Hepatol, 2013. **58**(1): p. 155-68.
170. Trauner, M., et al., *Bile acids as regulators of hepatic lipid and glucose metabolism*. Dig Dis, 2010. **28**(1): p. 220-4.
171. Lankisch, T.O., et al., *Aryl hydrocarbon receptor (AhR)-mediated regulation of the human estrogen and bile acid UDP-Glucuronosyltransferase 1A3 gene*. Arch Toxicol, 2008. **82**(9): p. 573-82.
172. Parola, M. and G. Robino, *Oxidative stress-related molecules and liver fibrosis*. J Hepatol, 2001. **35**(2): p. 297-306.
173. Itoh, K., et al., *Keap1 represses nuclear activation of antioxidant responsive elements by Nrf2 through binding to the amino-terminal Neh2 domain*. Genes Dev, 1999. **13**(1): p. 76-86.
174. Klaassen, C.D. and S.A. Reisman, *Nrf2 the rescue: effects of the antioxidative/electrophilic response on the liver*. Toxicol Appl Pharmacol, 2010. **244**(1): p. 57-65.
175. Xu, W., et al., *The Nrf2 transcription factor protects from toxin-induced liver injury and fibrosis*. Lab Invest, 2008. **88**(10): p. 1068-78.
176. Tanaka, Y., et al., *NF-E2-related factor 2 inhibits lipid accumulation and oxidative stress in mice fed a high-fat diet*. J Pharmacol Exp Ther, 2008. **325**(2): p. 655-64.
177. Munzel, P.A., et al., *Contribution of the Ah receptor to the phenolic antioxidant-mediated expression of human and rat UDP-glucuronosyltransferase UGT1A6 in Caco-2 and rat hepatoma 5L cells*. Biochem Pharmacol, 2003. **66**(5): p. 841-7.
178. Kalthoff, S., et al., *Interaction between oxidative stress sensor Nrf2 and xenobiotic-activated aryl hydrocarbon receptor in the regulation of the human phase II detoxifying UDP-glucuronosyltransferase 1A10*. J Biol Chem, 2010. **285**(9): p. 5993-6002.
179. Schmidt, J.V. and C.A. Bradfield, *Ah receptor signaling pathways*. Annu Rev Cell Dev Biol, 1996. **12**: p. 55-89.
180. Fujii-Kuriyama, Y. and J. Mimura, *Molecular mechanisms of AhR functions in the regulation of cytochrome P450 genes*. Biochem Biophys Res Commun, 2005. **338**(1): p. 311-7.
181. Kalthoff, S., et al., *Coffee induces expression of glucuronosyltransferases via the aryl hydrocarbon receptor and Nrf2 in liver and stomach*. Gastroenterology, 2010.
182. Strassburg, C.P. and S. Kalthoff, *UDP-Glucuronosyltransferases in Metabolism of Drugs and Other Xenobiotics*. Wiley-VCH, 2012: p. 67-116.
183. Larsson, S.C., *Coffee, tea, and cocoa and risk of stroke*. Stroke, 2014. **45**(1): p. 309-14.
184. Loftfield, E., et al., *Coffee Drinking Is Widespread in the United States, but Usual Intake Varies by Key Demographic and Lifestyle Factors*. J Nutr, 2016. **146**(9): p. 1762-8.
185. Morisco, F., et al., *Coffee and liver health*. J Clin Gastroenterol, 2014. **48 Suppl 1**: p. S87-90.
186. Marventano, S., et al., *Coffee and tea consumption in relation with non-alcoholic fatty liver and metabolic syndrome: A systematic review and meta-analysis of observational studies*. Clin Nutr, 2016. **35**(6): p. 1269-1281.
187. Ruhl, C.E. and J.E. Everhart, *Coffee and tea consumption are associated with a lower incidence of chronic liver disease in the United States*. Gastroenterology, 2005. **129**(6): p. 1928-36.
188. Freedman, N.D., et al., *Coffee intake is associated with lower rates of liver disease progression in chronic hepatitis C*. Hepatology, 2009. **50**(5): p. 1360-9.
189. Bravi, F., et al., *Coffee reduces risk for hepatocellular carcinoma: an updated meta-analysis*. Clin Gastroenterol Hepatol, 2013. **11**(11): p. 1413-1421 e1.
190. Alferink, L.J.M., J.C. Kiefte-de Jong, and S. Darwish Murad, *Potential Mechanisms Underlying the Role of Coffee in Liver Health*. Semin Liver Dis, 2018. **38**(3): p. 193-214.
191. Gressner, O.A., et al., *Pharmacological application of caffeine inhibits TGF-beta-stimulated connective tissue growth factor expression in hepatocytes via PPARgamma and SMAD2/3-dependent pathways*. J Hepatol, 2008. **49**(5): p. 758-67.
192. Salomone, F., F. Galvano, and G. Li Volti, *Molecular Bases Underlying the Hepatoprotective Effects of Coffee*. Nutrients, 2017. **9**(1).
193. Arauz, J., et al., *Coffee attenuates fibrosis by decreasing the expression of TGF-beta and CTGF in a murine model of liver damage*. J Appl Toxicol, 2013. **33**(9): p. 970-9.

194. Shi, H., et al., *Chlorogenic acid reduces liver inflammation and fibrosis through inhibition of toll-like receptor 4 signaling pathway*. Toxicology, 2013. **303**: p. 107-14.
195. Pang, C., et al., *Caffeic acid prevents acetaminophen-induced liver injury by activating the Keap1-Nrf2 antioxidative defense system*. Free Radic Biol Med, 2016. **91**: p. 236-46.
196. Muriel, P. and J. Arauz, *Coffee and liver diseases*. Fitoterapia, 2010. **81**(5): p. 297-305.
197. Ehmer, U., et al., *Gilbert syndrome redefined: a complex genetic haplotype influences the regulation of glucuronidation*. Hepatology, 2012. **55**(6): p. 1912-21.
198. Kalthoff, S., et al., *Protective effects of coffee against oxidative stress induced by the tobacco carcinogen benzo[alpha]pyrene*. Free Radic Biol Med, 2017. **108**: p. 66-76.
199. Paigen, B., et al., *Variation in susceptibility to atherosclerosis among inbred strains of mice*. Atherosclerosis, 1985. **57**(1): p. 65-73.
200. Paigen, B., *Genetics of responsiveness to high-fat and high-cholesterol diets in the mouse*. Am J Clin Nutr, 1995. **62**(2): p. 458S-462S.
201. Vergnes, L., et al., *Cholesterol and cholate components of an atherogenic diet induce distinct stages of hepatic inflammatory gene expression*. J Biol Chem, 2003. **278**(44): p. 42774-84.
202. Goel, R., et al., *The proinflammatory phenotype of PECAM-1-deficient mice results in atherogenic diet-induced steatohepatitis*. Am J Physiol Gastrointest Liver Physiol, 2007. **293**(6): p. G1205-14.
203. Matsuzawa, N., et al., *Lipid-induced oxidative stress causes steatohepatitis in mice fed an atherogenic diet*. Hepatology, 2007. **46**(5): p. 1392-403.
204. Zarrinpar, A., et al., *Diet and feeding pattern affect the diurnal dynamics of the gut microbiome*. Cell Metab, 2014. **20**(6): p. 1006-17.
205. Tolba, R., et al., *Diethylnitrosamine (DEN)-induced carcinogenic liver injury in mice*. Lab Anim, 2015. **49**(1 Suppl): p. 59-69.
206. Heindryckx, F., I. Colle, and H. Van Vlierberghe, *Experimental mouse models for hepatocellular carcinoma research*. Int J Exp Pathol, 2009. **90**(4): p. 367-86.
207. Nakatani, T., et al., *Sex hormone dependency of diethylnitrosamine-induced liver tumors in mice and chemoprevention by leuprorelin*. Jpn J Cancer Res, 2001. **92**(3): p. 249-56.
208. Holland, P.M., et al., *Detection of specific polymerase chain reaction product by utilizing the 5'---3' exonuclease activity of Thermus aquaticus DNA polymerase*. Proc Natl Acad Sci U S A, 1991. **88**(16): p. 7276-80.
209. Cheong, J.Y., et al., *Serum markers for necroinflammatory activity in patients with chronic viral hepatitis and normal or mildly elevated aminotransferase levels*. Liver Int, 2011. **31**(9): p. 1352-8.
210. Cardiff, R.D., C.H. Miller, and R.J. Munn, *Manual hematoxylin and eosin staining of mouse tissue sections*. Cold Spring Harb Protoc, 2014. **2014**(6): p. 655-8.
211. Liou, G.Y. and P. Storz, *Detecting reactive oxygen species by immunohistochemistry*. Methods Mol Biol, 2015. **1292**: p. 97-104.
212. Sanchez-Valle, V., et al., *Role of oxidative stress and molecular changes in liver fibrosis: a review*. Curr Med Chem, 2012. **19**(28): p. 4850-60.
213. Poli, G., *Pathogenesis of liver fibrosis: role of oxidative stress*. Mol Aspects Med, 2000. **21**(3): p. 49-98.
214. Laurent, A., et al., *Metabolism of 4-hydroxynonenal, a cytotoxic product of lipid peroxidation, in rat precision-cut liver slices*. Toxicol Lett, 2000. **114**(1-3): p. 203-14.
215. Claudel, T., et al., *Role of nuclear receptors for bile acid metabolism, bile secretion, cholestasis, and gallstone disease*. Biochim Biophys Acta, 2011. **1812**(8): p. 867-78.
216. Han, C.Y., *Update on FXR Biology: Promising Therapeutic Target?* Int J Mol Sci, 2018. **19**(7).
217. Lopez, J.B., et al., *The value of liver function tests in hepatocellular carcinoma*. Malays J Pathol, 1996. **18**(2): p. 95-9.
218. Aktas, C., et al., *Melatonin attenuates oxidative stress, liver damage and hepatocyte apoptosis after bile-duct ligation in rats*. Toxicol Ind Health, 2014. **30**(9): p. 835-44.
219. Modi, A.A., et al., *Increased caffeine consumption is associated with reduced hepatic fibrosis*. Hepatology, 2010. **51**(1): p. 201-9.
220. Kennedy, O.J., et al., *Systematic review with meta-analysis: coffee consumption and the risk of cirrhosis*. Aliment Pharmacol Ther, 2016. **43**(5): p. 562-74.

221. Perreault, M., et al., *Role of glucuronidation for hepatic detoxification and urinary elimination of toxic bile acids during biliary obstruction*. PLoS One, 2013. **8**(11): p. e80994.
222. Setiawan, V.W., et al., *Association of coffee intake with reduced incidence of liver cancer and death from chronic liver disease in the US multiethnic cohort*. Gastroenterology, 2015. **148**(1): p. 118-25; quiz e15.
223. Costentin, C.E., et al., *Association of caffeine intake and histological features of chronic hepatitis C*. J Hepatol, 2011. **54**(6): p. 1123-9.
224. Bonner, J.C., *Regulation of PDGF and its receptors in fibrotic diseases*. Cytokine Growth Factor Rev, 2004. **15**(4): p. 255-73.
225. Kocabayoglu, P., et al., *beta-PDGF receptor expressed by hepatic stellate cells regulates fibrosis in murine liver injury, but not carcinogenesis*. J Hepatol, 2015. **63**(1): p. 141-7.
226. Wang, X., et al., *Targeting the PDGF-B/PDGFR-beta Interface with Destruxin A5 to Selectively Block PDGF-BB/PDGFR-betabeta Signaling and Attenuate Liver Fibrosis*. EBioMedicine, 2016. **7**: p. 146-56.
227. Arauz, J., et al., *Coffee consumption prevents fibrosis in a rat model that mimics secondary biliary cirrhosis in humans*. Nutr Res, 2017. **40**: p. 65-74.
228. Setiawan, V.W., et al., *Coffee Drinking and Alcoholic and Nonalcoholic Fatty Liver Diseases and Viral Hepatitis in the Multiethnic Cohort*. Clin Gastroenterol Hepatol, 2017. **15**(8): p. 1305-1307.
229. Fisher, C.D., et al., *Hepatic cytochrome P450 enzyme alterations in humans with progressive stages of nonalcoholic fatty liver disease*. Drug Metab Dispos, 2009. **37**(10): p. 2087-94.
230. Hardwick, R.N., et al., *Diversity in antioxidant response enzymes in progressive stages of human nonalcoholic fatty liver disease*. Drug Metab Dispos, 2010. **38**(12): p. 2293-301.
231. Hardwick, R.N., et al., *Altered UDP-glucuronosyltransferase and sulfotransferase expression and function during progressive stages of human nonalcoholic fatty liver disease*. Drug Metab Dispos, 2013. **41**(3): p. 554-61.
232. Aranha, M.M., et al., *Bile acid levels are increased in the liver of patients with steatohepatitis*. Eur J Gastroenterol Hepatol, 2008. **20**(6): p. 519-25.
233. Lew, J.L., et al., *The farnesoid X receptor controls gene expression in a ligand- and promoter-selective fashion*. J Biol Chem, 2004. **279**(10): p. 8856-61.
234. Pineda Torra, I., et al., *Bile acids induce the expression of the human peroxisome proliferator-activated receptor alpha gene via activation of the farnesoid X receptor*. Mol Endocrinol, 2003. **17**(2): p. 259-72.
235. Fuchs, C.D., et al., *FXR controls CHOP expression in steatohepatitis*. FEBS Lett, 2017. **591**(20): p. 3360-3368.
236. Zhou, X., et al., *PPARalpha-UGT axis activation represses intestinal FXR-FGF15 feedback signalling and exacerbates experimental colitis*. Nat Commun, 2014. **5**: p. 4573.
237. Alnouti, Y., I.L. Csanaky, and C.D. Klaassen, *Quantitative-profiling of bile acids and their conjugates in mouse liver, bile, plasma, and urine using LC-MS/MS*. J Chromatogr B Analyt Technol Biomed Life Sci, 2008. **873**(2): p. 209-17.
238. Takahashi, S., et al., *Cyp2c70 is responsible for the species difference in bile acid metabolism between mice and humans*. J Lipid Res, 2016. **57**(12): p. 2130-2137.
239. Little, J.M., et al., *Glucuronidation of the dietary fatty acids, phytanic acid and docosahexaenoic acid, by human UDP-glucuronosyltransferases*. Drug Metab Dispos, 2002. **30**(5): p. 531-3.
240. Little, J.M., et al., *Glucuronidation of oxidized fatty acids and prostaglandins B1 and E2 by human hepatic and recombinant UDP-glucuronosyltransferases*. J Lipid Res, 2004. **45**(9): p. 1694-703.
241. Bushee, J.L., et al., *Identification of saturated and unsaturated fatty acids released during microsomal incubations*. Xenobiotica, 2014. **44**(8): p. 687-95.
242. Bock, K.W., *Roles of human UDP-glucuronosyltransferases in clearance and homeostasis of endogenous substrates, and functional implications*. Biochem Pharmacol, 2015. **96**(2): p. 77-82.
243. Jarrar, Y.B., et al., *Determination of major UDP-glucuronosyltransferase enzymes and their genotypes responsible for 20-HETE glucuronidation*. J Lipid Res, 2014. **55**(11): p. 2334-42.

244. Lemotte, P.K., S. Keidel, and C.M. Apfel, *Phytanic acid is a retinoid X receptor ligand*. Eur J Biochem, 1996. **236**(1): p. 328-33.
245. Stec, D.E., et al., *Bilirubin Binding to PPARAlpha Inhibits Lipid Accumulation*. PLoS One, 2016. **11**(4): p. e0153427.
246. Guillemette, C., et al., *Genetic polymorphisms in uridine diphospho-glucuronosyltransferase IA1 and association with breast cancer among African Americans*. Cancer Res, 2000. **60**(4): p. 950-6.
247. Innocenti, F., et al., *Genetic variants in the UDP-glucuronosyltransferase IA1 gene predict the risk of severe neutropenia of irinotecan*. J Clin Oncol, 2004. **22**(8): p. 1382-8.
248. de Vries, H.S., et al., *A functional polymorphism in UGT1A1 related to hyperbilirubinemia is associated with a decreased risk for Crohn's disease*. J Crohns Colitis, 2012. **6**(5): p. 597-602.
249. Schwertner, H.A. and L. Vitek, *Gilbert syndrome, UGT1A1*28 allele, and cardiovascular disease risk: possible protective effects and therapeutic applications of bilirubin*. Atherosclerosis, 2008. **198**(1): p. 1-11.
250. Cheriyath, P., et al., *High Total Bilirubin as a Protective Factor for Diabetes Mellitus: An Analysis of NHANES Data From 1999 - 2006*. J Clin Med Res, 2010. **2**(5): p. 201-6.
251. Choi, S.H., K.E. Yun, and H.J. Choi, *Relationships between serum total bilirubin levels and metabolic syndrome in Korean adults*. Nutr Metab Cardiovasc Dis, 2013. **23**(1): p. 31-7.
252. Lin, Y.C., et al., *Variants in the UGT1A1 gene and the risk of pediatric nonalcoholic fatty liver disease*. Pediatrics, 2009. **124**(6): p. e1221-7.
253. Hjelkrem, M., et al., *Unconjugated hyperbilirubinemia is inversely associated with non-alcoholic steatohepatitis (NASH)*. Aliment Pharmacol Ther, 2012. **35**(12): p. 1416-23.
254. Hu, Z. and P.G. Wells, *In vitro and in vivo biotransformation and covalent binding of benzo(a)pyrene in Gunn and RHA rats with a genetic deficiency in bilirubin uridine diphosphate-glucuronosyltransferase*. J Pharmacol Exp Ther, 1992. **263**(1): p. 334-42.
255. Vienneau, D.S., U. DeBoni, and P.G. Wells, *Potential genoprotective role for UDP-glucuronosyltransferases in chemical carcinogenesis: initiation of micronuclei by benzo(a)pyrene and benzo(e)pyrene in UDP-glucuronosyltransferase-deficient cultured rat skin fibroblasts*. Cancer Res, 1995. **55**(5): p. 1045-51.
256. Wiench, K., et al., *1-C-glucuronidation of N-nitrosodiethylamine and N-nitrosomethyl-n-pentylamine in vivo and in primary hepatocytes from rats pretreated with inducers*. Carcinogenesis, 1992. **13**(5): p. 867-72.
257. Wiener, D., et al., *Characterization of N-glucuronidation of the lung carcinogen 4-(methylnitrosamino)-1-(3-pyridyl)-1-butanol (NNAL) in human liver: importance of UDP-glucuronosyltransferase IA4*. Drug Metab Dispos, 2004. **32**(1): p. 72-9.
258. Chen, G., et al., *Glucuronidation of tobacco-specific nitrosamines by UGT2B10*. Drug Metab Dispos, 2008. **36**(5): p. 824-30.
259. Strassburg, C.P., M.P. Manns, and R.H. Tukey, *Differential down-regulation of the UDP-glucuronosyltransferase IA locus is an early event in human liver and biliary cancer*. Cancer Res, 1997. **57**(14): p. 2979-85.
260. Bravi, F., et al., *Coffee and the risk of hepatocellular carcinoma and chronic liver disease: a systematic review and meta-analysis of prospective studies*. Eur J Cancer Prev, 2017. **26**(5): p. 368-377.
261. Vesselinovich, S.D. and N. Mihailovich, *Kinetics of diethylnitrosamine hepatocarcinogenesis in the infant mouse*. Cancer Res, 1983. **43**(9): p. 4253-9.
262. Tomasetti, C., L. Li, and B. Vogelstein, *Stem cell divisions, somatic mutations, cancer etiology, and cancer prevention*. Science, 2017. **355**(6331): p. 1330-1334.
263. Weinberg, R.A., *Oncogenes, antioncogenes, and the molecular bases of multistep carcinogenesis*. Cancer Res, 1989. **49**(14): p. 3713-21.

Supplements



```

Macro ImageJ Sirius Red Protocol - Editor
Datei Bearbeiten Format Ansicht ?

// Sirius Red Quantification - Galaxy protocol - Max Thr is
set at 118 - modified from
https://imagej.nih.gov/ij/docs/examples/stained-
sections/index.html
// select the green channel, which has the best contrast
run("RGB Stack");
setSlice(2);
// change scale from inches to microns
run("set scale...", "distance=317 known=200 pixel=1
unit=um");
// erase scale bar
setBackground(255, 255, 255);
makeRectangle(1019, 906, 320, 44);
run("Clear", "slice");
run("Select None");
// set threshold
setAutoThreshold();
getThreshold(min, max)
setThreshold(0, 160);
// measure area and area fraction
run("Set Measurements...", "area area_fraction limit
display redirect=None decimal=3");
run("Measure");
selectWindow("Results");

```

Figure 44: Manually written protocol used for computational quantification of liver fibrosis from Sirius red stained liver sections.

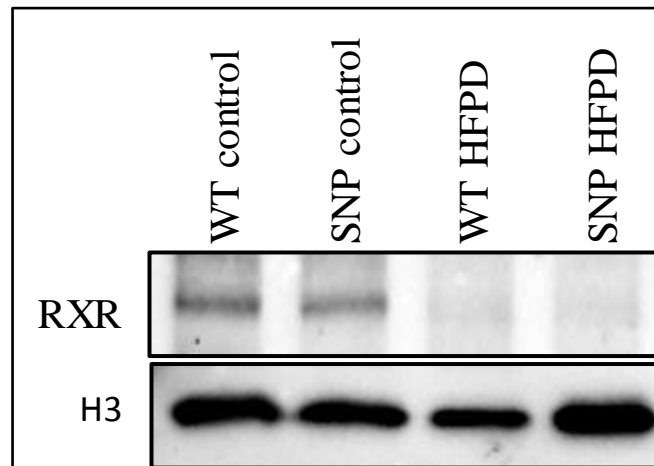


Figure 45: Western blot analysis of nuclear retinoid X receptor protein in *htgUGT1A*-WT and SNP mice after 24 weeks of control or high-fat Paigen diet (HFPD). (H3) histone H3, (RXR) retinoid X receptor.

Publications

Paper:

Landerer, S., Kalthoff, S., Strassburg, C. P. UDP-glucuronosyltransferases mediate coffee-associated reduction of liver fibrosis in bile duct ligated humanized transgenic *UGT1A* mice. *Hepatobiliary Surg Nutr* (accepted 13 April 2020)

Landerer, S., Kalthoff, S., Paulusch, S., Strassburg, C. P. A Gilbert syndrome-associated haplotype protects against fatty liver disease in humanized transgenic mice. *Sci Rep* 2020;10(1):8689

Kalthoff, S., Landerer, S., Reich, J., Strassburg, C. P. Protective effects of coffee against oxidative stress induced by the tobacco carcinogen benzo[alpha]pyrene. *Free Radic Biol Med* 108, 66-76 (2017)

Herz, C., Tran, H.T.T., Landerer, S., Gaus, J., Schlotz, N., Lehr, L., Schäfer, W. R., Treeck, O., Odongo, G. A., Skatchkov, I., Lamy, E. Normal human immune cells are sensitive to telomerase inhibition by brassica-derived 3,3-diindolylmethane, partly mediated via ER α / β -AP1 signaling. *Mol Nutr Food Res*, 61 (9) (2017)

Poster:

Landerer, S., Kalthoff, S., Winkler, A., Strassburg, C.P. Differential regulation of human UDP-glucuronosyltransferases (UGTs) during chronic ethanol exposure in a humanized transgenic UGT1A mouse model.

AASLD 2016

Landerer, S., Kalthoff, S., Strassburg, C.P. Coffee mediated effects on transcriptional regulation of human UDP-glucuronosyltransferases (UGTs) during obstructive cholestasis (BDL) in a humanized transgenic UGT1A mouse model.

AASLD 2017

Landerer, S., Kalthoff, S., Paulusch, S., Strassburg, C.P. Gilbert syndrome-associated single nucleotide polymorphisms (SNPs) of the human UDP-glucuronosyltransferase 1A (UGT1A) gene locus are associated with milder hepatic steatosis in humanized transgenic *UGT1A* mice after 24 weeks of a high fat Paigen diet.

AASLD 2018 (oral presentation)

Landerer, S., Kalthoff, S., Paulusch, S., Strassburg, C.P. UDP-glucuronosyltransferase 1A (*UGT1A*) gene polymorphisms affect diethylnitrosamine-induced hepatocellular carcinoma development in humanized transgenic *UGT1A* mice.

AASLD 2019